TURUN YLIOPISTO
UNIVERSITY OF TURKU

TUNING PHOTOCHROMIC SODALITES ACROSS THE VISIBLE SPECTRUM

Hannah Byron

TURUN YLIOPISTO
UNIVERSITY OF TURKU

TUNING PHOTOCHROMIC SODALITES ACROSS THE VISIBLE SPECTRUM

Hannah Byron

University of Turku

Faculty of Science
Department of Chemistry
Intelligent Materials Chemistry Group
Doctoral Programme in Exact Sciences

Supervised by

Professor Mika Lastusaari
Intelligent Materials Chemistry Group
Department of Chemistry
University of Turku
Turku, Finland

Reviewed by

Assoc. Professor Maria Luisa Saladino
Department of Biological, Chemical and
Pharmaceutical Sciences and
Technologies (STEBICEF)
Università degli Studi di Palermo
Palermo, Italy

Professor Dmitry Murzin
Faculty of Science and Engineering
Åbo Akademi University
Turku, Finland

Opponent

Professor Mark T. Weller
Cardiff University
Wales, United Kingdom

"Colour is a power which directly influences the soul."
- Wassily Kandinsky

UNIVERSITY OF TURKU
Faculty of Science
Department of Chemistry
Chemistry
Hannah Byron: Tuning Photochromic Sodalites across the Visible Spectrum
Doctoral Dissertation, 165 pp.
Doctoral Programme in Exact Sciences
June 2023

ABSTRACT

Photochromic sodalite, $Na_8(AlSiO_4)_6(Cl,S)_2$, has been a topic of research for almost 100 years, though only recently has a deep understanding of its remarkably fatigue-resistant colour change been obtained. Aside from the cathodochromic displays proposed in the 1970s, photochromic sodalites have only been seriously considered for everyday and industrial applications in the last decade, and for some of these significant development was needed before potential commercialisation.

Following on from prior investigations into the colour and excitation threshold of photochromism, this thesis studies how the colour change of photochromic sodalite can be tuned to switch from white to any desired colour, presenting a range of possible absorption maxima from 420-680 nm: almost the entire visible spectrum. Particularly interesting was the effect of sodium substitution with calcium, which produced sodalites showing a remarkable white-to-yellow colour change. The relative efficiency of four different synthesis methods was considered for producing the best photochromic sodalites, including a thorough characterisation of the blue-white luminescence of photochromic sodalite produced without zeolite A. Post-synthesis treatment such as sintering of hydrothermal samples and nitrate-melt ion exchange is also discussed in the context of redshifting the F-centre's absorption maximum as much as possible. The suitability of a diverse range of photochromism colours from a single or mix of low-cost sodalite materials for several industrial applications, including X-ray imaging and blue light detection, is discussed.

The effect of selenium on the photochromism was also studied: selenium was gradually introduced into the sodalite structure to replace the usual sulfur activator. Selenium was found to lower the activation threshold of photochromism without affecting the energy levels of the F-centre's absorption, unlike potassium and rubidium. Selenium sodalites were then mixed with selenium-free materials of a complementary colour, and with the aid of a mathematical model, such mixtures were shown to be suitable for simultaneous passive dosimetry of two types of UV radiation.

The deeper scientific understanding of the photochromism mechanisms and the tuning methods presented in this work thus serve to improve these materials' suitability for further research and commercialisation.

KEYWORDS: Photochromism, sodalite, colour, dosimetry, tuning

TIIVISTELMÄ

Fotokromista sodaliittia, $Na_8(AlSiO_4)_6(Cl,S)_2$, on tutkittu jo lähes 100 vuoden ajan, mutta sen merkittävää pitkään kestävään värinmuutokseen liittyvää ominaisuutta on alettu ymmärtää paremmin vasta viime aikoina. Fotokromisen sodaliitin käyttöä teollisissa ja arkisissa sovelluksissa on harkittu varsinaisesti vasta viime vuosikymmenellä, vaikka sen soveltuvuutta katodokromisissa näytöissä on tutkittukin jo 1970-luvulla. Nämä sovellukset vaativat kuitenkin lisää kehitystyötä ennen niiden mahdollista kaupallista käyttöä.

Tämän väitöskirjan tutkimus pohjautuu aiempien fotokromismin väriä ja virityskynnystä käsitteleviin tutkimuksiin keskittyen siihen, miten fotokromisen sodaliitin värinmuutosta voidaan muokata valkoisesta mihin tahansa väriin. Väitöskirjatyön tuloksena saavutettiin laajennettu absorptiomaksimin väli 420-680 nm, joka vastaa lähes koko näkyvän valon spektriä. Eräänä poikkeuksellisen mielenkiintoisena tuloksena havaittiin keltainen fotokromismi korvattaessa natrium osittain kalsiumilla. Työssä tutkittiin neljän eri synteesimenetelmän sopivuutta ja tehokkuutta parhaan fotokromismin tuottamiseen, jonka lisäksi yhden zeoliitittoman menetelmän tuotteiden sinivalkoinen luminesenssi karakterisoitiin perusteellisesti. Synteesin jälkeisiä käsittelyjä, kuten hydrotermisesti valmistettujen näytteiden sintraaminen ja kaliumionin vaihto, käsitellään F-keskuksen absorptiomaksimin punasiirtämisen yhteydessä. Lisäksi työssä käsitellään erilaisten fotokromisten sodaliittien ja useiden fotokromisten sodaliittien sekoitusten mahdollista sopivuutta sovelluksiin, kuten röntgenkuvantamiseen ja sinivalodetektointiin.

Työssä tutkittiin myös seleenin vaikutusta fotokromismiin lisäämällä seleeniä asteittaisesti sodaliitin rakenteeseen korvaamaan sen tyypillistä aktiivista keskusta, rikkiä. Tutkimus paljasti, että seleeni pystyy laskemaan fotokromismin virityskynnyksen samalla tavalla kuin kalium tai rubidium, mutta näistä poiketen, seleeni ei vaikuta F-keskuksen energiatasoihin. Näitä seleenisodaliitteja sekoitettiin toisten, fotokromismiväriltään sopivien seleenittömien materiaalien kanssa, jolloin saatiin sekoitus, jonka voitiin osoittaa soveltuvan kahta eri UV-säteilyä samanaikaisesti mittaavaan passiiviseen dosimetriin.

Tässä työssä esitetty tieteellinen ymmärrys fotokromismin mekanismista ja viritysmenetelmistä parantaa sodaliittien soveltuvuutta jatkotutkimukseen ja kaupalliseen käyttöön.

ASIASANAT: Fotokromismi, sodaliitti, väri, dosimetria, virittäminen

Table of Contents

Abbreviations

a	Unit cell parameter (unit: Å)
Ca_2	Two Ca^{2+} surrounding V_{Cl} in the sodalite β-cage
DFT	Density functional theory
d_{vac}	Vacancy size
E	An element from the chalcogen group (S, Se)
E_a	Activation energy
FAU	Faujasite, zeolite with the faujasite structure
HT	Hydrothermal (synthesis)
IR	Infrared
LED	Light-emitting diode
LTA	Linde type A, zeolite with the Linde type A structure
$λ$	Wavelength (unit: nm)
$λ_{em}$	Emission wavelength (unit: nm)
$λ_{ex}$	Excitation wavelength (unit: nm)
$λ_{max}$	Wavelength of absorption maximum (reflectance minimum, unit: nm)
M	An element from the alkali metal group (Li, Na, K, Rb, Cs)
Na_2Ca	Two Na^+ and once Ca^{2+} surrounding V_{Cl} in the sodalite β-cage
Na_3Ca	Three Na^+ and one Ca^{2+} surrounding V_{Cl} in the sodalite β-cage
Na_4	Four Na^+ in a tetrahedral arrangement surrounding V_{Cl} in the sodalite β-cage (pristine sodalite)
Na_xK_y	Tetrahedral arrangement of x Na^+ and y K^+ surrounding V_{Cl} in the β-cage; $x + y = 4$
NIR	Near infrared, radiation in the wavelength range 800-2500 nm
NIST	National Institute of Standards and Technology
OSL	Optically stimulated luminescence
PeL	Persistent luminescence
PL	Photoluminescence
PXRD	Powder X-ray diffraction
SS	Solid-state (synthesis)
T	A tetrahedrally coordinated ion in the sodalite backbone (Al^{3+}, Ga^{3+}, Si^{4+}, Ge^{4+})

TD-DFT	Time-dependent density functional theory
t_{delay}	Delay time
t_{ex}	Excitation time
TL	Thermoluminescence
TT	Thermotenebrescence, thermal bleaching of tenebrescence
UV	Ultraviolet
UVA	Ultraviolet radiation in the wavelength range 315-400 nm
UVB	Ultraviolet radiation in the wavelength range 280-315 nm
UVC	Ultraviolet radiation in the wavelength range 100-280 nm
V_{Cl}	Chloride vacancy
V_O	Oxygen vacancy
V_{Sr}	Strontium vacancy
V_X	Halide ion vacancy
WLED	White light-emitting diode
X	An element from the halogen group (F, Cl, Br, I)
XANES	X-ray absorption near edge structure
XPS	X-ray photoelectron spectroscopy
XRF	X-ray fluorescence spectroscopy

List of Original Publications

This dissertation is based on the following original publications, which are referred to in the text by their Roman numerals:

I   **Byron, H.**, Norrbo, I. & Lastusaari, M., A zeolite-free synthesis of luminescent and photochromic hackmanites, *J. Alloys Compd.,* 2021*, 872,* 159671.

II   **Byron, H.**, Kreivilä, T., Colinet, P., Le Bahers, T. & Lastusaari, M., New shades of photochromism – yellow sodalites for the detection of blue light, *J. Mater. Chem. C*, 2023, 11(9), 3360-3374.

III   **Byron, H.**, Swain, C., Paturi, P., Colinet, P., Rullan, R., Halava, V., Le Bahers, T., & Lastusaari, M., Highly tuneable photochromic sodalites for dosimetry, security marking and imaging, *Manuscript under review in Advanced Functional Materials (May 2023).*

List of Other Related Publications

Colinet, P., **Byron, H.**, Vuori, S., Lehtiö, J.-P., Laukkanen, P., Van Goethem, L., Lastusaari, M., and Le Bahers, T., The structural origin of the efficient photochromism in natural minerals, *Proceedings of the National Academy of Sciences*, 2022, 119(23), e2202487119.

Vuori, S., **Byron, H.**, Norrbo, I., Tuomisto, M. and Lastusaari, M., Photochromic photography with hackmanite obtained by a large-scale synthesis, *Journal of Industrial and Engineering Chemistry*, 2023, 120, 316-373.

1   Introduction

Photochromic sodalite has in recent years been dubbed something of a miracle material.[1] This simple aluminosilicate compound of formula $Na_8(AlSiO_4)_6(Cl,S)_2$ is capable of showing a multitude of optical properties, depending on its exact composition and the wavelength of light it interacts with.[2] The most famous of these is its reversible photochromism (tenebrescence), i.e. a change in colour from white to purple under UV stimulation that fades away again in white light. Natural photochromic sodalites also carry the name hackmanite, after the Finnish geologist Victor Hackman,[3] though hackmanite is no longer classified as a separate mineral to sodalite by the International Mineralogical Association.[4] Throughout this work the natural mineral will still be called hackmanite, though its synthetic analogue will be referred to as (synthetic) photochromic sodalite.

Prior research into the optical properties of photochromic sodalite has revealed much about the species and mechanism responsible for the colour change, as well as many ways to tune the structure. Nevertheless, some options have remained unexplored until now, and publications about the development of these materials for applications beyond cathodochromic displays have only seriously begun to surface in the last decade. This work presents the experimental study of the full colour tuning of photochromic sodalite, including the introduction of novel white-to-yellow photochromism and a demonstration of how the colour and excitation threshold can be tuned independently.

Synthesis was carried out using four different methods and their advantages and disadvantages are evaluated. It was found that despite the limitations on tuning of the aluminosilicate backbone, zeolite A ($NaAlSiO_4$) was the best choice of starting material, and with small modifications to the composition, a very wide range of colours could be produced. In fact, it appears that by utilising the methods presented in this thesis, photochromic sodalite can be tuned to change from white to one of a broader range of colours than any other inorganic photochromic material, without the need for toxic or expensive elements. Moreover, the high stability of the material is not compromised, making it perfect for application as much in the home as in industry.

Following synthesis, materials were analysed using a wide range of methods to understand their structure and properties. Powder X-ray diffraction (PXRD) was the main method of structural analysis, and many of the decisions made in how to further study and tune the materials were made on the basis of the PXRD data. X-ray fluorescence (XRF) was also key in understanding the compositions of the products and thus the success of the syntheses.

Some studies on the luminescence of these materials were performed, particularly in **I**, though with time the focus shifted solely towards the photochromic property. Nevertheless, the photo- and persistent luminescence of photochromic sodalites only further strengthens their potential for applications in tagging and security marking, something that is highlighted in **III** when sodalite mixes and their combined optical properties are discussed.

Reflectance spectroscopy was the main method of studying the colour change, and was applied in a wide range of ways to study properties such as the excitation spectrum of tenebrescence, optical bleaching spectra, thermal bleaching energies, colouration intensity as a function of radiation dose and fading of colouration under different light sources. This method is the equivalent of UV-VIS spectroscopy for opaque powder samples and primarily tells the difference in light absorption properties (and thus, how much light is reflected from the sample) of the sample in its uncoloured and coloured forms.

Computational methods were also used, where required, to further understand the inner workings of these materials. These were essential to determining the cause of yellow photochromism in the calcium-containing photochromic sodalites of **II**, and computational data also complemented the experimental observations on the effect of selenium on the excitation threshold of colouration.

After the extensive characterisation of these materials, their suitability for application was studied in a variety of contexts. Some applications previously presented in the literature, such as X-ray imaging and UV dose determination,[5,6] were shown to work more efficiently when highly tuned photochromic sodalites were used in place of the sodium chlorosodalite found in nature. New applications were also developed, such as the blue light detector and dosimeter of **II**, and the sodalite mixes of **III**, which utilise these materials as photochromic pigments. Mixing sodalites together gives a very efficient route to cheap, robust photochromic materials with a reliable photochromic response from white to any desired colour, while retaining their luminescent properties.

This work therefore represents a significant step forward in the understanding and control of photochromic sodalites. There are still many avenues left unexplored, though it can be said that photochromic sodalites show greater potential and are closer to commercialisation than ever before.

2 Literature Review

2.1 Sodalite and related minerals

Sodalite is an aluminosilicate mineral of formula $Na_8(AlSiO_4)_6Cl_2$, which gets its name from the high proportion of sodium it contains.[7] First registered with the International Mineralogical Association in 1811,[4] it is a member of the feldspathoid mineral family[8] and is typically found in Greenland and Canada.[7,9] Sodalite has been used as a decorative stone due to its deep blue colour, somewhat reminiscent of lapis lazuli. In fact, blue lapis lazuli contains another member of the sodalite family, lazurite $(Na_7Ca(AlSiO_4)_6(SO_4)(S_3)\cdot H_2O)$. Both sodalite and lazurite, along with other members of the sodalite family such as haüyne $(Na_3Ca(AlSiO_4)_3(SO_4,S,Cl))$ and nosean $(Na_8(AlSiO_4)_6(SO_4)\cdot H_2O)$, get their rich blue colour from the presence of the radical anion S_3^-, though other colours such as pink and yellow are possible too.[8,10] Many of these minerals also fluoresce under longwave UV radiation, often an orange colour, which arises from the presence of S_2^- in the structure.[11,12] Lazurite is the exception to this, perhaps because any yellow emission produced would be subject to strong self-absorption by this dark blue mineral.[13]

Along with their luminescence and attractive colours, some members of the sodalite family boast another interesting property – that of tenebrescence, or reversible photochromism. Two members in particular display this property: tugtupite $(Na_4BeAlSi_4O_{12}Cl)$ and hackmanite $(Na_8(AlSiO_4)_6(Cl,S)_2)$. Scapolite $([Na,Ca]_4Al_3Si_9O_{24}[Cl,CO_3]_2)$ and spodumene $(LiAl(SiO_3)_2)$ are other tenebrescent natural minerals,[14,15] but are not members of the sodalite family. It is uncertain whether other members of the sodalite group are tenebrescent, as their strong body colours (lazurite, haüyne) conceal any possible change of colour on exposure to UV.

Hackmanite's white-to-purple tenebrescence (**Figure 1**a-b) has been know of the longest, and was first reported by Lee in 1936.[16] Tugtupite's pink tenebrescence (**Figure 1**c-d) was revealed in 1982,[17] and scapolite's blue photochromism **Figure 1**e-f) is the newest discovery, being first reported in 2005.[14] Kirk stated in 1954 that both chloride and sulfur are required for sodalites to display tenebrescence,[12] and studies from the last decade based on synthetic analogues and computational simulations have revealed the true intricacies of the mechanism. In 2022 Colinet *et al*. also sought to uncover the reasons behind the high efficiency of the reversible

photochromism in hackmanite, tugtupite and scapolite, and in turn confirmed that the mechanism of photochromism in tugtupite and scapolite is the same as in hackmanite (see section 2.3).[18] However, thus far synthetic tugtupites and scapolites displaying tenebrescence have not been produced,[18] meaning that for now their only applications are as unusual collectors' items and pieces of jewellery. Hackmanite, on the other hand, can easily be produced synthetically, making it suitable for a plethora of applications.[2]

Sodalite is a zeolite-type mineral with an aluminosilicate backbone and a silicon to aluminium ratio of 1:1. It crystallises in a cubic system and is related to other zeolites, such as Linde type A (LTA, zeolite A), zeolite X and zeolite Y (Faujasite-type zeolites, FAU), in that the structure is made up of sodalite cages, or β-cages (**Figure 1**g). The sodalite structure is the most compact of these, with the β-cages as tightly packed as possible, joined by both 4- and 6-rings.[19] In LTA zeolite, the β-cages are joined by the 4-rings only, and in FAU zeolites they are joined by 6-rings.[19] Sodalite is therefore the least porous of these three zeolite types, and either LTA or FAU can be used as precursors to sodalite synthesis.[2,20,21] In sodalite, the β-cages are not empty – rather they are filled with four sodium ions and one chloride ion (**Figure 1**g). In the case of natural hackmanite, in some β-cages, chloride ions are replaced with disulphide ions, S_2^{2-}, while in others the chloride ion is missing, leaving a vacancy, V_{Cl}. Electron transfer from S_2^{2-} to V_{Cl} in a nearby cage is responsible for the colour change, as discussed in section 2.3. During synthesis, such ions can enter the structure through the pores of the LTA or FAU precursors, where they remain trapped once the structure becomes more compact. It is this structure which is responsible for the photochromic property in photochromic sodalites and hackmanites, as well as their excellent chemical and physical durability.
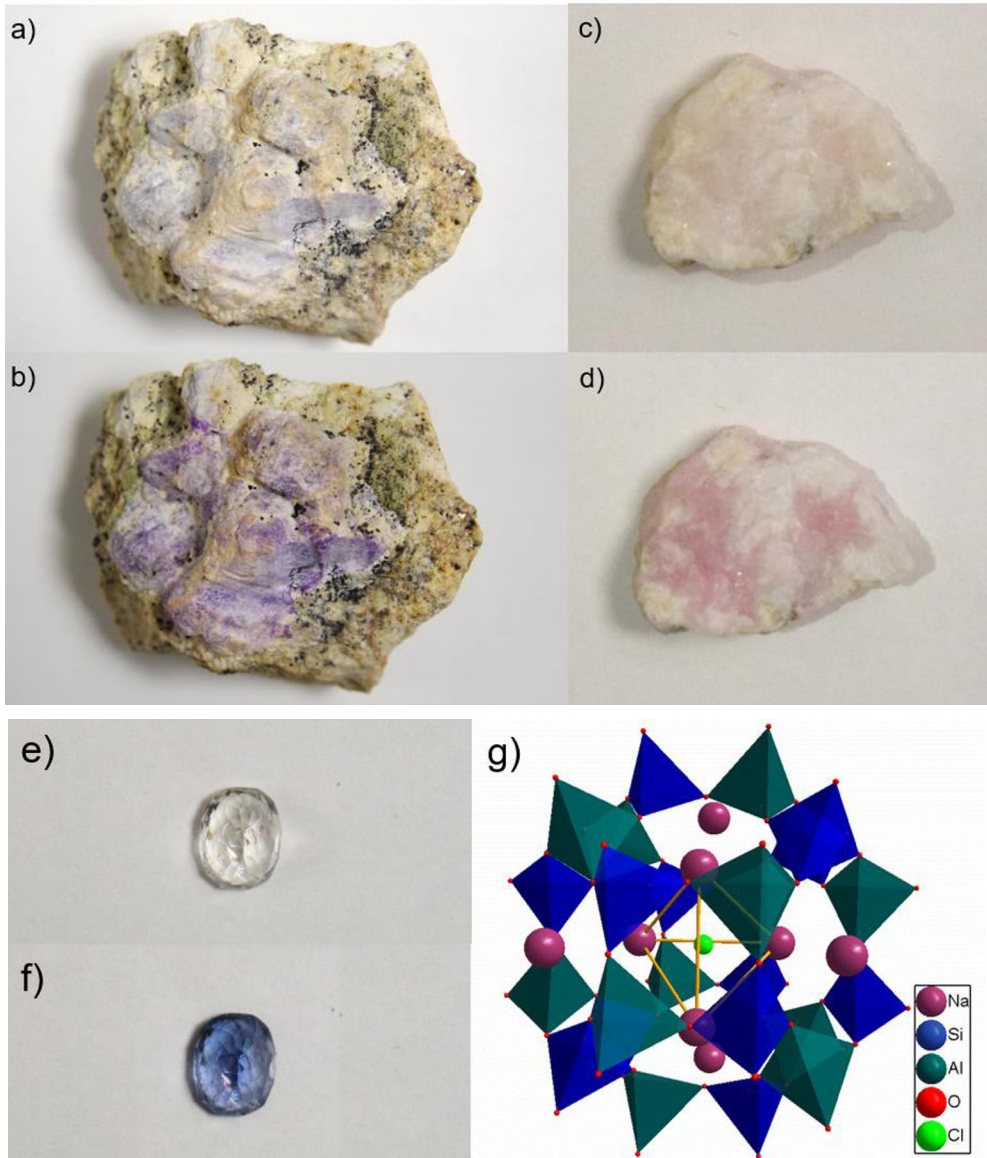
Figure 1.   Photographs of natural hackmanite (a, b), tugtupite (c, d) and scapolite (e, f) before (a, c, e) and after (b, d, f) colouration by UV. g) Structure of sodalite showing the aluminosilicate β-cage with Na_4 tetrahedron surrounding Cl^- inside. AlO_4^{5-} and SiO_4^{4-} corner-sharing tetrahedral are shown in dark green and blue respectively; coloured spheres represent Na^+ (purple), O^{2-} (red) and Cl^- (bright green).

2.2 Photochromic materials

The term "photochromic" comes from the Greek words "photos" (φωτός) meaning "light" and "chroma" (χρῶμα) meaning "colour". This term well indicates the nature of the phenomenon – namely, that when a photochromic substance interacts with light, it undergoes some change in colour. However, this is not the original term for the ability of a material to change colour upon exposure to light, which was first recorded by Marckwald in 1899. He observed that when exposed to light, two organic compounds (anhydrous benzo[c][1,8]naphthyridine hydrochloride and 2,3,4,4-tetrachloronaphthalen-1(4H)-one) became coloured, and that this colour faded when the compounds were returned to a dark room.[22] For around the next 50 years, Marckwald's term "phototropy" would be used to refer to materials with this property, until in the 1950s, when Yehuda Hirshberg renamed it "photochromism" after his studies on dianthrones.[23,24]

Both Marckwald's photochromic materials are organic, and their photochromism arises from their ability to easily interconvert between two different structures which have different light-absorbing properties. There are countless different families of organic photochromes, sometimes referred to as "molecular switches" due to their molecular nature and ability to switch from one colour to another. Upon exposure to UV, these molecular switches can undergo structural rearrangements, often with bonds breaking and new bonds forming to produce the chromophore. Perhaps the most simple of these are the azobenzenes, which rearrange upon 300-400 nm excitation from E-azobenzene to Z-azobenzene.[25] This rearrangement changes the symmetry of the molecule, thus rendering the n → π* transition allowed in Z-azobenzene (C_{2v} symmetry), whereas it is forbidden in C_{2h} E-azobenzene. In both forms, the absorption maximum of this band is around 440 nm, but the increase in extinction coefficient from 405 dm^3 mol^{-1} cm^{-1} (E-azobenzene) to 1250 dm^3 mol^{-1} cm^{-1} (Z-azobenzene) causes the colour change from almost colourless to yellow (**Figure 2**a).[26] The Z form is metastable, and will relax back to the E form either upon exposure to visible light of >400 nm,[25] or through thermal relaxation.[27] The energy gap of the n → π* transition is highly sensitive to substitution, and thus the colour of azobenzenes can be easily tuned.[26]

Another typical organic photochromic material is spiropyran, whose coloured form is the merocyanine isomer formed upon C-O bond cleavage by UV radiation (**Figure 2**b). Spiropyrans are able to switch between their colourless and coloured forms rapidly and with high quantum yields.[28] They are also capable of responding to other stimuli such as temperature, pH and redox potential.[25] Spiropyrans, azobenzenes and many other organic molecular switches have also been connected to other molecular systems to broaden their functionality:[29] for example, azobenzenes coupled to long chain hydrocarbons can produce photoresponsive pores in membranes.[25]

a)

λ_{max} 449 nm
$\varepsilon = 405$ dm^3 mol^{-1} cm^{-1}

λ_{max} 440 nm
$\varepsilon = 1250$ dm^3 mol^{-1} cm^{-1}

UV
Vis

b)

UV
Vis

Spiropyran
Colourless

Merocyanine
Coloured
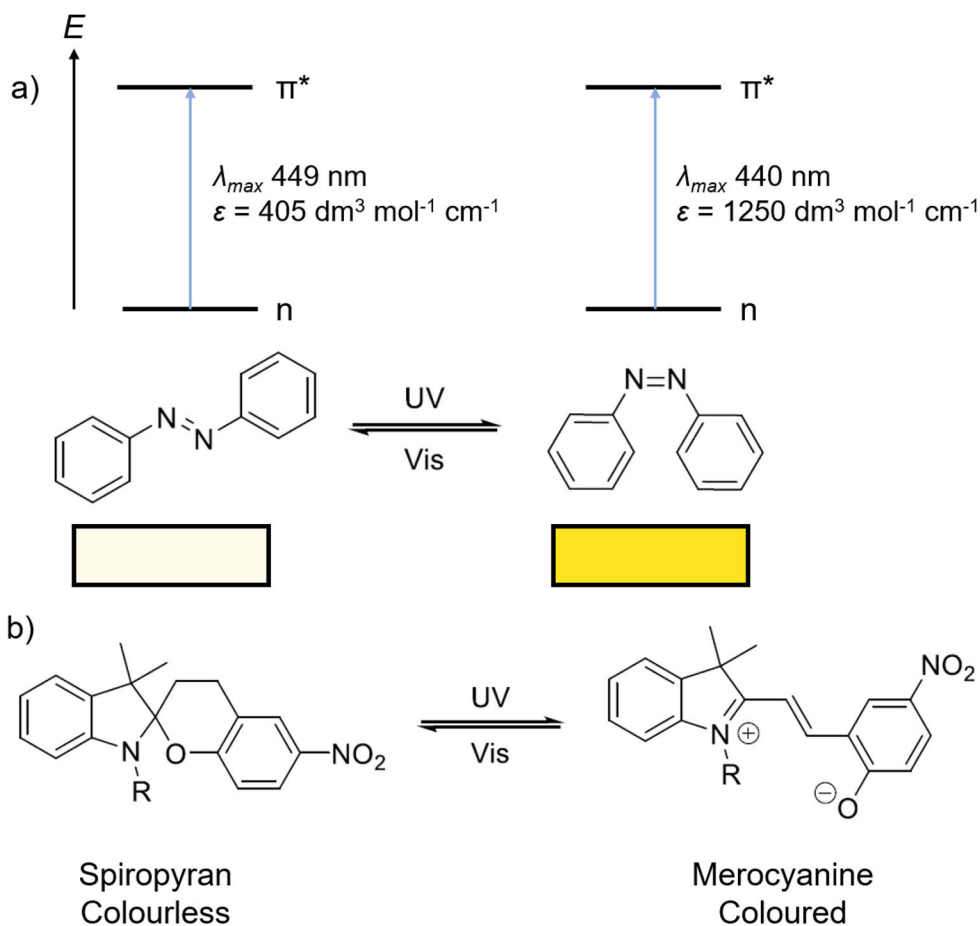
Figure 2. a) Structures of *E*- and *Z*-azobenzene, transition responsible for the colour and observed colour of each isomer.[26] b) Structures of spiropyran in its colourless and coloured forms.

Many inorganic materials are also known to be photochromic. Sodalite is one of these, though perhaps the most familiar example is the silver chloride present in photochromic eyeglasses.[30] Another classic inorganic photochrome is tungsten oxide, WO_x; other binary transition metal oxides such as molybdenum oxide, MoO_3, vanadium oxide, V_2O_5, zinc oxide, ZnO, and titanium oxide, TiO_2 have also been reported.[31,32] In general, inorganic photochromic materials do not undergo the significant structural rearrangements of their organic counterparts, as they are often not individual molecules, but rather ionic crystal lattices. Instead, their coloured forms may arise from photoreduction of metal ions (WO_3, MoO_3, V_2O_5, TiO_2), which absorb light via a charge transfer,[31,33] F-centres forming in structural defects

(photochromic sodalite, $Sr_3MLn(PO_4)_3F:Eu^{2+}$ (M = Li, Na, Ln = Y, Gd)),[34–36] or formation of nanoparticles (AgCl-doped glass, $Ag-TiO_2$ films).[30,37,38] Doping usually improves the photochromic property: for example, Cu doping of WO_3 to improve reversibility of the colour change,[39] or introduction of Ag nanoparticles to TiO_2 films.[37,38] It should be noted that the exact mechanism of WO_3/WO_x's photochromism is uncertain, with Bechinger *et al.* claiming the decomposition of water is involved, along with the formation of tungsten bronze H_xWO_3.[31,40]

Tungsten oxide changes from yellow to blue under UV irradiation, and as discussed the reversibility can be improved by doping with copper.[39] Altering the colour is also possible, as shown by Miyazaki *et al.* through molybdenum doping.[41] Zirconium and aluminium can also be incorporated into tungsten oxide to enhance the photochromism.[42,43] Molybdenum and vanadium oxides also take on a blue hue when exposed to appropriate wavelengths of light; V_2O_5 is particularly interesting due to its ability to change colour under visible light (515 nm) and the high reversibility of the colour change.[44] The aforementioned TiO_2 films containing Ag nanoparticles change from white to brown, similarly to AgCl-doped glasses.[37] The silver nanoparticles that form in these films are of all different sizes and thus absorb broadly in the visible spectrum, giving a brown colour. Interestingly, the colour can be selectively bleached with different colours of light, leaving behind particles which absorb other wavelengths to those used in bleaching, giving the film a multi-coloured appearance.[37,38]

While doping can be used to greatly enhance the reversibility and contrast of simple transition metal oxide-based inorganic photochromic materials, their intrinsic colours are rather limited. Some more complex ceramics, such as $Ba_{10}(PO_4)_6ClF:Eu^{2+},Gd^{3+}$ and $Sr_2SnO_4:Eu^{3+}$, have been shown to reversibly change from white to purple upon UV and possibly X-ray excitation,[45,46] while $Ca_2Ba_3(PO_4)_3F:Eu^{2+}$ changes from white to green.[47] For all of these, the presence of europium greatly enhances the photochromic property and is often essential for it. Further variety in the available colours is found with the $Sr_3MLn(PO_4)_3F:Eu^{2+}$ (M = Li, Na, Ln = Y, Gd) family of materials studied between 2015 and 2017 by Yang *et al.* These are, depending on M, Ln and the presence of other dopants, able to change from white to purple or blue.[35,36,48,49] Finally, in 2021, Yang *et al.* presented a grey-to-yellow inorganic photochromic material, $0.85(K_{0.5}Na_{0.5})NbO_3-0.15ZrSrO_3:0.5\%$ Sm^{3+}.[50] This, like many of the more complex oxide ceramics, shows good fatigue resistance. Some colours, however, still appear more challenging to obtain: for example, green and yellow are somewhat rarer than others, and an account of an inorganic photochrome changing from white to orange was not found.

Table 1. Summary of inorganic photochromic materials discussed in the text, the species responsible for their coloured forms, and range of colours available.

Inorganic photochromic material	Chromophore	Available colour change
WO_3	Bronze formation followed by charge transfer	Yellow → blue[39] Yellow → brown[41]
MoO_3	Photoreduction and charge transfer (Mo^{6+}-Mo^{5+})	Yellow → blue[51]
V_2O_5	Photoreduction and charge transfer (V^{5+}-V^{4+})	Pale brown → blue-black[44]
Ag-TiO_2	Ag nanoparticles	White → brown[37,38]
AgCl-doped borophosphate glass	Ag nanoparticles	White → brown[52]
$Ba_{10}(PO_4)_6ClF:Eu^{2+},Gd^{3+}$	F-centre, e^- from Eu^{2+}	White → purple[45]
$Sr_2SnO_4:Eu^{3+}$	F-centre in V_{Sr} stabilised by Eu^{3+}	White → purple[46]
$Ca_2Ba_3(PO_4)_3F:Eu^{2+}$	Photo-oxidation of Eu^{2+} to Eu^{3+}	White → green[47]
$Sr_3MLn(PO_4)_3F:Eu^{2+}$ (M = Li, Na, Ln = Y, Gd)	F-centre in V_O stabilised by Eu^{2+}	White → purple[36,48] White → blue[35,49]
$0.85(K_{0.5}Na_{0.5})NbO_3$-$0.15ZrSrO_3:0.5\%\ Sm^{3+}$	F-centre in V_O	Grey → yellow[50]
$Na_8(AlSiO_4)_6(Cl,S)_2$	F-centre in V_{Cl}	White → pink[2] White → purple[53] White → blue[53] White → turquoise[53]

Due to their simplicity and the sheer range of organic syntheses available, organic photochromic materials can truly be tuned to change to almost any possible colour under excitation by UV light. Rarely can the colour change be induced by lower energy radiation than UV, but this is also true of inorganic photochromes. However, due to nature of small organic molecules, their thermal and structural stability is not always on par with their inorganic counterparts, which are generally robust metal oxides, sulfides and halides.[52] The dramatic structural rearrangements some organic photochromic molecules undergo when switching forms may also lead to reduced performance over time.

Recent advancements in the study of inorganic photochromic materials mean it can no longer be said that their colour range is limited, and inorganic materials are generally superior in their robustness and stability. However, all the examples discussed in the text above contain one or more rare elements, which could limit their availability for any application in the future.[54] Unlike the other materials

presented in **Table 1**, synthetic photochromic sodalite has all the benefits of an inorganic photochromic material, without containing any "endangered elements".[54] Furthermore, it has great potential to be tuned, in terms of colour, colouration activation energy and bleaching rate, amongst other properties. The tunability of photochromic sodalite is discussed in section 2.4.

2.3   Mechanism of photochromism in sodalite

As discussed in section 2.1, the importance of sulfur in sodalite's photochromism has been known since 1954.[12] Since then, gradual advances in understanding the exact nature of the sulfur species involved, the significance of the ratio of sulfur and chlorine, and the presence of an F-centre inside the β-cage giving rise to the coloured form, have been revealed.[21,55] In 2016, Norrbo *et al.* conducted an extensive study into the mechanism of tenebrescence in photochromic sodalites, including studying the precise transitions, energy levels and energies involved.

The work of Goettlicher *et al.*, who studied the sulfur species present in natural hackmanite using X-ray absorption near-edge structure (XANES), provided the foundation for Norrbo's mechanistic study. XANES results revealed that in hackmanite, sulfur is present either as S^{2-} or S_2^{2-} pre-colouration, and after colouration converts to S^- or S_2^- respectively.[56] XPS measurements made by Norrbo *et al.* are in agreement with Goettlicher *et al.*'s XANES study.[6] After measuring the orange-red emission of synthetic photochromic sodalite excited with synchrotron radiation, and finding within the emission band of coloured sodalite a vibrational fine structure characteristic of S_2^-, Norrbo *et al.* concluded that S_2^{2-} was the species involved in the tenebrescence phenomenon. Upon establishing that the basis of the transition was an electron transfer from S_2^{2-} to a chloride vacancy (**Scheme 1**), they went on to use spectroscopic measurements to determine the energy gaps between the valence and conduction bands, and the ground and excited states of S_2^{2-} and the vacancy (**Figure 3**a).[34]

$$(S_2)_{Cl}{}' + V_{Cl}{}^{\bullet} \leftrightarrow (S_2)_{Cl}{}^{X} + V_{Cl}{}^{X}$$
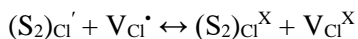
Scheme 1.[34]
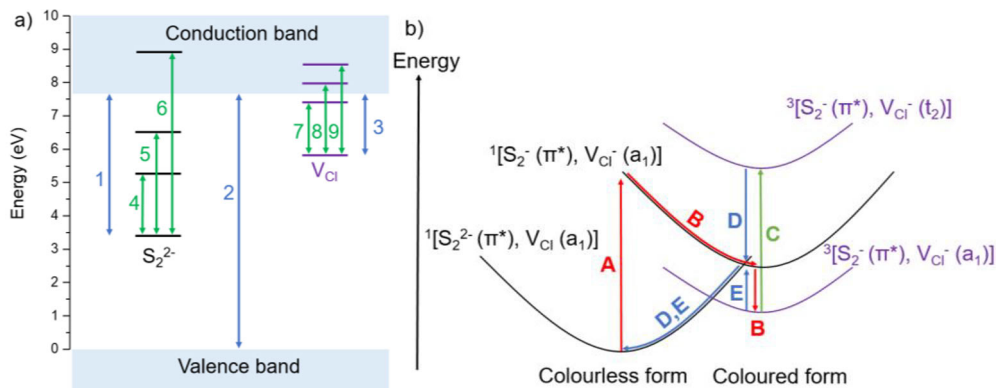
Figure 3.   a) Spectroscopically determined energy levels significant to the tenebrescence mechanism in photochromic sodalite. The energies of gaps 1-9 are given in **Table 2**.[34] b) Detailed mechanism of colouration and bleaching of photochromic sodalite, including involved molecular orbitals and spin states.[6,18]

Table 2.   Spectroscopically determined energies of the nine energy gaps in **Figure 3**a.[34]

Energy level gap	Energy (eV)
1	4.3
2	7.7
3	2.0
4	1.8
5	3.1
6	5.5
7	1.8
8	2.3
9	2.9

Figure 3b shows the mechanism in detail, including the orbitals and spin states involved. In **A**, an electron is excited by a photon of energy 4-5 eV from the π^* orbital of S_2^{2-} to the a_1 orbital of V_{Cl} (see **Figure 3**a, energy level gap **6**, also **Table 2**). After excitation the system heads towards an energy minimum, and spin relaxation occurs during **B** to a triplet state. The electron remains in the a_1 orbital of V_{Cl}, where it is able to absorb visible light of energy 1.8-2.9 eV (**Figure 3**a **7-9**), with the absorbance maximum at 2.5 eV or 500 nm (**C**). There are two pathways for the fading of the coloured form: optical bleaching (**D**) and thermal bleaching (**E**). The

optical bleaching pathway **D** first requires absorption of visible light (**C**), so the electron reaches the t_2 excited state of V_{Cl}. After that, through non-radiative relaxation it passes back to the π^* orbital of S_2^{2-}. During thermal bleaching, when activated by thermal energy of 0.5 eV or greater, the electron transfers from the a_1 orbital of V_{Cl} directly to the π^* orbital of S_2^{2-} (**E**). It can also be noted that in **Figure 3**a, excitation via **5**, followed by non-radiative relaxation and emission via **4**, correspond to excitation of the S_2^- species present in the coloured form by UVA radiation (3.1 eV, 400 nm), followed by orange-red 1.8 eV (680 nm) emission. These energies were determined spectroscopically, while the intricacies of the mechanism were confirmed using TD-DFT simulations.[18,57]

Most recently, the reason for the stability of the colour change was found. The unique structure of photochromic sodalite provides a stable cage structure in which the Na_4 tetrahedron can freely expand and contract around S_2^{2-} or V_{Cl}, stabilising these species in the coloured form.[18] This improves the stability of the F-centre, before the electron returns to its ground state after activation by visible light. It was during this work that Colinet *et al.* also carried out simulations for tugtupite and scapolite assuming the same mechanism as for hackmanite, and found that the simulated results again matched the experimental data well.[18] The assumption that the mechanism of tenebrescence was the same in all three minerals was made based on their compositional and structural similarities, despite scapolite crystallising in a tetragonal system (rather than cubic) and having a significantly different geometry around V_{Cl}. It is this difference in geometry that explains why scapolite's absorption spectrum is so different from that of hackmanite and tugtupite, and in this study Colinet highlighted the sensitivity of the F-centre's transitions to the surrounding cationic polyhedron.[18]

Finally, Vuori *et al.* have worked on understanding the mechanism of tenebrescence when photochromic sodalite is exposed to X-rays and γ-radiation. In 2021 Vuori *et al.* published a work discussing the X-ray detection abilities of photochromic sodalites, and discussed possible mechanisms based upon those already presented in the literature. The main mechanism is believed to be one in which the X-ray radiation creates a cascade of electrons in the conduction band and holes in the valence band. These charge carries move through their respective bands until the system relaxes, with the hole ending up in the π^* orbital of S_2^{2-} and the electron in V_{Cl}.[5] This means that upon exposure to X-rays, the whole material is capable of colouring, due to the penetrating nature of the radiation; upon exposure to UV, only the surface changes colour, as UV radiation cannot penetrate further than that. Finally in 2022 Vuori *et al.* discuss the effect of γ-radiation on the colouring of photochromic sodalites, and conclude the mechanism is the same as for X-rays, i.e., a cascade of electrons and holes is produced, rather than direct excitation from S_2^{2-} to V_{Cl}. They also observed that the extremely high energy γ-radiation is

capable of converting the Na_4V_{Cl} tetrahedra to Na_3V_{Cl}, which has a slightly different absorption profile. They coined this "γ-exposure memory", and is thus far unique only to photochromic sodalites.[58]

2.4   Synthetic sodalites as tuneable photochromes

In the 1960s and 70s, synthetic sodalites became a popular topic of research due to their photo- and cathodochromism, rendering them potential energy storage materials. In 1964, Radler and Chenot explored the effects of halogen substitution on photochromic sodalite's colour, finding that replacing chlorine with bromine or iodine altered the colour.[59] Following this, in 1969 Williams *et al.* studied the sulfur-to-chlorine ratio for the first time, and observed that too much sulfur "slows down the bleaching rate" and that excessive amounts "will produce a pigment", likely some kind of ultramarine.[21] Phillips went on to study the effect of halogen substitution on cathodochromic sodalites, and found that the position of the absorption band in the coloured form was related to the lattice parameter of the structure.[60] He likened this relationship to that of the F-centre formed in alkali metal chlorides when they are exposed to ionising radiation.[61] Another key observation made by Phillips was that iodosodalites did not colour under the electron beam as well as their chloro- and bromo- counterparts. He also noticed that iodosodalites faded most quickly of the three, which is in agreement with Williams's statement that Br and I speed up the rates of colouration and fading.[21] TD-DFT calculations also predict that iodosodalites bleach faster than their chloro- and bromosodalite counterparts, due to the trapped electron being less stable in an expanded structure.[62]

Further attempts to tune the structure continued throughout the 1970s and beyond as researchers tried to understand better these materials. Doorn and Schipper investigated different synthesis methods for chloro-, bromo- and iodosodalites, with a focus on studying their cathodochromic properties.[63,64] Todd began introducing germanium into the structure, replacing 1-54 mol% of silicon with germanium, and with emphasis on the luminescence of the materials.[65,66] Only larger quantities (25-54 mol%) of germanium appeared to affect the photochromism in any way, redshifting the F-centre's absorption maximum.[65] Todd also discussed the negative effects of increasing germanium content on the growth of good sodalite crystals, and other sources also discuss the collapse of the sodalite structure with incorporation of greater quantities of increasingly large ions.[65,67] This can be put down to a combination of tetrahedral tilting and change in the T-O-T bond angle (where T = a tetrahedrally coordinated ion such as Al^{3+}. Si^{4+}. Ga^{3+} or Ge^{4+}), as well as the large size of gallium and germanium consequently favouring 6-fold coordination.[68,69]

In 2010, Williams *et al.* decided to explore the effects of gallium and germanium on the photochromism of sodalite further. Until this point, the tuning of sodalite's

photochromism was of less interest to scientists - the focus had been much more on cathodochromism and its applications. However, Williams sought to study further the relationship between unit cell size and tenebrescence colour, and to do so they introduced sulfur and a reduction step to their group's previous work on gallosilicate and aluminogermanate chloro- and bromosodalites.[70] In this study, they were able to determine the relationship between vacancy size and absorption energy of the F-centre (**Equation 2**), and found it to be in relatively good agreement with the particle in a box model (**Equation 1**), though the unit cell size does not perfectly correlate to that of the vacancy.[53] In this way the F-centre in photochromic sodalite behaves similarly to that of the alkali metal halides (**Equation 3**).[61]

$$E_a = \frac{3\pi^2}{2a^2} = fa^{-2}$$

Equation 1. Solution to the particle in a box model for energy transfer of an electron in a cubic box from the ground state to its first excited state. E_a is the activation energy, and the size of the box corresponds to a.[53]

$$E_a = (39.4 \pm 2.5)d_{vac}^{-1.8}$$

Equation 2. Relationship between absorption maximum, E_a, and vacancy size, d_{vac}, in the coloured form of photochromic sodalite.[53]

$$E_a = (60.5 \pm 9.8)a^{-1.81 \pm 0.10}$$

Equation 3. Relationship between absorption maximum, E_a, of the F-centre formed in alkali halides and the alkali halide's unit cell parameter, a.[61]

Most recently, Norrbo *et al.* have sought to tune the tenebrescence of photochromic sodalite. As well as optimising the sulfur-to-chlorine ratio for both tenebrescence and luminescence,[2] they found that addition of lithium weakened the photochromic property.[71] In 2018, they studied the effect of sodium substitution with other alkali metals on the tenebrescence more closely, something which had not yet been studied so thoroughly by other researchers. They found through computational and experimental studies that substitution of sodium with lithium raised the energy at which colouration occurs, i.e., the gap between the energy levels of S_2^{2-} and V_{Cl} broadens; conversely substitution of potassium and rubidium lowers this energy gap.[6] Whilst substitution of sodium with larger ions was limited, due to their large sizes and slow mobilities during synthesis, their effect on the photochromism activation energy is still immediately obvious, with potassium lowering the threshold energy by 0.6 eV and rubidium by 0.8 eV. The larger ions also lower the thermal bleaching energy, meaning these materials not only colour with lower energy UV radiation, they also fade more quickly.[6]

During their study of the effect of heavy cations on the photochromism activation energy, Norrbo *et al.* briefly mention that the reflectance minimum (i.e., absorption maximum) of their potassium-substituted sodalite had shifted to a longer wavelength than that of the pure sodium sodalite.[6] However, they do not comment on this further. The cation's effect on the colour is yet to be properly studied, though in 2023, Colinet and Le Bahers presented simulated absorption spectra for the F-centre in sodalites where between 0-4 sodium ions surrounding V_{Cl} are replaced by potassium. They discussed that the simulations based on TD-DFT predict a broadening of the band, due to loss of degeneracy of the F-centre's energy levels, but no significant shift in absorption maximum.[72]

Table 3.   Summary of how the photochromism of photochromic sodalite ($Na_8(AlSiO_4)_6(Cl,S)_2$) has been tuned in the literature.

Element substituted	Substituted with	Observed effect
Cl	Br, I	Absorbance maximum of coloured form shifts to longer wavelengths[59,60,73] Unit cell expansion[53,60] Faster rates of colouration and fading[21,72]
Cl	S	Increasing S:Cl ratio slows bleaching rate and eventually the material is permanently coloured[21]
Si	Ge	Absorbance maximum of coloured form shifts to longer wavelengths[53,65] Unit cell expansion[53,65] Structure collapse in large quantities[65,67,69,70]
Al	Ga	Absorbance maximum of coloured form shifts to longer wavelengths[53] Unit cell expansion[53]
Na	Li	Weakened photochromic property[71] Raised colouration energy threshold[6]
Na	K, Rb	Lowered colouration energy threshold[6] Broadens absorption band[72]
S	Se, Te	Reversible photochromism similar to materials with sulphur[74]

Thus far substitution of all elements in the photochromic sodalite formula ($Na_8(AlSiO_4)_6(Cl,S)_2$) has been discussed, with the exception of oxygen and sulfur. Framework oxygen substitution would likely have detrimental effects on the structure and thus the properties, and no record of such a study on sodalites has been

found, though some research into nitrogen substitution in zeolite Y has determined that it may be possible.[75] Replacement of sulfur, however, is more feasible. Ballentyne and Bye showed in 1970 that substitution of sulfur with selenium or tellurium in sodalite produced a similar photochromic effect to sulfur when the material had been fired in hydrogen and subsequently exposed to UV radiation.[74] Their seleno- and tellurosodalites' photochromism was reversible, and the F-centre's absorption maximum was in the same place as that of their sulfur-containing sodalite material. Following this, most of the studies on selenosodalites focused on the production of red ultramarine pigments,[69,76–78] and studies of their luminescence,[78,79] though recent TD-DFT simulations predict that Se_2^{2-} and Te_2^{2-} activators would significantly lower the activation energy of F-centre formation and thus the colour change.[62,72]

Extensive studies into the tuning of photochromic sodalites have been carried out in the last sixty years (**Table 3**). However, until the mid-2010s these have mostly been studies for the sake of understanding the nature and versatility of the sodalite cage. Aside from as an energy storage material, applications of photochromic sodalites have only recently begun to be seriously researched. These will be discussed more thoroughly in section 2.6.

2.5   Other properties of photochromic sodalites

As discussed in section 2.1, natural sodalites, hackmanites and other members of the sodalite family fluoresce orange under long-wave UV excitation, as a result of S_2^- impurities in the structure (**Figure 4**a).[11] In their studies of photochromic sodalites doped with selenium and tellurium, Ballentyne and Bye did not comment on any luminescence. In 1999 Reinen and Lindner did measure the corresponding emission from Se_2^- and Te_2^- in sodalite, specifically in ultramarines, with the emission wavelength increasing from sulfur to selenium to tellurium, and the intensity also weakening.[78]

However, while rare in natural hackmanites, both natural and synthetic materials have been known to display blue-white photoluminescence (PL, **Figure 4**b). Kirk already observed this in 1955, but did not comment on it further.[80] The white PL of synthetic photochromic sodalite (**Figure 4**c) was studied Van Doorn and Schipper, who concluded the presence of manganese and O_2^- were responsible.[81] A year later, Deb and Gallivan noticed a similar blue-green emission in oxygen-doped synthetic sodalites, complete with vibrational fine structure of the O-O bond.[82] Gaft studied the blue-white emission of natural hackmanite in 2009,[83] but it was not until 2016 when a detailed explanation of this phenomenon was published.
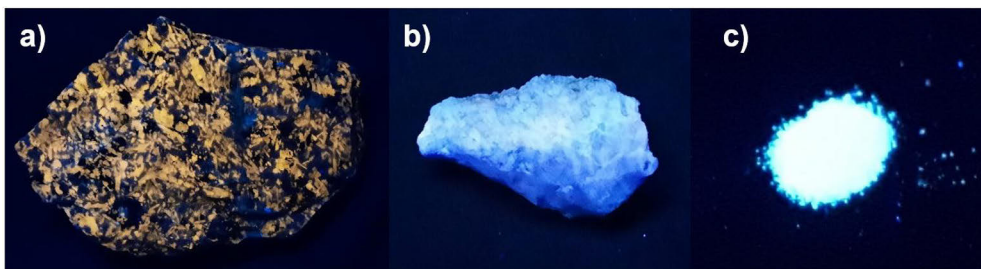
Figure 4.   a) Orange luminescence of natural hackmanite under 365 nm excitation. b) White luminescence of natural hackmanite under 302 nm excitation. c) White luminescence of synthetic photochromic sodalite powder under 254 nm excitation.

Natural hackmanite is capable of displaying yet another optical property – that of persistent luminescence (PeL, afterglow). In a similar way to tenebrescent materials, persistent luminescent materials are capable of storing energy, in the form of trapped electrons, for a period of time before thermal stimulation releases the electrons, which in turn emit light as they return to a lower energy state. Natural hackmanite was said to emit "a prolonged after-glow of white light" by Warner in 2011,[84] and the intricacies of natural hackmanite's PeL were studied in depth by Agamah *et al.* in 2020.[11] Prior to this, when investigating synthetic photochromic sodalites, Norrbo *et al.* noticed that depending on the sulfur-to-chlorine ratio in the materials, they presented a blue-white afterglow after excitation with 365 nm UV detectable up to 1 h after irradiation ceased.[2] Norrbo then began to investigate the mechanism of the PeL properly, and in doing so discovered that PeL arises from the interaction of a Ti^{3+} ion located in an Al^{3+} or Si^{4+} tetrahedral site, and an oxygen vacancy. The energy level gaps involved in the mechanism were determined using spectroscopy (**Figure 5**a **1-3**, **Table 4**) and thermoluminescence (TL) measurements (**Figure 5**a **4-6**, **Table 4**). The mechanism can be summarised as follows: upon UV excitation of ≥ 3.3 eV, electrons transfer from Ti^{3+} to V_O, the orbitals of which overlap with the conduction band (**Figure 5**b, **A**). A non-radiative relaxation transfers the electron either to V_O, which acts as a trap, or to Ti^{3+} located in a sodium site (**Figure 5**b, **D**). Thermal energy of 0.6-1.1 eV is capable of releasing the electron from the trap (**E**), where it returns to the $[Ti^{4+}\text{-}V_O^-]$ excited state, undergoes non-radiative relaxation (**B**) and eventually returns to the ground state, emitting a photon of ~480 nm light upon doing so (**C**). The PL mechanism is much the same, however after excitation (**A**), there is immediate non-radiative relaxation (**B**) and emission (**C**), i.e., the electron does not temporarily reside in any traps. Norrbo also commented that the emission of O_2^- likely still contributes to the PL spectrum of photochromic sodalite, however the $Ti^{3+}\text{-}V_O$ interaction is the dominant source of emission.[34]
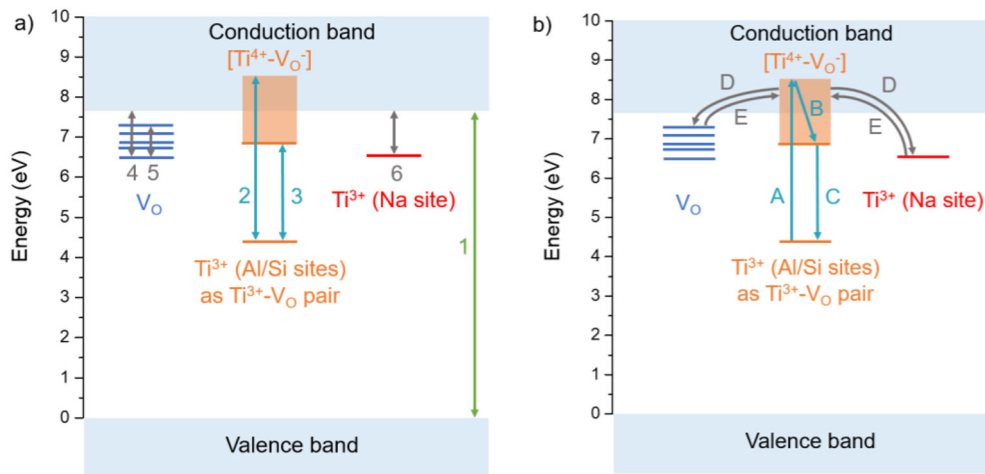
Figure 5.   a) Energy levels significant in the mechanisms of PL and PeL in photochromic sodalite. The energy levels determined spectroscopically and using thermoluminescence measurements are given in **Table 4**.[34] b) Dominant mechanism for PL (A, B, C only) and PeL (A, B, C, D, E) in photochromic sodalite.[34]

Table 4.   Energies of the six energy gaps in **Figure 5**a as determined by spectroscopy and thermoluminescence measurements.[34]

Energy level gap	Energy (eV)
1	7.7
2	≥ 3.3
3	≈ 2.5
4	1.1
5	0.6
6	1.1

After uncovering the mechanism behind synthetic photochromic sodalite's PeL, Norrbo went on to improve this property through doping with titanium and partial substitution of sodium with lithium. At the cost of the photochromism, this dramatically increased the lifetime of the PeL from one to seven hours, already outlasting commercial red phosphor $Y_2O_2S:Eu^{3+},Mg^{2+},Ti^{4+}$.[71] This long-lived white afterglow, combined with the advantage of sodalite not containing rare earth or heavy elements, led Norrbo *et al.* to begin developing these materials for commercial applications. In 2017 they attempted to add yet another property to the mix – that of up-conversion, by introducing a Yb^{3+}-Er^{3+} sensitizer-activator pair capable of

converting 970 nm IR radiation to green and red luminescence, which was moderately successful.[85]

2.6 Applications of photochromic materials

Several possible applications of photochromic sodalites are discussed in this thesis, including its use in blue light detection, passive dosimetry and X-ray imaging. This section discusses the background of these applications, as well as other applications for which photochromic sodalite has been considered in recent years.

2.6.1 Blue light detection

The human body has evolved to respond to the natural cycle of day and night, giving rise to the circadian rhythm. As the sun rises in the morning, light levels increase and levels of melatonin in the body drop. Melatonin production is best suppressed by blue light of around 460 nm,[86] which incidentally is very similar to the emission peak of blue LEDs used in lighting systems, computer and television screens, and many other areas of everyday life.[87] Blue light therapy has been proven to help regulate the circadian rhythm and help those suffering from sleep disorders and seasonal depression.[88–90] However, with the rise of technology, humans are exposed to far more blue light than their bodies have evolved to cope with, and too much melatonin suppression can lead to problems falling asleep at night, and in turn dry eyes and irritation.[91] Excessive exposure to blue light can cause cataract formation and potential retinal damage, particularly if exposure happens at night, when there are no natural sources of blue light present.[91–94] Thus, practising good sleep hygiene measures such as reducing and monitoring exposure to blue light, particularly in the evenings and before sleeping, is important to improve sleep quality and minimise the risk of eye damage.

It is known that the colour of photochromic sodalite induced by UV excitation fades under visible light.[18] Optimal optical bleaching occurs under light of a wavelength close to that of the F-centre's absorption maximum (~520 nm in pristine sodalite), though blue light in the range 420-490 nm can also bleach the colour, provided the blue light is not of high enough energy to form any F-centres.[34] As the degree of bleaching depends on the exposure time and thus dose of visible light,[18] photochromic sodalite could theoretically be used in detection and dosimetry of blue light. Photochromic sodalite could serve as a low-cost dosimeter for use at home or in the office, particularly if it were to be optimised to improve sensitivity to blue light over other wavelengths of visible light.

2.6.2   Passive dosimetry

When working with ionising radiation, whether in a scientific or other professional context, it is important to be able to quantify the dose of radiation a sample, test subject or worker is exposed to. Ionising radiation refers to any radiation capable of removing electrons from atoms, and includes high frequency UV, X-ray and γ-radiation, as well as subatomic particles such as α-, β- and neutron radiation. Radiation dose is usually measured in grays (Gy, J kg^{-1}), i.e. the amount of energy absorbed by unit mass,[95] but for the less penetrating UV radiation it can be given in J m^{-2}, though this is technically a unit of fluence (radiant energy per unit area). Radiation dose in grays is then multiplied by a weighting factor to obtain the equivalent dose in sieverts (Sv), which is an indication of the likely biological damaged induced by the radiation. The exact value of the weighting factor depends on the type of radiation in question.[95]

There are two ways to measure the dose of radiation a person or subject is exposed to: actively or passively. Active dosimetry involves the use of a dosimeter, an electronic device which contains a detector material sensitive to radiation. When the detector is exposed to radiation, it gives an electrical signal which the device then converts to a meaningful dose reading.[96] Typical dosimeters contain metal-oxide-semiconductors like hafnium oxide.[97] Before the days of portable electronics, those working frequently with radiation carried around photographic film, which darkened on exposure to radiation, as Röntgen observed when he imaged his wife's hand with X-rays in 1896.[98,99] This is a form of passive dosimetry: a radiation-sensitive material is exposed to radiation for some time, and only after the material is removed and studied can the dose be quantified. Radiation films are single-use, but modern devices make use of thermoluminescent materials, or those displaying optically stimulated luminescence (OSL), which can be reused.[100] These methods require an external reader, which then gives information on the received dose.

Photochromic materials can also function as reusable passive radiation dosimeters, provided the intensity of the colour change can be quantified easily, and behaves as some clear function of radiation dose. In 2018, Norrbo *et al.* demonstrated how photochromic sodalite responds to UV dose and proposed its application in UV indexing. They particularly emphasised how potassium-substituted sodalite's colouration threshold matched the erythemal action spectrum of human skin. The colour intensity can be read using a smartphone camera and after calibration, a simple application on said smartphone can indicate the UV index and dose the sample was exposed to.[6]

Following this, Vuori *et al.* also demonstrated that photochromic sodalite's colour deepens in a systematic fashion on exposure to X-rays and γ-rays.[5,58] They went on to demonstrate applications of this property: photochromic sodalite can be used to make dose distribution maps for products exposed to γ-radiation: for example, food

products sterilised with γ-radiation. The colour of the sodalite placed below the product being sterilised would directly indicate when sufficient exposure has been completed, without the need for special detection equipment. They emphasise the cost-effectiveness of this method, not only because the sodalite film is re-useable and the dose can be read with a simple smartphone, but also because of its high durability and the lack of toxic and expensive elements in the composition.[58] Further comparisons to existing radiochromic films emphasise sodalite's robustness in high temperature conditions, water resistance and ability to quantify significantly higher doses than other available films.

2.6.3   X-ray imaging

In a similar fashion, a dose map can be created using photochromic sodalite films when the radiation source is X-radiation. In this case, an X-ray image is produced (**Figure 6**). In his 2021 publication, Vuori discusses how the doses required to produce X-ray images with sodalite are high (approx. 105 mSv), certainly too high for medical use at this stage, but would potentially suitable for quality control tests such as imaging of welds or mechanical parts.[5] Unlike other modern computed radiography (CR) X-ray imaging systems, the image does not require any external equipment to read it. The film is also not immediately light-sensitive, reducing waste from disposable cassette coatings and removing the need for a dark room, though the image will fade upon prolonged exposure to light. The films are non-toxic and completely re-useable.[58] Thus, this material may find a future in X-ray imaging, for example in developing countries where expensive CR or even more costly direct radiography (DR) systems are not accessible.[1] However, some development is needed to improve the sensitivity of photochromic sodalite, particularly when it colours optimally only under very soft X-rays with an energy range of 2-4 keV. Industrial imaging, for example in quality control and non-destructive testing, uses much harder X-rays of 20-150 keV and beyond.[101–103]
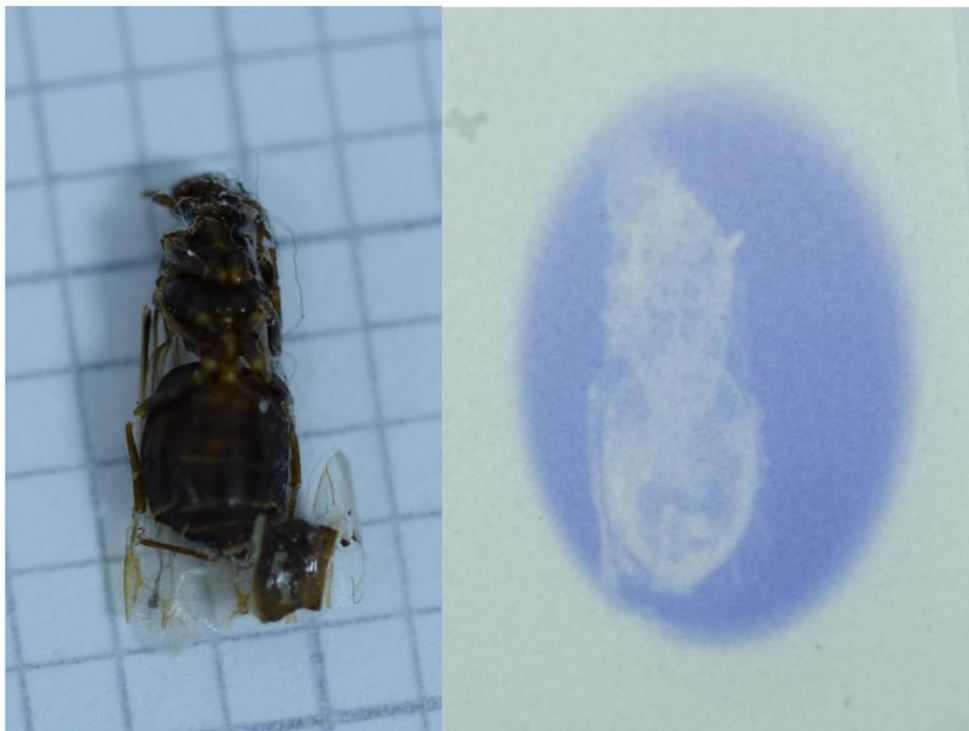
Figure 6.   A dead flying ant (left) used as the subject of an X-ray image (right) taken using photochromic sodalite film following exposure to 107 mSv of 22 keV X-rays. Each square is 1 mm × 1 mm in size.

2.6.4   Other applications

Photochromic sodalites displaying luminescent properties have been proposed several times for optical multiplexing applications. More specifically, these materials are able to give different responses based upon which wavelengths of radiation they are exposed to.[2,85] Such materials are often found as security markers and invisible tags, and in fact many of the photochromic materials discussed in section 2.2 also display luminescence, meaning they are also suitable for such applications.[35,47,104] Sodalite is, however, once again unique in that all its optical properties can be produced without the need for rare elements.[54]

Still more applications for photochromic sodalites have been proposed in recent years, usually based upon their luminescent and persistent luminescent properties, such as in medical and bioimaging.[34] Norrbo *et al.* discuss how the long-lasting afterglow allows sodalite to be excited ex situ, removing the need to expose the patient to UV radiation. They also discuss sodalite's high stability in water, making it even more suitable for biological applications.[71] Titanium-doped white luminescent sodalite is a low-cost and attractive alternative to other white

luminescent phosphors for lighting applications, particularly in safety lighting, since its emission spectrum overlaps closely with the scotopic response of the eye.[71]

One final and extremely unique application of sodalite's photochromism was proposed by Vuori *et al.* in 2022. He studied how photochromic sodalites respond to α-, β- and γ-radiation, and found that the absorption spectrum of photochromic sodalite coloured by γ-radiation differed from that of photochromic sodalite only exposed to UV. Upon further investigation, this change turned out to be permanent, with the high-energy γ-radiation generating some Na_3V_{Cl} species in place of the usual Na_4V_{Cl} present in photochromic sodalite.[58] This led to him proposing that photochromic sodalites can be used in places where it is of interest to know if a γ-exposure has occurred, for example in nuclear facilities, outer space and defence infrastructure.[58]

3   Aims of the Experimental Work

The aim of this study was to tune the photochromism of synthetic photochromic sodalites to produce materials that change from white to any other colour. In doing this, a variety of compositions were tested, as were several synthesis methods, in order to expand upon the range of tenebrescence colours available before this work. The study also sought to alter the colouration threshold of photochromic sodalite in a simple and reliable way. Other properties of these sodalites were also studied, such as their PL and PeL. Finally, some applications were proposed for the materials, based on the precise combination of optical properties present in each composition.

The more specific aims of each publication were:

I.   To produce photochromic sodalites which also displayed photo- and persistent luminescence from starting materials other than zeolite A using a solid-state synthesis method. To optimise the synthesis parameters so that all three optical properties were present.

II.   To provide a thorough characterisation of photochromic sodalites displaying a new white-to-yellow colour change, which occurs when sodium is partially substituted by calcium. Both experimental and computational studies were done to fully understand the phenomenon, including determining the precise Na:Ca ratios required for yellow photochromism, the mechanism involved, and the impact of other halides than chloride on the colour. These materials were then proposed as blue light detectors due to their sensitivity to fading under blue light.

III.   To demonstrate further methods of tuning the colour and activation threshold of photochromic sodalite, including pushing the limits of the range of possible absorbance maxima with potassium, iodine and germanium, lowering the activation energy with selenium, and mixing multiple sodalites together to combine their optical properties. Tuned sodalites were also used to significantly improve photochromic sodalite's function as a material for re-useable X-ray imaging plates.

4 Materials and Methods

4.1 Synthetic Procedures

4.1.1 Solid-state synthesis from zeolite

The majority of samples were prepared from zeolite 4A (Sigma Aldrich) using a solid-state method (**II, III**). 0.7 g dried zeolite was ground together by hand with in total 0.0040 mol of salts (**Table 5**) and 0.06 g Na_2SO_4 (E. Merck, 99 %). One or more salts were used in varying ratios, but the total number of moles of salt with respect to the metal were always the same. These masses and ratios were taken from the works of Norrbo *et al.* and Williams *et al.*[53,71]

The mixture was transferred to an alumina boat and heated in air in a tube furnace to 850 °C at a rate of 3 °C/min for 5 h. Once the furnace had cooled, the mixture was ground again, placed in the same boat, and returned to a tube furnace, where it was heated again in a reducing atmosphere of 12 % H_2/88 % N_2 at 850 °C for 2 h, heating rate 19 °C/min. After the furnace was cool, the sample was removed, in some cases washed with distilled water to remove soluble impurities, and characterised. The effect of washing on the optical properties was minimal, and thus was generally only done to improve reliability in XRF analyses.

In some syntheses, zeolite 3A (Zeochem) was used instead of zeolite 4A (**II**). The mass of zeolite and other parameters were the same in both cases. In **III**, some or all Na_2SO_4 was replaced with Na_2SeO_3 (Sigma Aldrich, 99 %) The masses used are given in **Table 6**. Due to the toxicity and low decomposition temperature of Na_2SeO_3, these samples were prepared inside a quartz reactor with the furnace inside a fume hood at all times.

Table 5.   Salts used in solid-state syntheses of photochromic sodalites, their masses corresponding to 0.0040 mol, and manufacturer information.

Salt	Mass (g)	Manufacturer	Purity (%)
LiF	0.104	Aldrich-Chemie	-
LiCl	0.170	Acros	99
LiBr	0.349	Sigma Aldrich	99
LiI	0.538	Fluka Chemie	> 98
NaF	0.169	Merck	-
NaCl	0.240	Sigma Aldrich	99.5
NaBr	0.414	J. T. Baker	-
NaI	0.603	E. Merck	-
KF	0.234	Riedel de Haën	99
KCl	0.300	Merck	99.5
KBr	0.479	Merck	-
KI	0.668	Ega-Chemie	> 99
RbF	0.420	Alfa Aesar	99.1
RbCl	0.468	Merck	-
RbBr	0.665	Alfa Aesar	99.8
RbI	0.854	Sigma Aldrich	99.9
CsF	0.611	Sigma Aldrich	99
CsCl	0.677	Serva	-
CsBr	0.856	Merck	-
CsI	1.045	Sigma Aldrich	99.9
$CaCl_2 \cdot 6H_2O$	0.881	Riedel de Haën	99
$CaBr_2$	0.804	British Drug Houses	-
CaI_2	1.182	Alfa Aesar	99.5

Table 6.   Masses of Na_2SO_4 and Na_2SeO_3 used in solid-state syntheses of selenium sodalites.

mol% S replaced with Se	Mass Na_2SO_4 (g)	Mass Na_2SeO_3 (g)
0	0.060	0.000
25	0.045	0.018
33	0.040	0.024
50	0.030	0.037
100	0.000	0.073

4.1.2   Zeolite-free synthesis methods

Zeolite-free syntheses were done using three different methods: solid-state synthesis (**I**), synthesis from a silicate glass precursor, and hydrothermal synthesis (**III**).

4.1.2.1   Solid-state method

Samples were prepared using a solid-state reaction based on that of Medved[105] by mixing the following dried reagents: 0.251 g Al_2O_3 (Merck, Aluminium oxide 90 standardised), 0.296 g SiO_2 (Sigma, 99.8 %), 0.240 g NaCl (Sigma Aldrich, 99.5 %), 0.060 g Na_2SO_4 (E. Merck, 99 %) and 0.261 g Na_2CO_3 (E. Merck, 99.5 %) or 0.197 g NaOH (Merck, 99 %) and grinding together by hand. H_3BO_3 (E. Merck, 99.8 %) was added as a flux (10 % by mass) to some samples. 0.300 g KCl (Merck, 99.5 %) was also used instead of NaCl in one sample. The mixtures were heated in air at 800-1060 °C for 48–72 h, then allowed to cool freely. Once cool, the mixtures were ground again and subsequently heated at 850 °C under a flowing 12 % H_2/88 % N_2 atmosphere for 2 h and allowed to cool. Samples were washed with distilled water to remove soluble impurities such as NaCl, and thoroughly dried.

4.1.2.2   Silicate glass method

This method was adapted from Armstrong and Weller's 2006 work on synthetic tugtupites.[106] Stoichiometric amounts of dry Na_2CO_3 and K_2CO_3 (Merck, 99 %) corresponding to Na:K ratios of 0-100 % were ground together with a stoichiometric amount of SiO_2. The mixtures were heated at 975 °C in alumina crucibles in air for 48 h and allowed to cool to yield sodium-potassium silicate glasses of differing compositions. Each glass was ground and mixed with stoichiometric amounts of dry Al_2O_3, NaCl and Na_2SO_4 and heated in a tube furnace at 800 °C in an alumina boat

in air for 48 h. After cooling, the samples were ground and heated at 850 °C for 2 h in a reducing atmosphere (12 % H_2/88 % N_2). Once cooled the samples were washed with distilled water and dried at 500 °C for 1 h.

4.1.2.3   Hydrothermal method

Samples were prepared by mixing 0.400 g $NaAlO_2$ (Sigma Aldrich), 0.300 g SiO_2 (Sigma, 99.8 %), 0.060 g Na_2SO_4 (E. Merck, 99 %) and in total 0.0040 mol of salts (**Table 5**) in an adaptation of the methods of Williams *et al*.[53] The powders were ground together by hand and then dissolved in a few ml of distilled water and transferred to a 23 ml Teflon cup that fitted in a small autoclave. The autoclave was sealed and placed into an incubator at 180 °C for 48 h. After this stage, the resulting paste-like solution was transferred to an evaporating dish and placed in a drying oven (Termaks TS 8056) at 100 °C for 1-2 h to evaporate the remaining water. The resulting powder was collected, ground and transferred to an alumina boat. Some samples were subsequently sintered in air at 850 °C for 5 h, and all samples were reduced in the same was as described in 4.1.1.

In some cases, stoichiometric amounts of $NaGaO_2$ and Na_2GeO_3 were used to substitute for some or all $NaAlO_2$ or SiO_2. These starting materials were prepared by grinding stoichiometric amounts of Na_2CO_3 and Ga_2O_3 (Sigma Aldrich, 99.99 %) or GeO_2 (Sigma Aldrich, 99.99 %) respectively and heating them in air at 800 °C for 48 h. The products were analysed by PXRD and found to be pure.

4.1.3   Ion exchange of synthetic sodalites

Some materials in **III** were subjected to potassium ion exchange using a nitrate melt method as described by Johnson *et al*.[69] Sodalites of varying composition, prepared by solid-state and hydrothermal syntheses, were ground by hand with potassium nitrate (Alfa Aesar, 99 %) in a 1:4 ratio by mass of sodalite to KNO_3. The mixture was transferred to an aluminium boat and heated in a tube furnace at 370 °C for 16 h. Once the product had cooled, it was washed with distilled water, centrifuged for 30 s and the liquid poured away. This was repeated four times.

Likewise, lithium ion exchange was also tested. This was also done using a nitrate melt method described by Johnson and Weller.[68] Chlorosodalite prepared from zeolite A was ground by hand with lithium nitrate (J. T. Baker, > 97 %) in a 1:4 ratio by mass of sodalite to $LiNO_3$. The mixture was transferred to an aluminium boat and heated in a tube furnace at 240 °C for 3 h. Once the product had cooled, it was washed with distilled water, centrifuged for 30 s and the liquid poured away. This was repeated four times.

4.1.4　Preparation of sodalite mixes

Different sodalites were mixed together in **III** to combine their optical properties, for example to produce new tenebrescence colours or mixes whose colour change depended on the irradiation wavelength.

4.1.4.1　Mixes showing new tenebrescence colours

Two or more sodalites were selected based on their observed tenebrescence colours, including the intensity of the absorption band. Samples with similar absorption intensities but at different wavelengths were selected and mixed together in equal proportions with a pestle and mortar. The resulting mixture was irradiated for 1 minute with 254 nm radiation to check the resulting colour. More of a particular component was then added, if necessary, to adjust the colour to that which was desired.

4.1.4.2　Mixes whose colour depends on excitation wavelength

Two sodalites were chosen based upon their measured tenebrescence excitation spectra such that one was excited by UVA and the other by only UVB or UVC. The two materials also had to have significantly different absorption maxima in their coloured forms so that the two colours were distinguishable to both a spectrometer and the human eye. Once chosen, the two sodalites were mixed together in equal proportions with a pestle and mortar.

4.1.5　Tape casting

In **III**, some sodalites were mixed with an organic polymer matrix and cast into thin, flexible films. The tape casting method is based on that of Abhinay *et al.*,[107] modified to account for the equipment available.[108] Sodalite (40 m-%), 2-butanone (30 m-%), ethanol (15 m-%) and Triton X-100 (2 m-%) were first mixed together in a Philips Minimill PW4018/00 ball mill at speed 1 for 10 min, after which polyvinyl butyral (7 m-%) and benzyl butyl phthalate (6 m-%) were added to the mixture, which was mixed in the same mill for 2 min at speed 5. The subsequent suspension was cast as a 350 μm coating using an Erichsen Coatmaster 510 with doctor blade onto a 0.1 mm thick Folex® Premium Universal Copy Film X-100 A4 (art no. 39100.100.44000) polyethylene film.

4.2 Analysis Methods

4.2.1 Structural and compositional analyses

4.2.1.1 Powder X-ray diffraction (PXRD)

PXRD analyses were done using three different methods, due to the acquisition of a new PXRD instrument partway through the doctoral studies. Different devices were used in data acquisition for different publications, but in all publications the instrument used to obtain diffraction data is stated clearly. Data collected for **I** and **III** were measured with a Huber G670 detector and copper $K_{\alpha 1}$ radiation (λ = 1.54060 Å). Exposure time was 30 min, with 10 readings of the imaging plate. Data for **II** suitable for quantitative phase analysis and unit cell refinement and data for **III** were collected as follows: PXRD was performed using a PANalytical Aeris benchtop instrument, with copper $K_{\alpha 1,2}$ radiation (λ = 1.5406 Å ($K_{\alpha 1}$) and 1.5444 Å ($K_{\alpha 2}$)) with a step size of 2θ = 0.011 ° and a measurement time of 29 min 45 s across the range 8-85 °. Some samples were measured multiple times and their diffractograms added to produce a good enough signal-to-noise ratio for quantitative phase analysis and unit cell refinement. Other routine measurements were performed using the Huber G670 and parameters mentioned previously, or the PANalytical Aeris using a step size of 0.022 ° and a measurement time of 6 min 11 s across the range 5-85 °.

4.2.1.2 Unit cell refinement and quantitative phase analysis

Unit cell refinements and quantitative phase analyses (**II**, **III**) were performed using the Rietveld analysis function in PANalytical HighScore Plus software v. 4.9.0.27512 connected to the ICDD PDF4+ 2021 database v. 4.21.0.2. The background was determined with a bending factor of 2 and a granularity of 20. The peaks were then searched with a minimum significance of 2.00, a minimum tip width of 0.01, a maximum tip width of 1.00, a peak base width of 2.00, using as a method Minimum 2nd derivative. The peaks were fitted with HighScore's default profile fit function using the available background as the background function and using a separate shape function and split width and shape methods due to peak asymmetry. The search and match pattern list was drawn from the PDF4+ database, with appropriate reference patterns being chosen manually from those found by the algorithm. The peaks were fitted with HighScore's default Rietveld function. The refinement was then further improved by manually releasing and refining other parameters such as profile variables Caglioti U, V and W Left and Peak Shape 1, 2 and 3 Left to optimise the fit.

4.2.1.3   Crystallite size determination with the Scherrer method

Crystallite sizes were estimated by analysing the most intense reflection (around 2θ = 24.3 °) using the Scherrer formula $D = K\lambda/\beta \cos \theta$ (**I**).[109,110] In this formula, D = mean crystallite size, K = Scherrer constant, usually 0.89, λ = X-ray wavelength, β = full width at half maximum (FWHM) in radians and θ = half of 2θ. This formula assumes that broadening of the peak is due only to domain size, that domains are spherical and that there is no size distribution. This is largely true for very small domains (1-30 nm), however for larger crystallites the instrumental contribution to the signal width becomes significant, and thus it must be corrected for using the following equation: $\beta^2 = \beta_{sample}^2 - \beta_{ref}^2$.[110] In this work, microcrystalline silicon was used for the corrections, with its FWHM being 0.140 ° for the setup used here. Note that this formula generally only holds for values of $D < 100$ nm, though the exact limit depends on the degree of instrumental broadening.

4.2.1.4   X-ray fluorescence (XRF)

Sample compositions were investigated with X-ray fluorescence spectroscopy (**I-III**) (XRF) using a PANalytical Epsilon 1 device with internal Omnian calibration and a 50 kV Ag-anode X-ray tube. Results were compiled from the device's own deconvolution of four scans using a silver filter, a copper filter, an aluminium filter and no filter, respectively.

4.2.1.5   Thermogravimetric analysis (TGA)

Loss of chloride was investigated using thermogravimetric analysis with a TA Instruments SDT Q600 (**I**). Approximately 10 mg of reaction mixture was heated from 20 °C to 1300 °C at a rate of 10 °C/min in air, flow rate 100 mL/min.

4.2.1.6   Raman spectroscopy

Raman spectroscopy (**III**) was performed using a Renishaw inVia Raman microscope equipped with a 532 nm laser as an excitation source, a Leica microscope at 20× magnification, a CCD detector, and a 1800 l/mm grating. The device was calibrated with silicon before use. The beam power, measurement time and number of acquisitions per sample depended on the strength of sample interaction with the laser and thus intensities were not comparable. The baseline was corrected using WiRE 5 software. Only normalised curves are presented.

4.2.2   Characterisation of photochromism

4.2.2.1   Reflectance spectroscopy

Reflectance spectroscopy (**I-III**) was the main method for characterising the colour change of photochromic sodalites. There was some variation in the method between publications, due to different spectrometer availability, but all measurements presented in a particular publication were done using the same method.

In **I**, reflectance was measured as follows: the change of colour of the materials after UV irradiation was investigated using reflectance measurements under illumination of a 60 W incandescent lamp, with incident irradiance kept constant in all measurements. The reflectance of the sample before excitation was measured using Al_2O_3 as the white reference. Samples were excited with 254 nm radiation from a UVP model UVLS-24 EL, 4 W 254/365 nm handheld lamp for 5 min (irradiance approx. 1.1 mW cm^{-2}) and their reflectance measured again 20 s after irradiation ceased to show the change in reflectance. Spectra were collected using an Avantes FC-IR600–1-ME-HTX optical fibre connected to an Avantes AvaSpec-2084 × 14 CCD spectrometer with a data collection time of 1.6 s (160 ms integration time, 10 averages). The difference of the two reflectance curves was calculated to show the colour change.

In **II** and **III**, the measurements were performed as follows: the change of colour of the materials after UV irradiation was investigated using reflectance measurements under illumination of a 40 W incandescent lamp, with an incident irradiance of 1.34 W m^{-2} in all measurements. The reflectance of the sample before excitation was measured and then used as the white reference colour. Samples were excited with 254 nm radiation from a UVP model UVLS-24 EL, 4 W 254/365 nm handheld lamp (UVC irradiance approx. 3.0 mW cm^{-2}) and their reflectance measured again 5 s after the lamp was switched off to show the change in reflectance. Spectra were collected using an Avantes FC-IR600-1-ME-HTX optical fibre connected to an Avantes HS-TEC CCD spectrometer with a data collection time of 1.6 s (160 ms integration time, 10 averages). Where the body colour of the material before irradiation required characterisation, MgO was instead used as a white reference.

4.2.2.2   Colour quantification as *L*a*b** coordinates

The materials' colours were quantified as *L*a*b** coordinates (**II-III**) after 5 min irradiation with 254 nm from the aforementioned 4 W handheld lamp using a Konica Minolta CM-2300d handheld spectrometer with its own white calibration disc and internal light source (D65 standard illuminant).

4.2.2.3   Thermotenebrescence i.e., thermal bleaching of tenebrescence

Thermotenebrescence[6,18] (**II**-**III**) was measured using the same optical fibre and HS-TEC spectrometer as in 4.2.2.1, with a data collection time of 1 s (50 ms integration time, 20 averages). The sample's reflectance was measured before irradiation and used as the background. Similarly to before, the sample's reflectance was measured before irradiation and set as the white reference, then measured again after 2 min of excitation using a 254 nm handheld lamp as mentioned before (UVC irradiance approx. 2.2 mW cm^{-2}). After coloration, the sample was heated from 20 to 250 °C at a rate of 3 °C/s using a MikroLab Thermoluminescent Materials Laboratory Reader RA'04. Using the data collection time of 1 s, a reflectance spectrum was acquired every second during the heating. The reflectance signal was corrected to account for the effects of heating on an uncoloured sample and spontaneous fading under white light, and then the curves were integrated to calculate the colour intensity at each temperature. Colour intensity with respect to temperature was plotted to obtain the thermotenebrescence curve. Thermotenebrescence data was handled in a similar way to thermoluminescence data to calculate the activation energy of thermal bleaching. The curves were analysed and the activation energies calculated using the initial rise method.[111]

4.2.2.4   Tenebrescence excitation spectra

Tenebrescence excitation spectra were measured either cumulatively (**II**) or absolutely (**III**).

Cumulative tenebrescence excitation spectra (**II**) were measured by irradiating the sample with 340-220 nm radiation produced by a SB522 150 W Xe-arc lamp coupled to a LOT MSH 300 monochromator, for 7.5 minutes per wavelength. 10 nm intervals were used between irradiation wavelengths. The sample was not changed between measurements. The reflectance of the sample was measured using the same HS-TEC spectrometer and optical fibre as previously mentioned in 4.2.2.1 under the illumination of a LS-1-CAL OceanOptics incandescent torch. The data collection time was 1.6 s (160 ms integration time, 10 averages). Reflectance was measured before irradiation and set as the white reference; after irradiation reflectance was measured again. The reflectance wells were integrated to give the colour intensity.

Absolute tenebrescence excitation spectra (**III**) were measured by irradiating the sample for 5 minutes with the following radiation wavelengths produced by the aforementioned monochromator: 220, 240, 260, 280, 300, 325, 350, 375 and 400 nm. Fresh sample was used for each excitation wavelength. The reflectance of the sample was measured using the same HS-TEC spectrometer and optical fibre as previously mentioned in 4.2.2.1 under the illumination of a LS-1-CAL OceanOptics incandescent torch. The data collection time was 1.6 s (160 ms integration time, 10

averages). Reflectance was measured before irradiation and set as the white reference; after irradiation reflectance was measured again. The reflectance wells were integrated to give the colour intensity.

4.2.2.5 Optical bleaching of tenebrescence

Optical bleaching of tenebrescence (**II-III**) was measured by first measuring the sample's reflectance and setting this as the white reference. The sample was then excited with 260 nm radiation from the SB522 150 W Xe-arc lamp coupled to a LOT MSH 300 monochromator for 5 minutes and its reflectance measured. The sample was allowed to sit in darkness for a further 5 min, after which its reflectance was measured to obtain the spontaneous fading in darkness of the sample. The sample was subsequently re-coloured using 260 nm radiation for 5 min, then bleached with light ranging from 300-680 nm. The cycle was repeated using 20 nm steps in the bleaching wavelength. The reflectance wells were integrated to give colour intensity, and the decrease in colour intensity caused by each bleaching wavelength relative to the previous intensity after 260 nm excitation was calculated accounting for spontaneous fading in darkness. These results produced the optical bleaching spectra. Reflectance was measured using the same HS-TEC spectrometer and optical fibre as previously mentioned in 4.2.2.1 under the same OceanOptics incandescent torch as before. The data collection time was 1.6 s (160 ms integration time, 10 averages).

4.2.2.6 Rise of tenebrescence colouration

In **II**, the rise of tenebrescence coloration was measured by constantly exciting samples with 254 nm radiation from a UVP model UVLS-24 EL, 4 W 254/365 nm handheld lamp (UVC irradiance approx. 1.3 mW cm^{-2}) or with 302 nm radiation from a UVP model UVM-57, 6 W lamp (UVB irradiance approx. 1.3 mW cm^{-2}) while measuring their reflectance under a 40 W incandescent lamp giving constant incident irradiance. For powder samples, MgO was used as the white reference. Reflectance spectra were measured using the same optical fibre coupled to the same HS-TEC spectrometer as in 4.2.2.1 with a 200 ms integration time and 10 averages. In this way, samples were irradiated for 60 minutes with data collected every two seconds. The integrals of the reflectance curves were used to give the colour intensity.

In **III**, flexible films made according to 4.1.5 were subjected to 254 nm radiation using the handheld lamp from 4.2.2.1 with an irradiance of 4.4 mW cm^{-2}. The films were irradiated for between 15 s and 10 min to expose them to different doses of radiation. The reflectance of the coloured region was then measured, and the

reflectance curve integrated to obtain the colour intensity after that UV dose. The reflectance of an uncoloured portion of film was used as the white reference. Reflectance was measured using an Avantes AvaSpec-ULS2048CL-EVO CCD spectrometer coupled to an Avantes FC-UVIR600-1 optical fibre (200 ms integration time, 10 averages), under illumination from a 40 W incandescent lamp at constant irradiance.

4.2.2.7   Fade of tenebrescence colouration

The fade of tenebrescence (**II**) was measured after the sample was excited for at least 10 minutes by 254 nm UV radiation. The reflectance mas measured every two seconds for two hours, using uncoloured sample as the white reference and the same spectrometer and measurement parameters as in 4.2.2.6. Samples were measured under various light sources, including a 40 W incandescent lamp, an Airam 2700 K 9 W warm white LED light, cool white LED ambient lighting, a blue LED from a North GLGID-02 RGB lamp, and a HP Compaq LA2306x WLED-backlit LCD computer monitor. The reflectance curves were integrated to give the colour intensity. Dose correction for different light sources was carried out using the measured irradiances of each light source as given in the 400-1050 nm range by a Delta Ohm HD 2102.1 photo/radiometer coupled to a LP 471 RAD irradiance meter; for different F-centres exposed to the same light source dose correction was done using the relative intensities of the light source in question in the F-centres' absorption ranges.

4.2.2.8   Rise of tenebrescence colouration under X-rays

Flexible films made according to 4.1.5 were subjected to X-ray irradiation (**III**) using the PANalytical Epsilon 1 device in 4.2.1.4. The films were irradiated for between 1 min and 3 h, corresponding to doses of between 4-320 mSv as measured using a Thermo Scientific RadEye B20-ER.[5] The reflectance of an uncoloured portion of film was measured immediately after irradiation and set as the white reference. The reflectance of the coloured region was then measured, and the reflectance curve integrated to obtain the colour intensity after that X-ray dose. Reflectance was measured using an Avantes AvaSpec-ULS2048CL-EVO CCD spectrometer coupled to an Avantes FC-UVIR600-1 optical fibre (200 ms integration time, 10 averages), under illumination from a 40 W incandescent lamp at constant irradiance.

4.2.2.9   X-ray imaging with photochromic sodalite

X-ray images (**III**) of a deceased flying ant and micro-SD reader were taken by placing the subject in the sample chamber of the PANalytical Epsilon 1 device of 4.2.1.4 and a flexible tape of desired sodalite composition on top of the ant. The subject and the tape were then subjected to X-ray irradiation for 4.5-61 min, after which an X-ray image was produced on the tape. The image was photographed with a digital camera as soon as possible following exposure to record the X-ray image digitally.

4.2.3   Characterisation of luminescence properties

4.2.3.1   Photo- and persistent luminescence spectroscopy

PL and PeL spectra (**I**, **III**) after UV excitation were measured at room temperature using a Varian Cary Eclipse Fluorescence Spectrophotometer containing a Hamamatsu R928 photomultiplier and a 150 W xenon lamp. For PL spectra, the internal light source was used, with a delay of 0.1 ms, an excitation slit width of 10 nm, an emission slit width of 2.5 nm, a gate time of 5 ms, and a step size of 0.2 nm. For PeL spectra, samples were excited using the 254 nm lamp or 302 nm lamp from 4.2.2.6 for 5 min at room temperature (irradiance approx. 2.3 mW cm^{-2}), followed by a 30 s (**III**) or 1 min (**I**) delay before measurement with emission slit 20 nm and step size 1 nm. Measurement of the PeL spectrum from 350-750 nm took 4 s in total.

4.2.3.2   Fading of PeL

The fading of persistent luminescence (**I**) was investigated using a Hagner ERP-105 photopic luminance photometer at room temperature. Samples were excited with the lamps of 4.2.2.6 for 5-30 min (irradiance approx. 2.3 mW cm^{-2} (302 nm), 3.1 mW cm^{-2} (254 nm)); measurement started immediately after irradiation ceased and continued until the luminance dropped below 0.3 mcd m^{-2}.[112] Lifetimes were obtained by fitting a bi- or triexponential function to the obtained data.

4.2.3.3   Thermoluminescence

Optical energy storage properties were investigated using thermoluminescence measurements (**I**) with a MikroLab Thermoluminescent Materials Laboratory Reader RA'04. Samples were excited with 302 nm and 254 nm UV from the lamps of 4.2.2.6 for 5 min (dose approx. 1.7 mW cm^{-2} (302 nm), 1.3 mW cm^{-2} (254 nm)), and the thermoluminescence measurement taken using a heating rate of 9 °C s^{-1} after

a 1 min delay. Preheated measurements were taken to investigate deep traps. Samples were excited for 5 min with a handheld 254 nm lamp, then preheated to 180-250 °C. Preheated samples were measured using a heating rate of 9 °C s^{-1} 1 min after excitation ceased. Corrections to the glow curves to account for thermal quenching of luminescence were carried out.[113] Glow curves were analysed using the initial rise method to obtain the trap depths in the material.[111]

4.2.3.4   Cathodochromism

Cathodochromism (**I**) was measured under the light of an Ocean Optics LS-1 Cal torch located approximately 3 cm from the sample. The reflectance of the sample before bombardment was measured using Al_2O_3 as the white reference, and the sample was then subjected to an electron beam for 5 min using a Nuclide Corp. ELM2EX Luminoscope at 50–100 mTorr pressure. The reflectance was measured again 10 s after electron bombardment ceased using an Avantes FC-IR600–1-ME-HTX optical fibre connected to an Avantes AvaSpec-2084 × 14 CCD spectrometer with a data collection time of 1.6 s (160 ms integration time, 10 averages). The difference of the two reflectance curves was calculated to show the colour change.

4.3   Computational Methods

4.3.1   Partial substitution of Na with Ca

The following method was used in **II** to simulate the 2x2x2 supercell of photochromic sodalite with partial substitution of Na with Ca. During the computational study, only calcium substitutions of sodium atoms in the pristine sodalite of formula $Na_8(Al_6Si_6O_{24})Cl_2$ were considered.

The methodology includes 3 main steps:
1. Optimisation of the geometry of pristine sodalite's bulk in PBC, followed by the generation and optimisation of the corresponding 2x2x2 supercell.
2. From this supercell, the defect (F-centre/trapped electron) was added to a Cl$^-$ site, along with substitution of 1-4 of the sodium atoms surrounding this site with calcium ones, and the corresponding 2x2x2 supercells' geometries were optimised. Three possibilities were considered in order to go from the unmodified $[Na_4V_{Cl}]^{3+}$ composition to: $[Na_3CaV_{Cl}]^{4+}$, $[Na_2CaV_{Cl}]^{3+}$ and $[Ca_2V_{Cl}]^{3+}$. They correspond to systems that are referred to as Na_3Ca, Na_2Ca and Ca_2 in relation to the unmodified Na_4 structure. In the case of Na_3Ca, the addition of one positive charge was offset by the substitution of one Si^{4+} by one Al^{3+} in the surrounding β-cage.

3. Extraction of a cluster containing the β-cage and the corresponding modified "tetrahedron" structures for the simulation of the F-centre's absorption with an embedded cluster approach. Atom positions are fixed to the ones of the geometry optimised in periodic boundary conditions.

All optimised structures obtained with the ab initio CRYSTAL17[114] code were conducted at the DFT/PBE0[115] level of theory using localised basis sets. HF and KS equations were solved self-consistently with convergence criterion for the SCF cycles fixed at 10^{-7} Ha per unit cell. The reciprocal space was sampled according to a sublattice with a 12x12x12 k-point mesh for the geometry optimisation of the bulk system, while a single k point (the Γ point) was used for the geometry optimisation of the supercells. When considering the F-centre in the structure (*i.e.,* a trapped electron), calculations were performed in an unrestricted formalism to account for the singly-occupied orbital. A numerical frequency calculation was performed to assess the nature of the stable geometry found. This calculation was performed only on the sodium and calcium atoms since the β-cage is known to be very rigid and not to be affected by chemical modifications in the sodium tetrahedron.[18,53]

Localised basis sets used in CRYSTAL PBC calculations were then kept for the F-centre's absorption simulations. The basis set for the electron in the vacancy has been previously optimised and is of the form 111G(d).[57] All-electron double-ζ basis sets with polarisation functions were used for Si ([4s3p1d]/(20s12p1d))[116], Al ([4s3p1d]/(17s9p1d))[117], O ([3s2p1d]/(10s4p1d))[118], and Cl ([4s3p1d]/(16s10p1d))[119]. All-electron triple-ζ basis sets with polarisation functions were used for Na ([4s3p1d]/(15s7p1d)[120] and Ca ([6s4p1d]/(17s11p1d)).[121]

Spectroscopic investigations led on the extracted clusters (embedded in a sphere of pseudopotentials and an array of point charges)[57], were done at the TD-DFT/B3LYP level with the same basis set as the one used for periodic boundary condition calculations with the Gaussian 16 package based on benchmark calculations.[57,122]

4.3.2   Different dichalcogenide activators

The following method was used in **III** to simulate the excitation thresholds of colouration for S_2^{2-}, SeS^{2-} and Se_2^{2-} activators in sodalite.

All optimised structures obtained with the ab initio CRYSTAL17[114] code were conducted at the DFT/PBE0[115] level of theory using localised basis sets. HF and KS equations were solved self-consistently with convergence criterion for the SCF cycles fixed at 10^{-7} Ha per unit cell. The reciprocal space was sampled according to a sublattice with a 12x12x12 k-point mesh for the geometry optimisation of the bulk system, while a single k point (the Γ point) was used for the geometry optimisation of the supercells. The basis set for the electron in the vacancy has been previously

optimised and is of the form 111G(d).[57] All-electron double-ζ basis sets with polarisation functions were used for Si ([4s3p1d]/(20s12p1d))[116], Al ([4s3p1d]/(17s9p1d))[117], O ([3s2p1d]/(10s4p1d))[118], and Cl ([4s3p1d]/(16s10p1d))[119]. All-electron triple-ζ basis sets with polarisation functions were used for Na ([4s3p1d]/(15s7p1d)[120] and S ([6s5p2d]/(20s14p2d)).[121] A pseudopotential was used for the 10 core electrons of selenium along with a ([5s4p2d]/(15s14p7d)) basis set for the 24 remaining electrons.

Spectroscopic investigations led on the extracted clusters (embedded in a sphere of pseudopotentials and an array of point charges)[57], were done at the TD-DFT/CAM-B3LYP level with the same basis set as the one used for periodic boundary condition calculations with the Gaussian 16 package.[122]

5 Results and Discussion

5.1 Zeolite-free synthesis

5.1.1 Solid-state method

The rationale for performing the study in **I** was to work towards improving the tunability of photochromic sodalite by removing the need for zeolite A as a starting material, which itself contributes six of the eight alkali metal ions present in sodalite, as well as aluminium and silicon, and thus limits the ability to adjust the composition. The basis for the synthetic method dates back to at least 1954,[105] and the idea to add a sulfur source to produce tenebrescence was also previously discussed by Kirk,[12] however no white PL or PeL had been reported for photochromic sodalites prepared in this way prior to **I**. In fact, white PL and PeL had only been reported and thoroughly studied in synthetic photochromic sodalites prepared from zeolite A from 2015 onwards by Norrbo *et al*.,[2] leading to the question of whether it was possible to obtain such properties without this starting material.

It was no surprise that the simple starting materials of Al_2O_3, SiO_2, NaCl and Na_2CO_3 were able to form the desired structure during synthesis once the temperature had been optimised to control the amount of chlorine that escapes the structure (**Figure 7**a, b), as similar methods for making sodalite have been reported to be successful.[12,105]
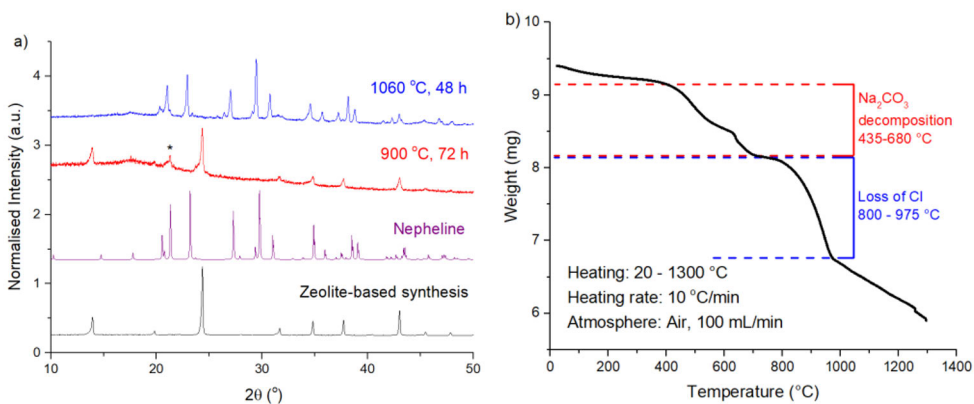
Figure 7. a) PXRD patterns for materials produced by optimised (900 °C, 72 h) and non-optimised (1060 °C, 48 h) zeolite-free synthesis compared to a zeolite-based reference material and a database pattern for nepheline (PDF 00-035-0424), which forms at high temperatures.[I] * indicates a signal from the sample mount. b) TGA curve for the reaction heated in air showing decomposition of Na_2CO_3 and loss of chloride.[123,I]

It was, however, a pleasant surprise to find that these materials all displayed the typical blue-white photoluminescence and afterglow of sodalites synthesised from zeolite A. Prior to this, no mention of such luminescence was given in the literature for photochromic sodalite prepared this way. In fact the PL was the easiest of the properties to achieve (**Figure 8**a), and most samples also displayed PeL (**Figure 8**b). The luminescence properties, such as the shape and position of excitation and emission bands, persistent luminescence emission spectra, and thermoluminescence trap depths, were studied closely (**Figure 8**c).[I] Upon comparison to a reference material, they were found to match those of sodalite produced from zeolite A very well, confirming that sodalites produced with this method have the same optical properties as their zeolite-based counterparts. While the deeper trap present in the zeolite-based reference (> 1.0 eV) was not found in the sample of zeolite-free photochromic sodalite presented in **Table 7**, other examples presented in **I** do show multiple traps.[I]

The synthesis had to be finely optimised to achieve the tenebrescence property, but eventually a transition from brown to purple with an absorbance band similar to that of zeolite-based photochromic sodalite was achieved (**Figure 8**d). The characteristic yellow emission of S_2^- observed by Kirk and Deb was never observed.[12,80,82]
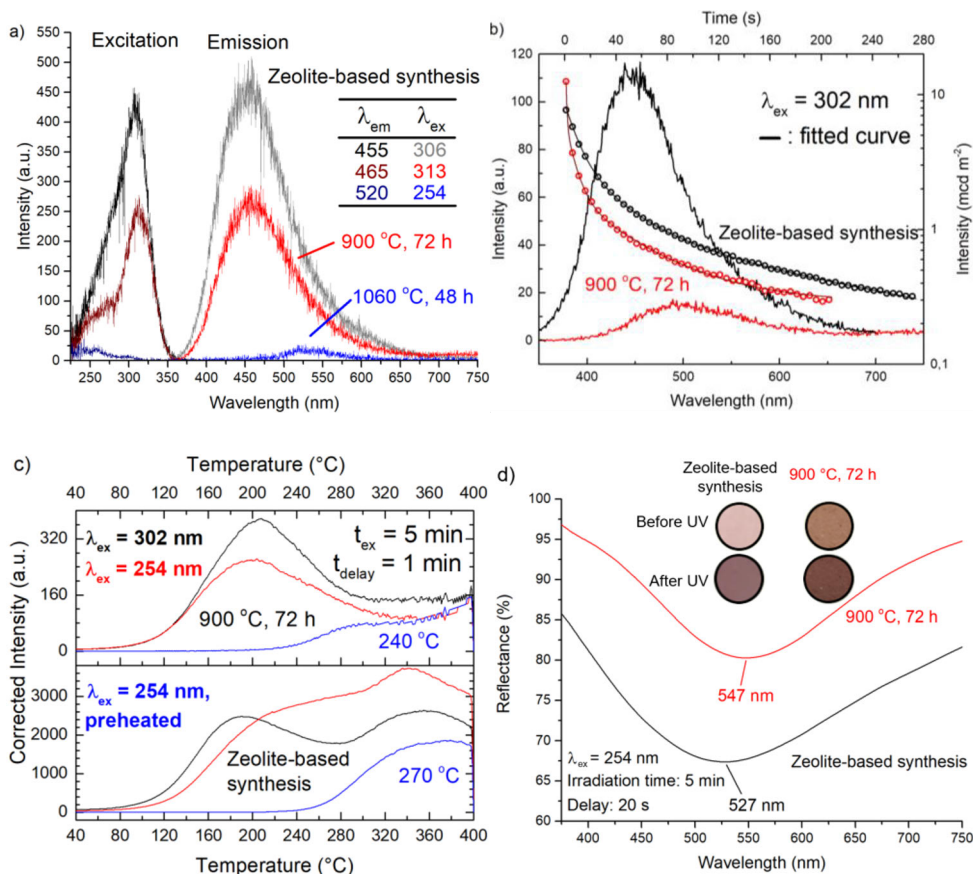
Figure 8. a) PL emission and excitation curves. λ_{ex} used to produce the emission curves and λ_{em} used to produce the excitation curves are indicated.[I] b) PeL emission spectra (*t_{ex}*: 5 min, *t_{delay}*: 1 min) and fading of PeL with respect to time.[I] c) Thermoluminescence glow curves measured after excitation with 302 nm, 254 nm and 254 nm with preheating. Curves have been corrected for thermal quenching of luminescence.[I] d) Reflectance curves and photographs showing the materials' changes in reflectance after irradiation with 254 nm.[I]

Table 7. Time constants of PeL fading and trap depths calculated from thermoluminescence glow curves of materials prepared from zeolite A and using the optimised zeolite-free synthesis. Trap depth values have been corrected for thermal quenching of luminescence. Lifetime refers to the length of time the PeL emission's intensity remains above 0.3 mcd m^{-2}.[112,I]

Synthesis method	τ_1 (s)	τ_2 (s)	τ_3 (s)	Lifetime (s)	Trap depth (eV)	Glow curve max (°C)
Zeolite-based	9.7 ± 0.4	36 ± 6	240 ± 200	273	0.52 ± 0.01	192
					1.40 ± 0.01	371
900 °C, 72 h	0.75 ± 0.01	7.1 ± 0.2	51 ± 1	198	0.52 ± 0.01	207

During Norrbo *et al.*'s 2018 investigation into the alkali cation's effect on the tenebrescence property, they commented that while nominally 25 % of Na$^+$ in the structure should have been replaced by K$^+$ and Rb$^+$ in samples prepared with KCl and RbCl respectively, measurements showed this was not the case. They proposed size constraints as the reason behind this – namely that the larger K$^+$ and Rb$^+$ ions are not so soluble in the sodalite lattice.[6] However, during this work it was postulated that if the lattice were able to grow around these larger ions, perhaps more of them would pass into the structure. The assumption was that any K$^+$ and Rb$^+$ ions introduced in this way would still end up in the correct sites, namely those usually occupied by Na$^+$. A brief study using an alternative method beginning with a silicate glass adapted from Armstrong and Weller's work on synthetic tugtupites[106] was conducted. The results showed that upon substitution of Na$^+$ by >38 % K$^+$, the halogen-free leucite (K[Al$_2$SiO$_6$]) structure forms instead (**Figure 9**a). Thus, this zeolite-free method fails upon introduction of too much potassium. NaCl substitution with KCl was also tested using the optimised zeolite-free solid-state synthesis, and again the main phase produced was leucite rather than sodalite (**Figure 9**b). This was not repeated using potassium carbonate in the optimised synthesis in light of the results in **Figure 9**. It is possible that the leucite phase is an intermediate in the synthesis of potassium sodalites using these methods, and further addition of KCl followed by heating and reduction may produce the desired product.[124] However, the product produced is unlikely to be worth the extra time and energy this would require. Thus, it was concluded that these kinds of zeolite-free syntheses are not feasible routes to incorporating more potassium into the sodalite structure.
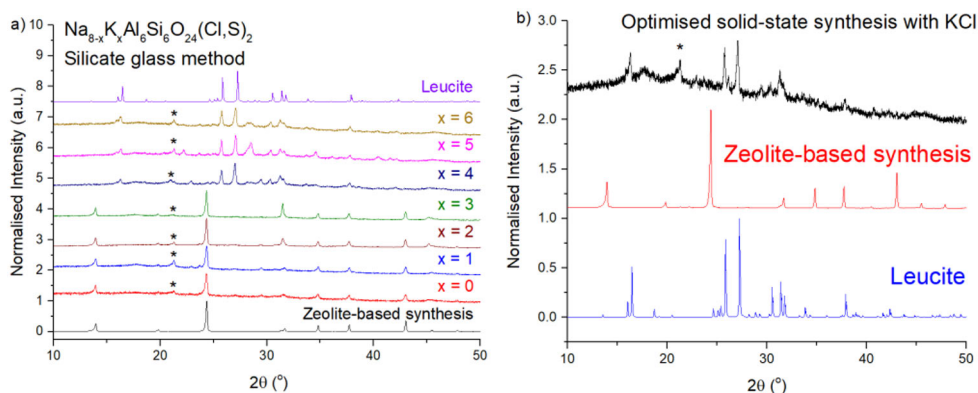
Figure 9.   a) PXRD patterns for sodalites prepared using a zeolite-free silicate glass method with different Na:K ratios compared to a reference prepared from zeolite and a database diffractogram of leucite (K[Al$_2$SiO$_6$], PDF 01-076-8732). * indicates a peak from the sample mount. b) PXRD pattern of a sodium-potassium material prepared using the optimised solid-state synthesis and KCl instead of NaCl. Comparison is made to a database diffractogram of leucite (K[Al$_2$SiO$_6$], PDF 01-076-8732) and a zeolite-based reference material. * indicates a peak from the sample mount.

The end results of the optimisation of this synthesis left much to be desired, especially when comparing to materials prepared from zeolite. The intensity of the luminescence, longevity of the afterglow and depth of the tenebrescence colour are all significantly poorer than the reference to which these materials were compared, and said reference was not a particularly high-performing sample. Thus, while this aspect of the doctoral research did prove that it was possible to synthesise sodalites with multiple optical properties without zeolite A using a solid-state method, the end products were not considered successful enough to warrant more time being spent using this method. Furthermore, the results in **Figure 9** indicate that these kinds of zeolite-free methods do not particularly facilitate large changes in stoichiometry. Hence, further tuning of photochromic sodalites and their properties has not been performed using these methods.

5.1.2   Hydrothermal method

5.1.2.1   Heavy cations: K⁺, Rb⁺, Cs⁺

The hydrothermal method for preparing photochromic sodalite is also one which dates back to the mid-20th century.[21,55] Tuning of the composition has been more widely tested using this method: Ballentyne and Bye prepared seleno- and tellurosodalites this way,[74] while Phillips and Chang tested hydrothermally prepared cathodochromic bromo- and iodosodalites,[20,60] and Williams *et al*. replaced

aluminium and silicon with gallium and germanium via a hydrothermal synthesis.[53] All these materials were made using sodium as the only alkali metal cation. Sodalites containing other alkali metal cations have been prepared hydrothermally, but these were not known to be photochromic, and the other alkali metal cations were introduced post-synthesis.[68,69,125]

Similarly to section 5.1.1, this method was considered for its potential to improve concentrations of large alkali metal ions such as K^+, Rb^+ and Cs^+ in the structure. Potassium and rubidium are known to lower the excitation threshold of F-centre formation, though their solubilities in the lattice perhaps limited this effect.[6] Incorporating a greater amount of such ions could greatly enhance tuning of the excitation threshold, and caesium sodalites have not yet been studied. It was hoped that if the sodalite cage is grown around these ions in solution, more of them may remain in the product, mitigating the solubility problem discussed by Norrbo *et al.*[6] The first tests of this theory were done by replacing only NaCl with the appropriate amounts of MX (M = K, Rb, Cs; X = Cl, Br, I), due to poor availability of $KAlO_2$ and heavier alkali metal aluminates. Note that the formulae used in this and following sections of the form $M_2Na_6(AlSiO_4)_6(X,S)_2$ are nominal in terms of the stoichiometry of M and Na, as solubility issues may affect the true ratios of M:Na in each material.[6]

Two sets of samples of nominally identical compositions were compared: one set prepared from zeolite A via solid-state synthesis and the other hydrothermally. Initial observations indicated that the sodalites obtained were much closer in quality and performance to those produced with zeolite when compared to the solid-state zeolite-free methods. XRF analyses of washed samples initial revealed the expected higher proportions of Rb or Cs in the hydrothermally prepared samples (**Table 8**). However, upon analysis of the PXRD diffractograms, it was observed that for samples made with RbX and CsX, sodalite was not the only significant phase, and the heavy cations instead were present in their respective aluminosilicates, $MAlSiO_4$ (**Figure 10**). Samples prepared hydrothermally had greater proportions of this phase, and also smaller unit cells, suggesting that the majority of the large cations are located in the aluminosilicate by-product, and the sodalite phase contains comparatively more sodium (**Table 9**). This is further confirmed by comparing the obtained values of unit cell parameter *a* given in **Table 9** to those of sodium sodalite containing the same respective halogens: 8.889 Å (X = Cl), 8.934 Å (X = Br) and 9.008 Å (X = I).

Table 8. XRF results for samples with the nominal formula $M_2Na_6(AlSiO_4)_6(X,S)_2$, where M and X are indicated by the row titled "Sample" in the table. SS indicates a sample prepared using a solid-state method; HT refers to hydrothermal synthesis. Concentrations determined by XRF are given as percentages. Only select elements are included in the table.

Sample	KI		RbCl		RbBr		RbI		CsBr	
Method	SS	HT	SS	HT	SS	HT	SS	HT	SS	HT
Element	%	%	%	%	%	%	%	%	%	%
Al	26.8	18.3	17.6	17.0	7.85	19.4	22.7	20.2	23.1	26.0
Si	30.4	22.2	18.7	22.9	69.7	23.5	0.69	22.8	27.8	26.4
S	0.66	0.50	0.55	0.71	0.34	0.76	0.66	0.42	2.4	0.35
Cl	0.32	0.35	5.9	11.1	0.08	0.68	0.20	0.17	2.3	0.20
K	16.7	14.8	2.5	0.36	0.72	0.79	2.4	1.6	6.0	0.26
Br	0.07	0.01	7.1	0.0	10.2	16.5	0.05	1.6	14.5	11.2
Rb	0.04	0.01	30.3	46.5	6.54	35.7	22.5	32.0	2.7	3.8
I	8.64	34.1	0.04	0.0	0.08	2.2	33.5	18.2	0.15	2.1
Cs	0.0	0.0	8.1	0.20	0.45	0.16	14.6	0.12	20.3	28.8
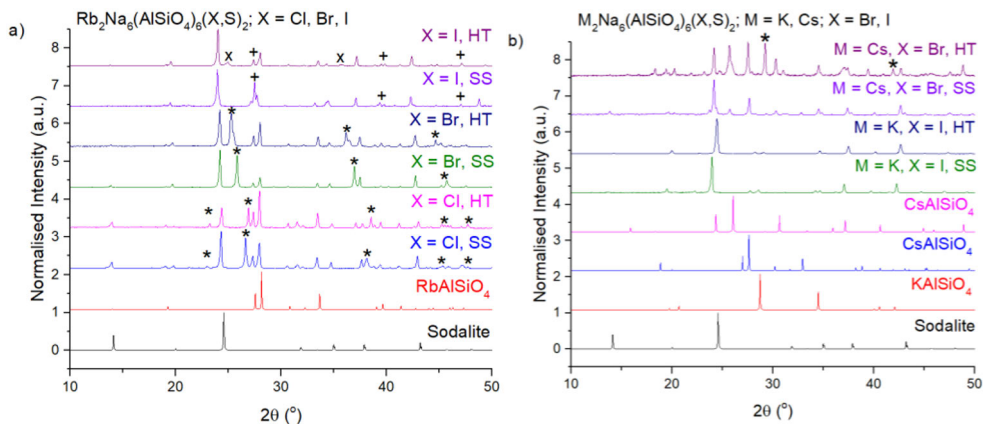
Figure 10. PXRD patterns for sodalites prepared using a solid-state (SS) and hydrothermal (HT) method. Compositions are indicated in the figures. In (a), peaks arising from impurities are indicated as follows: * = RbX, + = NaX and x = KI. Samples are compared to sodalite (PDF 00-037-0476) and RbAlSiO$_4$ (04-016-6279) references. In (b), peaks arising from impurities are indicated as follows: * = CsBr. Samples are compared to a sodalite (PDF 00-037-0476), a KAlSiO$_4$ (PDF 00-066-0070) and two CsAlSiO$_4$ references (blue: PDF 04-016-6278, pink: PDF 04-002-8335).

Table 9. Unit cell refinement and quantitative phase analysis results for samples of nominal formula $M_2Na_6(AlSiO_4)_6(X,S)_2$, where M and X are indicated by "Sample" in the table. SS indicates a sample prepared using a solid-state method; HT refers to hydrothermal synthesis.

Sample	Synthesis method	Sodalite (%)	MX (%)	NaX (%)	Other (%)	MAlSiO₄ (%)	a (Å)
KI	SS	75.5	0.0	0.0		24.5	9.033
	HT	89.0	0.0	0.0		11.0	9.064
RbCl	SS	50.8	15.3	1.3		32.6	8.902
	HT	42.4	10.0	6.4		41.2	8.877
RbBr	SS	60.1	23.1	0.0		16.8	8.931
	HT	51.3	22.6	0.0		26.1	8.864
RbI	SS	51.7	4.8	5.9		37.5	9.015
	HT	69.0	0.0	0.4	3.7 (KI)	27.0	9.007
CsBr	SS	83.8	0.0	3.0		13.2	8.954
	HT	20.9	8.3	0.0		70.8	8.943

Despite the presence of impurities, these materials typically showed good tenebrescence similar to that of their zeolite-based counterparts. In the case of the material made with potassium iodide, the hydrothermal synthesis was successful in expanding the unit cell. However, the XRF results suggest this could be due to a greater concentration of iodine in the material, rather than increased potassium content. The majority of Rb^+ and Cs^+ ions ended up in an aluminosilicate by-product rather than inside the sodalite structure, and the hydrothermal method failed to mitigate this problem, in fact exacerbating it. Hence, it was not considered advantageous as a way to introduce larger cations into the structure.

5.1.2.2 Fluorosodalites

The hydrothermal method was also used to prepare fluoride sodalites. Photochromic fluorosodalite has been mentioned in a few previous publications,[21,73] with Williams *et al.* stating that "Fluorine may shift the visible absorption maximum from 5300 to 5100 Å".[21] This observation fits with the theory that the F-centre's absorption maximum is related to the size of the unit cell and V_{Cl}, with smaller fluoride decreasing both these parameters and thus blueshifting the F-centre's absorption maximum. The literature does not, however, present fluorosodalite's absorbance spectra, nor the PXRD diffractograms of such materials. Hence, in this work the

synthesis of fluorosodalite was repeated, in the hope that it would produce a sodalite capable of changing from white to orange or red upon UV exposure.

Initially the solid-state synthesis from zeolite A was tried but was unsuccessful. The typical products were $MAlSiO_4$ (M = Li, Na, K) and NaF, though small amounts of the sodalite phase were detected (**Figure 11**). The usual sodalite synthesis temperature of 850 °C is at least 50 °C above the melting point of the MX salt used (X = Cl, Br, I), however the alkali metal fluorides have very high melting points (>850 °C). Even with increased synthesis temperatures, the correct structure did not form, likely due to the exceptionally high stability of NaF. The hydrothermal method was therefore tested, to see if the MF salts would react any more readily in solution.
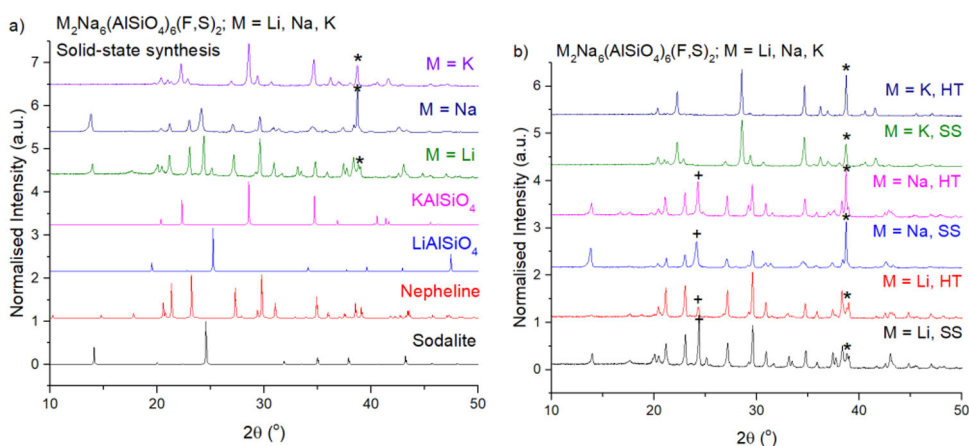
Figure 11.   a) PXRD patterns of fluorosodalites prepared by a solid-state method. Peaks arising from impurities are indicated as follows: * = NaF. Samples are compared to sodalite (PDF 00-037-0476), nepheline (PDF 00-035-0424), LiAlSiO₄ (PDF 00-017-0533) and KAlSiO₄ (PDF 01-079-5905) references. b) Comparison of diffractograms of fluoride sodalites prepared by solid-state (SS) and hydrothermal (HT) synthesis. Significant peaks are indicated as follows: * = NaF, and + = main peak of the sodalite phase, when present.

The diffractograms in **Figure 11**a show that for materials prepared from zeolite A, the majority of the material is composed of other aluminosilicate phases than sodalite, such as nepheline ($Na_3KAl_4Si_4O_{16}$), $LiAlSiO_4$ and $KAlSiO_4$. Some sodalite phase is present in materials prepared from LiF and NaF, however in the case of potassium, the main phase is $KAlSiO_4$, and no sodalite was detected by PXRD. When comparing these to the materials prepared by hydrothermal synthesis (**Figure 11**b), the peaks corresponding to impurities are generally stronger, suggesting this method is even less suitable to fluorosodalite preparation than the solid-state one.
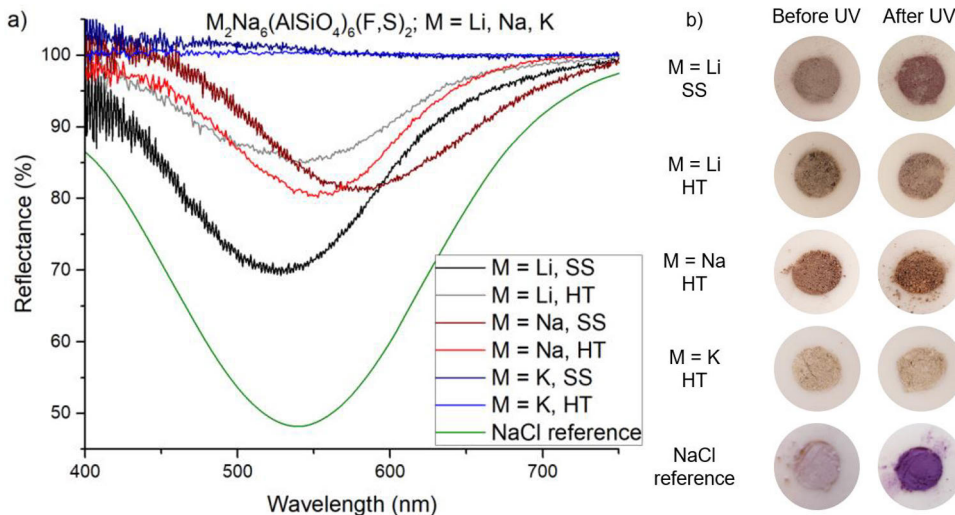
Figure 12. a) Reflectance curves of fluorosodalites prepared using a solid-state (SS) or hydrothermal (HT) method after 5 min irradiation with 254 nm. The NaCl reference has the formula $Na_8(AlSiO_4)_6(Cl,S)_2$. b) Photographs of fluorosodalites before and after irradiation with 254 nm.

Where sodalite was detected, the materials had tenebrescence. The sodium fluorosodalites did not show the blueshift in absorbance maximum as observed by Williams *et al.* in 1969 – in fact, the absorbance shifted to longer wavelengths than expected (**Figure 12**a). It is uncertain why this happened, and XRF analyses could not verify the fluorine content of these materials, as the available XRF device was unable to detect fluorine. The samples made with lithium fluoride show some colour change with an absorbance maximum of 530-545 nm, while often in the literature lithium sodalites have very poor tenebrescence.[71,73] As expected from the PXRD diffractograms, potassium sodalites showed no tenebrescence.

The texture of these materials was grainy, similar to coarse sand (**Figure 12**b), they had dark body colours, and they were somewhat more difficult to handle than regular sodalites. The poor purity led to the conclusion that fluorosodalites cannot easily be prepared, at least using the most straightforward synthesis methods. Introduction of fluorine also did not produce the desired effect of blueshifting the F-centre's absorption maximum, so another method must be employed to achieve this.

5.1.3 Conclusions

In general, the zeolite-free methods do not offer much in terms of improving the tunability of photochromic sodalite. The optimised solid-state method produces functional luminescent and photochromic materials, but the poor product quality

outweighs any increased compositional flexibility when compared to the zeolite-based synthesis. The hydrothermal method is able to produce photochromic materials of comparable functionality to those prepared from zeolite A, however this too does not offer any advantage when attempting to use more challenging precursors such as the highly stable alkali metal fluoride salts or very large cations. These methods are also incredibly slow, requiring 48-72 h of extra time for the first heating stage when compared to synthesis from zeolite, which only takes 5 h plus a 2 h reduction.

However, one area in which zeolite-free synthesis, particularly hydrothermal synthesis, proves invaluable, is in the tuning of the aluminosilicate backbone. Hydrothermal synthesis produces the best results when substituting Al for Ga or Si for Ge, as this is something that cannot be done using zeolite A. The use of hydrothermal synthesis to produce materials with the most redshifted absorption band, such as presented in **III**, is discussed in section 5.2.3.

5.2   Tuning the photochromism

5.2.1   Changing the alkali metal ion

5.2.1.1   Effects on the tenebrescence colour

As mentioned previously, the effect of the halogen on the unit cell size and thus the vacancy size, the F-centre's energy levels, and position of the absorption maximum, is well understood.[20,53,57] Similarly, the effects of Al and Si substitution with Ga and Ge have been studied both experimentally and computationally.[53,72] Alkali cation substitution for colour tuning has not been studied, though in their 2018 study Norrbo *et al.* did comment that their sodium-potassium sodalite showed a small shift in its reflectance minimum.[6] In this portion of the work, a range of sodalites were prepared using lithium, potassium and rubidium salts to study these ions' effects on the colour more closely. The effect of lithium, potassium and rubidium on the tenebrescence colour is apparent (**Figure 13**a).[III] Caesium sodalites may also behave similarly, but due to difficulties in their preparation (see section 5.1.2.1), caesium sodalites were not included in this section of the work.
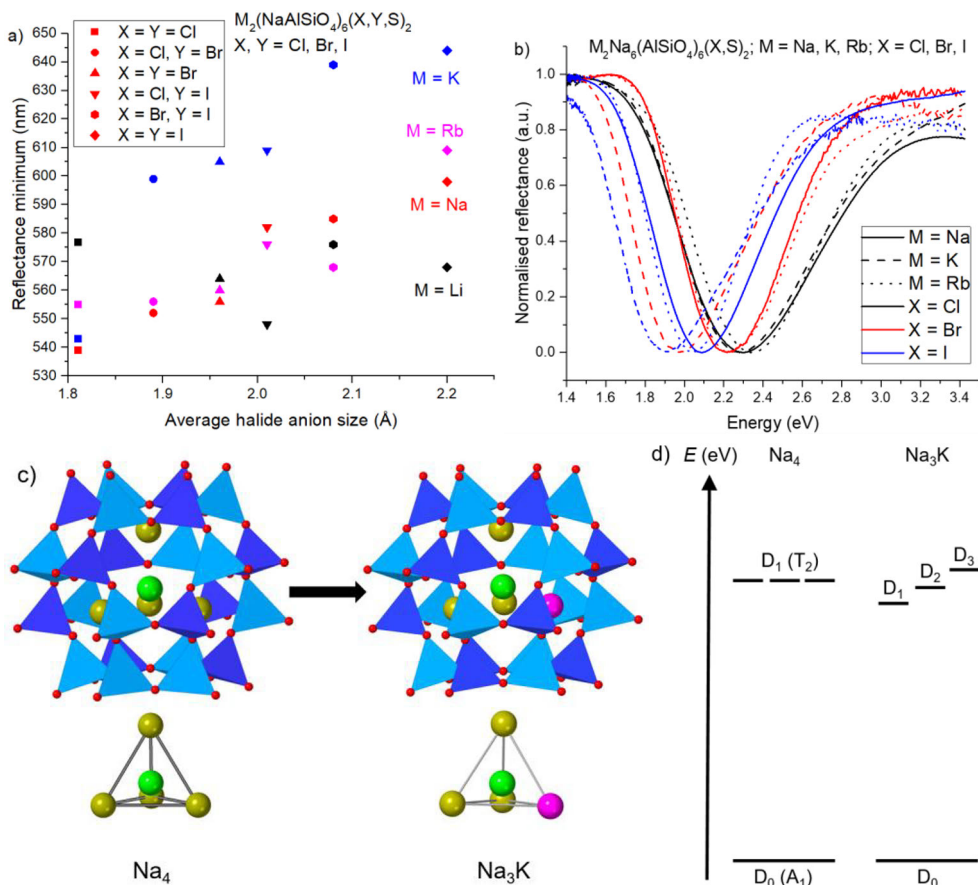
Figure 13. a) Effect of alkali cations on the position of the absorption maximum of the F-centre in photochromic sodalites made with different halogens.[III] b) Normalised reflectance curves showing band broadening and shift in absorption maximum.[III] c) Substitution of one sodium with potassium in the aluminosilicate β-cage. Aluminium and silicon are represented by light and dark blue tetrahedra respectively. Red, yellow, pink and green spheres represent oxygen, sodium, potassium and the centre of the cavity, respectively. Figure adapted from **II**.[II] d) Energy level diagram based on that in **II** showing the transitions of the F-centre in the pristine Na_4 system and in the Na_3K system. The loss of degeneracy of the LUMO upon introduction of potassium is visible. These states are of doublet spin-multiplicity explaining the notation D_0, D_1, D_2 and D_3 for the ground and excited states.[II,72]

The expected redshift in absorption maximum induced by increasing halide anion size is clear for sodium, potassium and rubidium sodalites, however potassium and rubidium have their own effect on the tenebrescence colour too, independent from that of the halogen. The reflectance minima of both potassium and rubidium sodalites generally fall at longer wavelengths than their sodium counterparts, though the effect is much more distinct for potassium. Unit cell refinement of the PXRD diffractograms reveal unit cell expansion when these ions are included in the

synthesis (**Table 10**). The generally greater expansion when M = K compared to M = Rb is put down to the relative solubilities of K^+ and Rb^+ in the lattice.[6] It is reasonable to assume that a larger ion would fill the sodalite cage more and potentially shrink the vacancy, which would result in a blueshift of the absorption maxima. However, this is clearly not the case. One explanation would be that introduction of another ion to the sodalite cage breaks the degeneracy of the F-centre's energy levels, resulting in multiple available transitions (**Figure 13**c, d).[62] This would be observed as band broadening, a phenomenon that is indeed seen in some compositions (**Figure 13**b, **Table 10**), though inconsistently. However, it is assumed that the dominant effect is bulk expansion of the structure caused by these large cations, which in turn expands the vacancy and negates any effect a large ion in the β-cage has on a particular vacancy's size.[III] Potassium is also known to be located further from the centre of the sodalite cage than sodium, which would cause potassium sodalites to have a larger vacancy and thus a redshifted absorption.[124] These effects are also presumed to dominate over any loss of degeneracy, as the shift in absorption maximum induced by K^+ and Rb^+ is consistent regardless of anion, while the band broadening is not.

Table 10.   Unit cell parameters of photochromic sodalites obtained by unit cell refinements of their PXRD patterns and change in absorbance band width through introduction of potassium and rubidium. Materials were of the nominal formula $M_2Na_6(AlSiO_4)_6(X,Y,S)_2$, where M = Li, Na, K or Rb and X, Y = Cl, Br or I. The average anion sizes were calculated from the ionic radii of Cl^-, Br^- and I^- weighted by the respective molar ratios of each ion in the sodalites.[126]

Average halide anion size (Å)	a (Å)				Absorption band FWHM (eV)		
	M = Li	M = Na	M = K	M = Rb	M = Na	M = K	M = Rb
1.81	8.762	8.899	8.920	8.902	0.87	0.84	0.77
1.89	8.844	8.910	8.957	8.928	0.81	0.66	0.59
1.96	8.894	8.934	9.011	8.931	0.64	0.69	0.65
2.01	8.899	8.949	8.985	8.974	0.52	0.57	0.55
2.08	8.937	8.963	9.017	8.954	0.51	0.56	0.57
2.20	8.954	9.008	9.033	9.015	0.66	0.74	0.85

The lithium sodalites are more unusual in their behaviour. Despite the decreased unit cell size compared to their sodium counterparts (**Table 10**), the position of the reflectance minimum stays roughly constant, even with increasing anion size. The lack of blueshift in reflectance minima is already discussed by Williams *et al.*, who explain that the high charge to radius ratio of Li^+ means it preferentially locates

closer to the framework oxygens, and thus expands the vacancy, despite the smaller unit cell parameter.[53] Lithium sodalites also show comparatively weak tenebrescence, meaning that despite their superior luminescence properties, they are of less interest to this study on photochromism than their potassium and rubidium counterparts.

From this, it is clear that potassium in particular has a strong effect on the tenebrescence colour in photochromic sodalites. By using potassium iodide the structure was expanded to the same extent as a chlorosodalite prepared with germanium,[53,69] but with an even greater shift in absorption maximum compared to that of Williams. Potassium is therefore more effective at tuning the colour than gallium or germanium, which is advantageous considering the relative availability of these elements.[54] The next section discusses how to increase potassium content to further lower the energy of the F-centre's absorption maximum.

5.2.1.2 Ion exchange to further shift the absorption maximum

Norrbo *et al.* determined that when all NaCl used in sodalite synthesis was replaced with KCl, resulting in a nominal substitution of Na with K of 25 mol%, in fact only 14 mol% K entered the structure.[6] Considering potassium's marked effect on the tenebrescence colour, increasing this substitution rate was of considerate interest. In 5.1.2.1, the hydrothermal method was shown to produce a purer potassium iodide sodalite with a larger unit cell than the solid-state synthesis (see **Table 9**), though it is not certain whether this is due to increased potassium or iodine content. The hydrothermal method is, however, slower and more complex than the solid-state method, and the benefits comparatively small, so a different method to increase potassium content was tested. The nitrate melt method employed by Johnson *et al.* in 2000 was able to substitute up to 50 mol% of sodium with potassium,[69] which would be a significant improvement to the 14-25 mol% substitution presumed to occur in the solid-state synthesis. This method was tested on a pure sodium bromosodalite and a potassium bromosodalite, as well as a potassium iodosodalite, and was found to further redshift the F-centre's absorption maximum without destroying the photochromism property.

XRF results indicate that the ion exchange was successful in increasing the amount of potassium in all three materials tested. Those sodalites already containing potassium showed the greatest unit cell expansion and change in absorption maximum (**Table 11**). This suggests that the solubility of K^+ is improved in an already expanded sodalite structure. Interestingly, the unit cell parameter of potassium-exchanged iodosodalite obtained is similar in size to that of the sodium aluminogermanate bromosodalites of Johnson and Williams,[53,69,125] though again with a much greater shift in absorption maximum compared to the literature.

Table 11. Summary of the effects potassium ion exchange had on the potassium concentration determined by XRF ([K]), the unit cell parameter and the absorption maximum of photochromic sodalites of nominal formula $M_2Na_6(AlSiO_4)_6(X,S)_2$.

Sodalite	Potassium exchanged	[K] (%)	Δ[K] (%)	a (Å)	Δa (Å)	λ_{max} (nm)	Δλ_{max} (nm)
M = Na;	No	0.68		8.938		559	
X = Br	Yes	4.65	+ 3.98	8.941	+ 0.003	562	+ 3
M = K;	No	16.28		9.011		627	
X = Br	Yes	20.06	+ 3.78	9.045	+ 0.034	652	+ 25
M = K;	No	16.25		9.064		648	
X = I	Yes	28.78	+ 12.54	9.103	+ 0.039	675	+ 27

Ion exchange with potassium did not induce further band broadening than that already achieved by substitution of sodium with potassium during the original synthesis, further supporting the idea that the redshift in absorption is not as much tied to loss of degeneracy as to expansion of the sodalite lattice (**Figure 14**a). It did, however, weaken the intensity of the colour change (**Figure 14**b). This may be the result of some nitrate ions becoming trapped in halide vacancies during ion exchange, which reduces the number of F-centres that can form. Nevertheless, the 65-75 % reflectance measured at the absorption maximum of the ion-exchanged sodalites is certainly enough for the colour change to be visible to the eye (**Figure 14**c). Whilst the tone of the coloured form of the sodium and potassium bromosodalites remains the same before and after potassium exchange, the potassium iodosodalite appears noticeably greener than its parent after ion exchange.
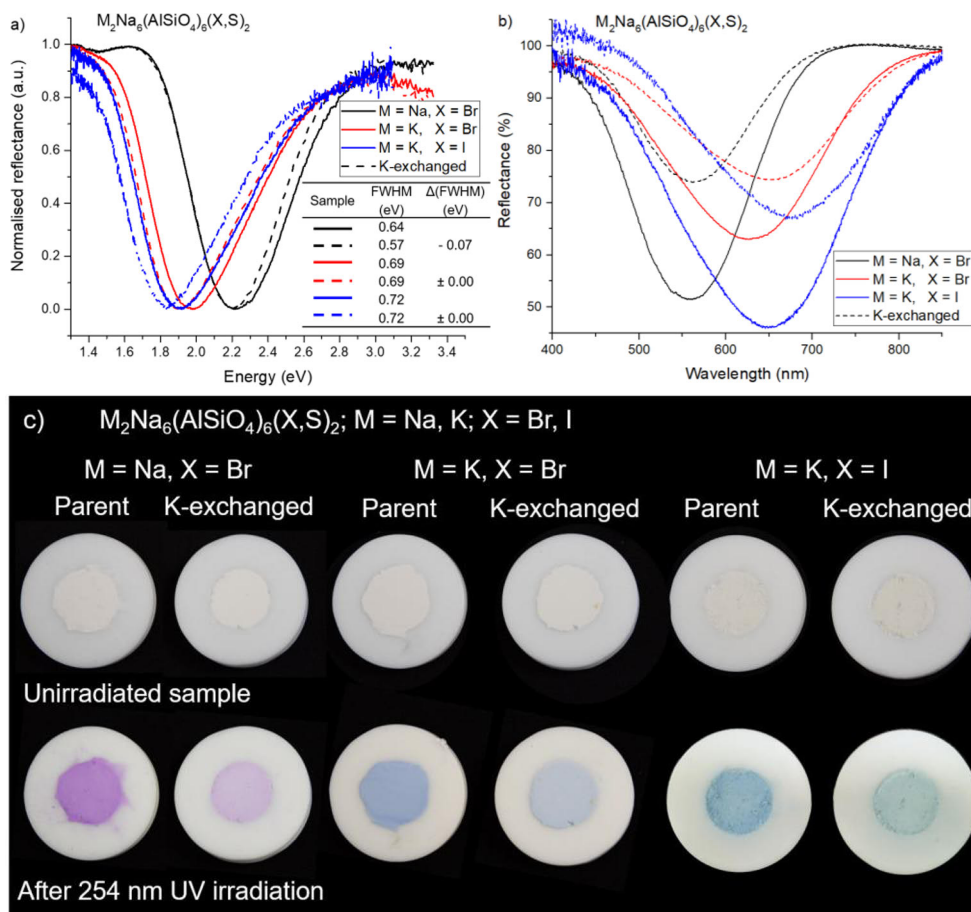
Figure 14. a) Effects of ion exchange on the width and maximum of the F-centre's absorption band. b) Effect of ion exchange on the intensity of the coloured form. c) Photographs of the parent and ion-exchanged sodalites after exposure to 254 nm UV radiation.

This method is, in conclusion, an effective way of tuning the absorption maximum. Combining the effects of potassium iodide and this ion exchange method, the absorption maximum has been pushed to a lower energy that that ever recorded before, bordering on the edge of the NIR region at 675 nm. This demonstrates that the somewhat costly and increasingly rare germanium is not necessary to produce sodalites with blue-green tenebrescence.

Lithium exchange was also attempted, since high lithium concentrations are known to expand the vacancy and thus redshift the absorption maximum. This was initially tested on chlorosodalite, and was indeed found to redshift the absorbance band, as well as significantly contracting the unit cell (**Figure 15**a), but also weakened the tenebrescence so much that the colour change was barely visible to the

eye (**Figure 15**b). Hence, potassium ion exchange is the better method for redshifting the absorption maximum. It is possible that rubidium exchange would produce even better results, though lattice solubility may be an issue. This was not tested.
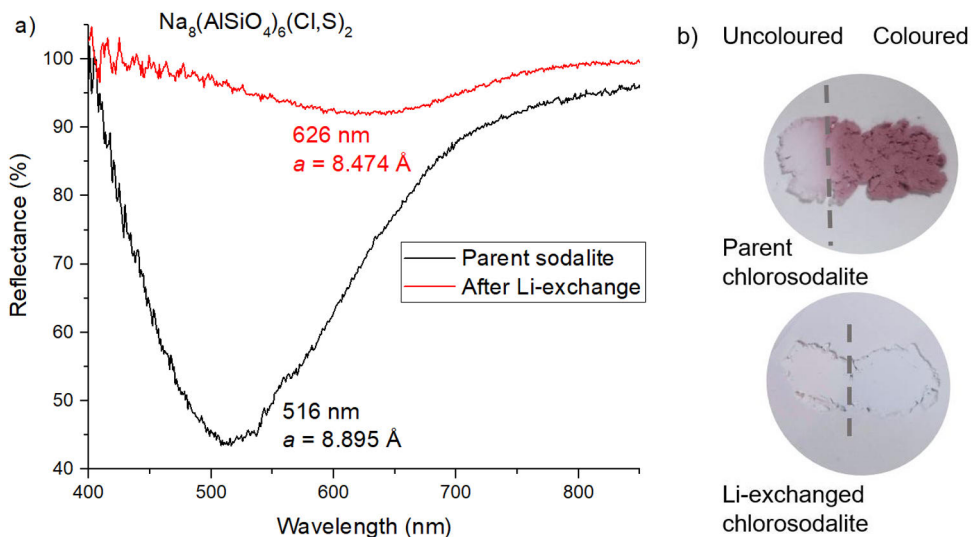
Figure 15.   a) Reflectance of chlorosodalite after exposure to 254 nm UV for 5 min, showing a strong absorbance in the green range before lithium ion exchange and a weak absorbance in the red after Li-exchange. The positions of the reflectance minima and unit cell parameters obtained by unit cell refinement are indicated. b) Photographs of chlorosodalite before and after ion exchange, showing its uncoloured and coloured forms.

5.2.1.3   Effects of ion exchange on the excitation threshold and thermal bleaching

Experimental and computational results predict that potassium substitution lowers the activation energy of F-centre formation.[6,62] Increasing potassium content should continually lower the excitation threshold,[62] so it was hoped that the ion-exchanged materials would show lower excitation thresholds than their parent sodalites. Likewise, potassium and rubidium have shown to alter the thermal bleaching energies of the F-centre in photochromic sodalites, and it was postulated that the ion exchange may have an effect on this too.

    Figure 16 shows the excitation spectra of the parent sodalites and their respective ion-exchanged counterparts. It is clear that the excitation threshold (activation energy) before and after ion exchange does not change significantly. Instead, the potassium already introduced during solid-state synthesis has more of an effect, as seen when comparing the parent sodalites made with NaBr and KBr.

TD-DFT calculations predict a gradual decrease in excitation threshold with increasing potassium content, falling from 3.6 eV (Na$_4$, 344 nm) to 3.1 eV (NaK$_3$, 400 nm).[62] However, as the nitrate exchange method is known to produce only up to 50 mol% substitution of sodium with potassium,[69] it can be assumed that at most Na$_2$K$_2$ systems (E_a = 3.35 eV, 370 nm) will be present after potassium exchange. It may be that for the materials with M = K, X = Br, I, despite the increased potassium content in the parent sodalites, this 50 mol% substitution is still a limiting factor, and thus the activation energy cannot be lowered further because of this. The method used to measure excitation spectra is also somewhat primitive, and may not be able to detect small changes in activation energy caused by ion exchange. Interestingly, the potassium iodosodalite shows a significantly lower excitation threshold than its bromide counterpart. This is not, however, an observation consistent across other tested compositions, nor does it agree with TD-DFT calculations.[62]
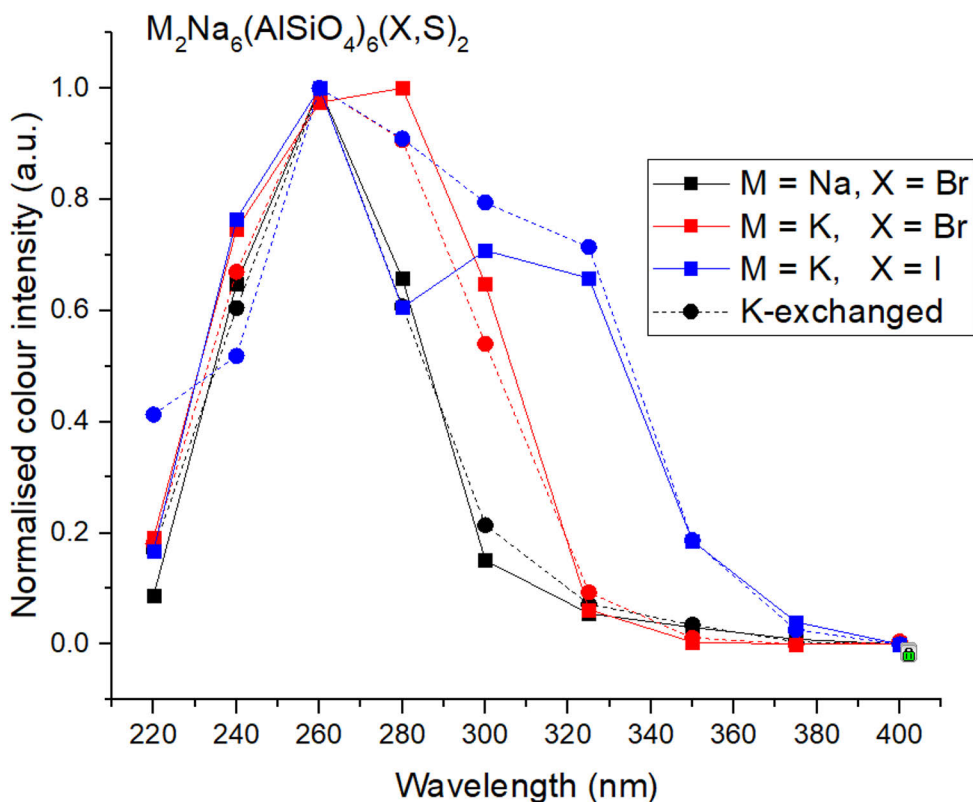
Figure 16.   Tenebrescence excitation spectra before and after potassium ion exchange.

Table 12. Thermal bleaching energies of sodalites of nominal formula $M_2Na_6(AlSiO_4)_2(X,S)_2$ before and after potassium ion exchange obtained by thermotenebrescence measurements.[6]

Sodalite	Potassium exchanged	Thermal bleaching energy, E_a (eV)	ΔE_a (eV)
M = Na; X = Br	No	0.48 ± 0.02	
	Yes	0.32 ± 0.03	- 0.16 ± 0.05
M = K; X = Br	No	0.28 ± 0.01	
	Yes	0.25 ± 0.01	- 0.03 ± 0.02
M = K; X = I	No	0.31 ± 0.03	
	Yes	0.25 ± 0.04	- 0.06 ± 0.07

The thermal bleaching energies in **Table 12** show that introduction of potassium by ion exchange to the sodium bromosodalite has a significant impact on its thermal bleaching energy, while the change is smaller for those parent sodalites already containing potassium before ion exchange, if there is any change at all. The obtained bleaching energies fit with those presented in the literature for sodium and sodium-potassium sodalites as the results of both experimental and computational studies.[6,62] This is in general agreement with the measured excitation spectra, i.e., the amount of extra potassium incorporated during ion exchange is not enough to significantly affect the colouration energy threshold or thermal bleaching energy, with the exception of the sodium sodalite. The sudden drop in thermal bleaching energy for the sodium bromosodalite, despite minimal change in tenebrescence excitation threshold, can be explained by considering that introduction of some potassium is enough to destabilise the F-centre somewhat, reducing the activation energy of thermal relaxation. This is detectable by thermotenebrescence – when the thermal bleaching curves are analysed by the initial rises method, they give only the lowest measurable bleaching energy.[111]

Whilst substitution of sodium with large alkali metal cations, particularly K^+, has a significant effect on the colour and position of the absorption maximum, which is further enhanced with ion exchange, the effect of said ion exchange on the excitation threshold of colouration was not so evident. This is therefore an attractive way to tune the photochromism colour and is essential to achieving the most redshifted absorption maxima, though another method is necessary to control the excitation threshold more easily. This is explored in further in section 5.2.4.

5.2.2   Yellow photochromism

As discussed in the literature and in section 5.2.1, inducing a redshift in the absorption band is somewhat straightforward: by expanding the unit cell, the vacancy V_X grows in size, and thus the energy gap between $a_1 \rightarrow t_2$ in the F-centre decreases. Both computational and experimental results support this,[53,57,62] and it can be logically assumed that the reverse would apply: if the unit cell could be shrunk somehow, V_X would decrease in size, and the $a_1 \rightarrow t_2$ energy gap would widen. This principle was tested in sections 5.1.2.2 (fluorosodalites), 5.2.1.1 (lithium halide sodalites) and 5.2.1.2 (lithium ion exchange in sodalite), and none of these syntheses produced the desired blueshift in absorption maximum. A different approach was therefore required. Here, the prediction by TD-DFT simulations that introduction of potassium to the tetrahedron surrounding V_{Cl} would break the degeneracy of the F-centre's orbitals, producing some higher energy level gaps, serves as a starting point.[62,72] While potassium is not an appropriate choice here, given its tendency to redshift the absorption maximum (section 5.2.1), the idea of breaking degeneracy remained plausible as a way to expand the gap between the F-centre's ground and excited state. Other cations were tested, and it was found that calcium (Ca^{2+}) was able to significantly affect the F-centre's energy levels. This became the basis of publication **II**.

5.2.2.1   Effect of the Na:Ca ratio on the structure and optical properties

Experimentally, it was found that substitution of sodium with calcium within a certain range of Na:Ca ratios changed the photochromism of sodalite significantly – namely the colour after exposure to UV was yellow, not pink. Materials of formula $Na_{2-2x}Ca_x(Na,K)_6(AlSiO_4)_6(Cl,S)_2$ were prepared from $0 \leq x \leq 1.00$, with particular focus on the values of x around which the photochromism colour changed from pink to yellow. The lowest value of x capable of producing clear white-to-yellow photochromism was 0.13, and for $x < 0.11$ the colour change was distinctly white-to-pink (**Figure 17**a).[II] The materials all had the desired sodalite structure, with the main impurities being NaCl and KCl (**Figure 17**b).
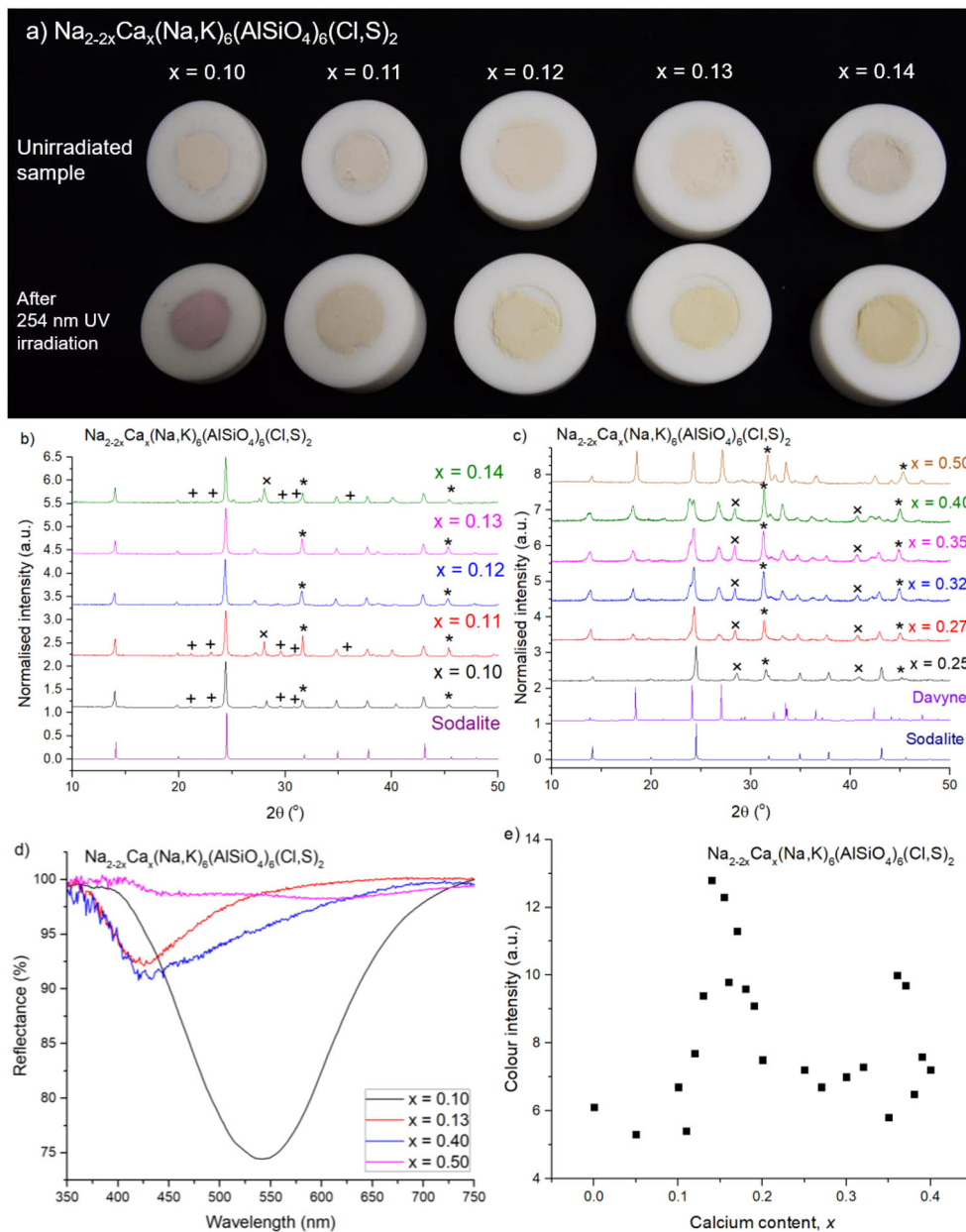
Figure 17. a) Photographs of samples close to the switch between pink and yellow photochromism ($0.10 \leq x \leq 0.14$) before and after irradiation with 254 nm UV.[II] b) Diffractograms of the samples in a)[II] compared to a sodalite reference (PDF 04-017-7136), with impurities indicated as follows: + = nepheline, * = NaCl, × = KCl. c) Diffractograms for samples with $0.25 \leq x \leq 0.50$ compared to a sodalite (PDF 04-017-7136) and a davyne (01-084-3796) reference.[II] Impurities are indicated as follows: * = NaCl, × = KCl. d) Reflectance spectra of samples either side of the upper and lower limits for yellow tenebrescence after exposure to UV. e) Absorption intensity at 420-435 nm for $0.00 \leq x \leq 0.40$.[II]

The upper limit of calcium substitution was found to be $x \leq 0.50$. From $x \geq 0.27$, a second phase is seen to appear in increasing concentrations in the PXRD diffractograms: this phase was identified to be davyne $((Na,K)_6Ca_2(Al_6Si_6O_{24})(Cl_2,SO_4)_2)$, and by $x = 0.50$ it is the dominant phase, with no sodalite observed in the diffractogram (**Figure 17**c). From this, it can be concluded that the range of x capable of producing white-to-yellow tenebrescence is $0.13 \leq x < 0.50$ (**Figure 17**d), though **Figure 17**e shows that the strongest yellow colour is produced by $0.13 \leq x \leq 0.18$.[II]

The yellow colour displayed by materials containing $0.13 \leq x < 0.50$ after exposure to UV was the result of an absorption band with maximum between 420-435 nm. The possibility of this arising from S_2^- or S_3^- was ruled out, as these ions contribute to a permanent body colour and thus their absorption would be unaffected by UV excitation.[8,78,127] It was postulated whether this band was the absorption of the same kind of F-centre as in $Na_8(AlSiO_4)_6(Cl,S)_2$, which forms only following UV excitation. 6-coordinate Na^+ and Ca^{2+} have very similar ionic radii (1.02 and 1.00 Å respectively),[126] so calcium was expected to have reasonable solubility in the sodalite lattice, but not to affect the unit cell parameter or vacancy size significantly. However, calcium has a different charge to sodium, which alters both the crystal field felt by the electron trapped in V_{Cl} and the symmetry around V_{Cl}, thus affecting the energy levels of the F-centre. The changed crystal field induces a blueshift in the absorption, while the change in symmetry breaks the degeneracy in the F-centre's energy levels, splitting the t_2 LUMO into three separate energy states (**Figure 18**i). This was confirmed using computational studies of three different arrangements of Na^+ and Ca^{2+} inside the sodalite cage (**Figure 18**a-h).[II] Comparison to experimental results led to the conclusion that the species responsible for the absorption at 420-435 nm was an F-centre inside a sodalite cage surrounded by an Na_2Ca system (**Figure 18**j).[II]
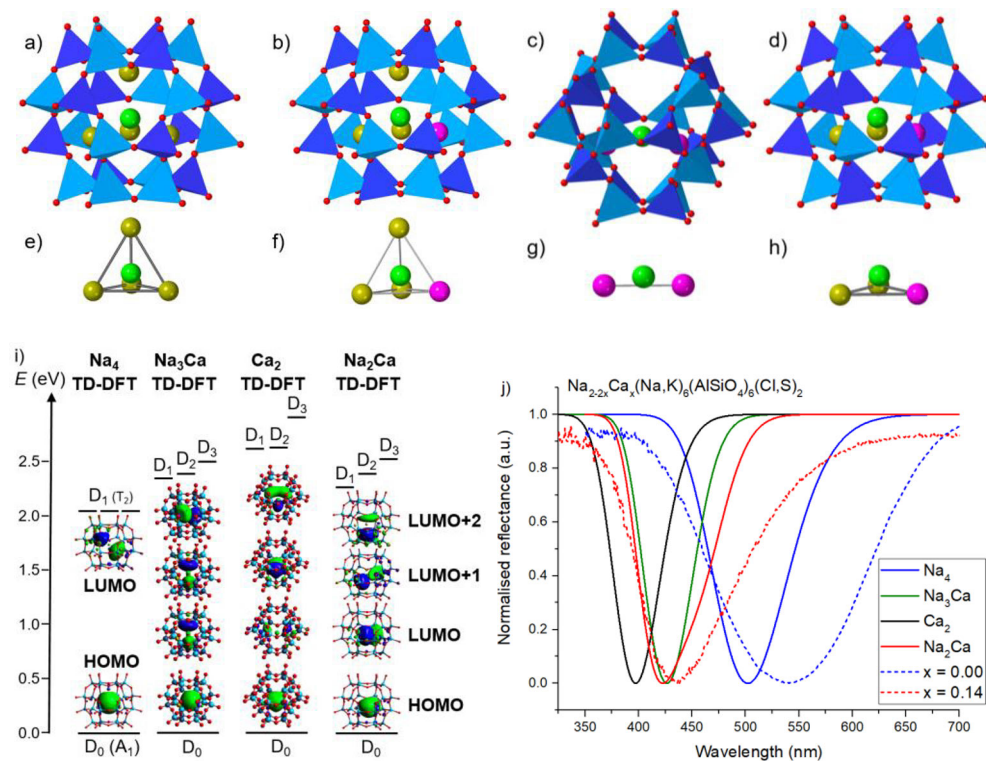
Figure 18. a-h) Structures of the pristine system called Na_4 (a, e) and the defective systems Na_3Ca (b, f), Ca_2 (c, g) and Na_2Ca (d, h) system from DFT optimised geometries showing the full β-cage (a-d) or focusing on the inside of the β-cage (e-h). Dark and light blue polyhedra surround the Si and Al atoms respectively. Red, yellow, pink and green spheres represent the oxygen, sodium, calcium atoms and the centre of the cavity respectively.[II] i) Energy level diagram of the three first electronic transitions for the Na_4, Na_3Ca, Ca_2 and Na_2Ca systems computed by TD-DFT. The transitions are dominated by the HOMO to the three lowest LUMOs' characters (presented as inserts). Excited states are of doublet spin-multiplicity, hence the notation D_0, D_1, D_2 and D_3 for ground and excited states.[II] j) Quantum chemically calculated absorbance spectra of the coloured form of the F-centre formed when V_{Cl} is located in a cage containing Na_4, Na_3Ca, Ca_2 and Na_2Ca systems (solid lines) compared to experimental absorbance spectra of a pink ($x = 0.00$) and yellow ($x = 0.14$) photochromic sodalite material.[II]

It was observed that the experimentally obtained reflectance spectrum of the yellow photochromic sodalites had a shoulder in the 475-600 nm range that the simulated spectrum of the Na_2Ca system did not (**Figure 18**j). This is particularly evident close to the switchover (**Figure 19**a), where for $x = 0.11$ and $x = 0.12$ a second band is clearly visible, and also for $x \geq 0.27$, the point at which the davyne phase begins to appear in the PXRD patterns (**Figure 19**b). This band aligns with the absorption maximum of an F-centre in a Na_4 system very well. It was thus postulated that two types of F-centres were present in these materials: those in Na_4 systems, which

absorb at 500-540 nm, and those in Na_2Ca systems, which absorb at 420-435 nm. The relative intensities of the two bands depended on the relative ratios of V_{Cl} present in each system within the structure: at very low x, the majority of V_{Cl} are found in Na_4 systems and at $x \geq 0.27$, calcium begins to preferentially locate in the davyne phase, leaving behind comparatively more sodium for the sodalite phase, and thus explaining the strengthening of the band at 500-540 nm in these materials. At $0.13 \geq x \geq 0.25$, enough V_{Cl} are located in Na_2Ca systems for the dominant absorption to be at 420-435 nm.[II]
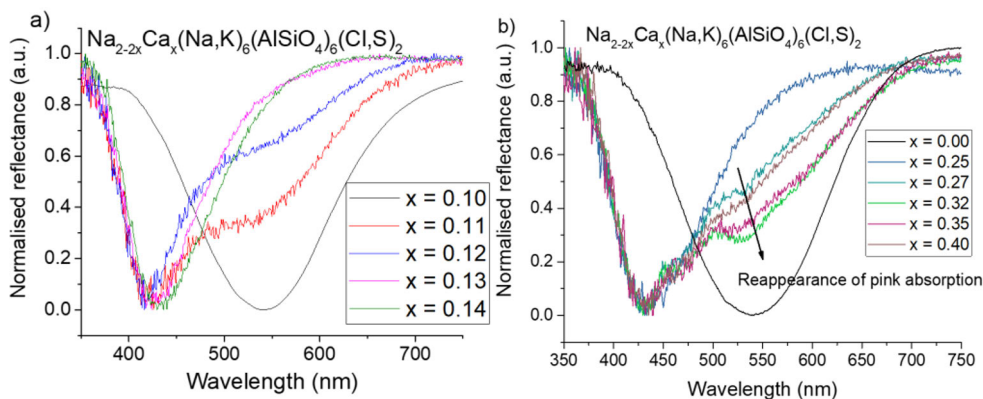
Figure 19.   a) Normalised reflectance of samples with $0.10 \leq x \leq 0.14$ after exposure to 254 nm UV, showing the changes of intensity of the pink and yellow absorption bands of the coloured form.[II] b) Normalised reflectance of samples with $0.25 \leq x \leq 0.40$ after exposure to 254 nm UV, showing the reappearance of the pink absorption band resulting from the appearance of the davyne phase.[II]

This theory was tested by studying the optical bleaching spectra and bleaching rates of materials showing both bands. The two bands were shown to have different bleaching spectra (**Figure 20**a), and also faded at different rates under visible light (**Figure 20**b, **Table 13**), confirming that they interact with visible light differently and thus arise from two different types of F-centre within the structure.[II] The two bands also had different thermal bleaching energies: the pink band in a sodalite with $x = 0.18$ fully bleached at 220 °C (thermal bleaching energy = 0.39 eV), while the yellow band remained visible at 250 °C (**Figure 20**c).[II]
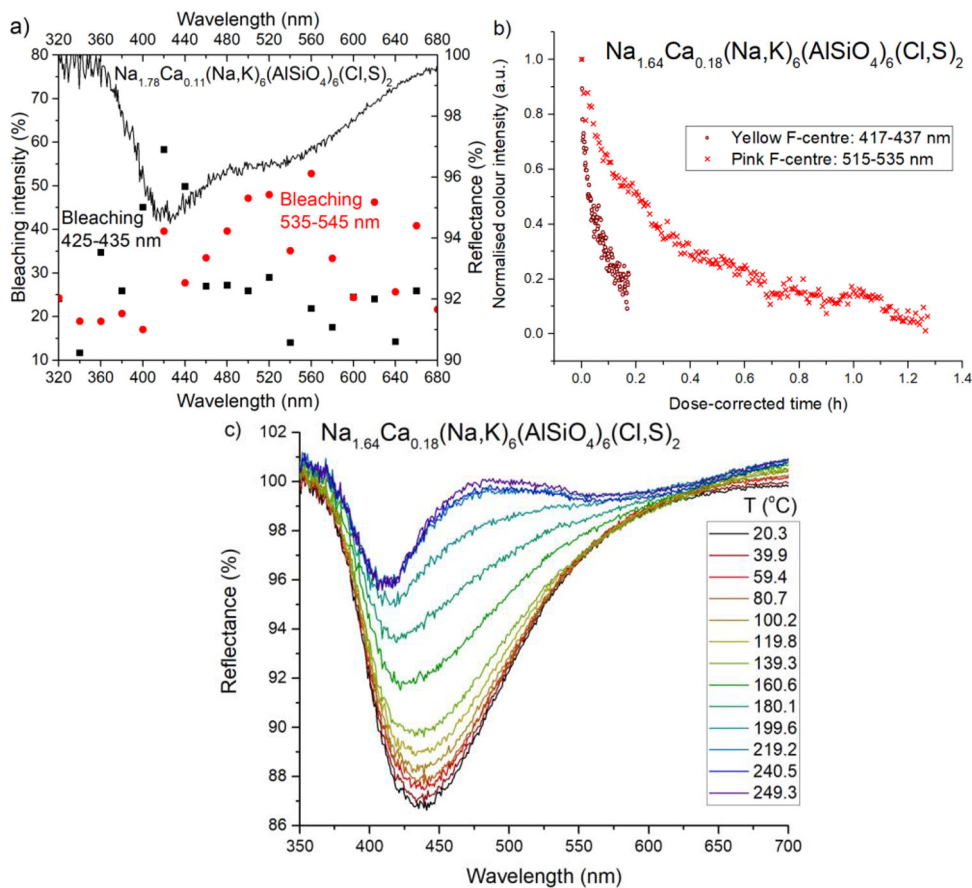
Figure 20. a) Optical bleaching spectra of the pink and yellow absorption bands of a material with $x = 0.11$ showing two independent bleaching spectra. The reflectance spectrum of the coloured form showing the two bands is also presented.[II] b) Dose-corrected bleaching curves of the pink and yellow bands in the same sample showing their different fading rates.[II] c) Change in reflectance of the coloured form of a yellow photochromic sodalite upon heating, measured using the thermotenebrescence method.[II]

Table 13. Dose-corrected parameters describing the fading of the pink and yellow F-centres in a material with $x = 0.18$.[II]

Integrated region (nm)	τ_1 (h)	$A(\tau_1)$ (%)	τ_2 (h)	$A(\tau_2)$ (%)
417-437	0.0124 ± 0.0004	32	0.202 ± 0.009	68
515-535	0.10 ± 0.01	23	0.47 ± 0.02	77

5.2.2.2   Further tuning for orange photochromism

The discovery of calcium's ability to change the position of the F-centre's absorption added another colour to sodalite's photochromism portfolio. These yellow photochromic sodalites retain the colour change's reversibility and, as for their pure sodium counterparts,[6] the colour intensity is dose-sensitive. Photochromic sodalite's F-centre absorption can as of section 5.2.1 be tuned to have a maximum anywhere between 510-680 nm. With the addition of these calcium materials, the range is expanded to 420-680 nm, which covers almost the entire visible spectrum. However, there is a gap between 440-510 nm which is yet to be filled, which would correspond to a white-to-orange colour change. Inorganic materials capable of changing from white to orange are rare, with the closest colours being pink, yellow or brown (section 2.2). It was therefore desirable to attempt to further tune sodalite such that it would exhibit a change from white to orange upon exposure to UV.

Indeed, the similar concentrations of pink and yellow F-centres in materials of formula $Na_{2-2x}Ca_x(Na,K)_6(AlSiO_4)_6(Cl,S)_2$ with $0.11 \leq x \leq 0.12$ produces a weak orange photochromism (**Figure 17**a).[II] However, this colour is very faint, and a higher contrast between coloured and uncoloured forms was desired. Based on previous evidence that larger halide ions are able to redshift the absorption maximum (Section 5.2.1, Phillips, Radler and Chenot, Williams *et al.*),[53,59,60] it was hypothesised that introducing bromine or iodine to the sodium-calcium systems discussed in 5.2.2.1 would redshift the 420-435 nm absorption band of an F-centre in the Na_2Ca system. Cl substitution with Br and I was done in small increments keeping $x = 0.25$. Samples in this study had the general formula $Na_{2-2x}Ca_x(Na,K)_6(AlSiO_4)_6(Cl,X,S)_2$, where X = Br or I.
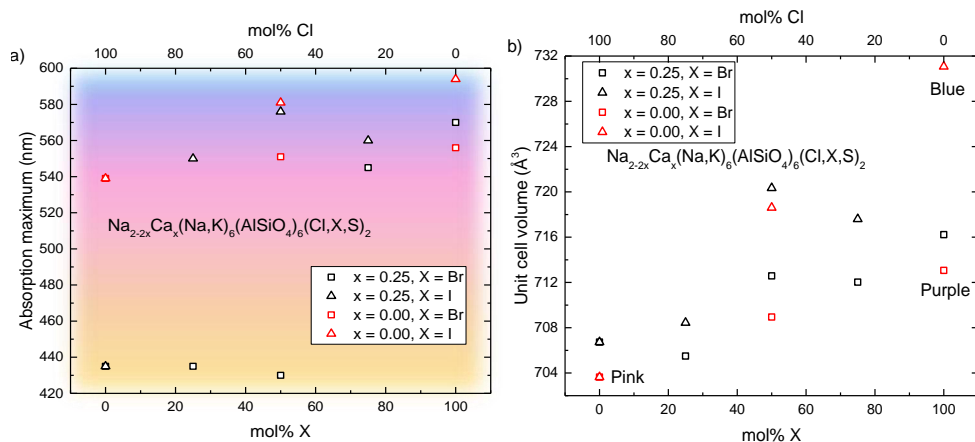
Figure 21. a) Absorption maxima after colouration with 254 nm UV of photochromic sodalites with different Cl:X ratios (X = Br, I), both with and without calcium. The background indicates the colour the material appears to the eye.[II] b) Unit cell volumes obtained by unit cell refinement of the same two sets of sodalite materials.[II]

Whilst substitution of up to 50 mol% Cl with Br retained the yellow photochromism, the position of the absorption maximum did not shift to a longer wavelength, and upon substitution of ≥ 75 mol% of Cl with Br the colour reverted back to pink (**Figure 21**a). In the case of iodine, substitution of ≥ 25 mol% of Cl with I was enough to restore the photochromism to its original pink-purple colour. A closer analysis of the reflectance minima of the materials with $x = 0.25$ compared to those with $x = 0.00$ with the same molar ratios of Cl:Br and Cl:I revealed little difference. That is, when pink or purple photochromism was observed in a material with $x = 0.25$, the absorption maxima was close to that of a similar material without calcium (**Figure 21**a). This suggests the F-centres responsible for the pink or purple colour are inside cages containing the pristine Na_4 system, rather than Na_2Ca.[II] Unit cell refinement of the PXRD data for these materials also revealed that the unit cell of a material with a certain Cl:X ratio was similar for $x = 0.25$ and $x = 0.00$ (**Figure 21**b). In **II** it was proposed that the reason for this was related to the size of the anions and the relative amounts of space in cages with Na_4 and Na_2Ca systems: larger ions locate more readily in the more spacious Na_2Ca cage, leaving the majority of V_X in Na_4 cages. Thus, the absorbance of F-centres in these types of vacancies dominates the reflectance spectra.

It remains inconclusive whether the substitution of Cl with Br or I would ever be able to redshift the absorption band of an F-centre in the Na_2Ca system. Larger concentrations of calcium would be required to increase the likelihood of a vacancy occurring in a Na_2Ca cage despite bromine and iodine's preferences to locate in such cages. However, testing this experimentally is hindered by the formation of the

davyne phase, which limits the amount of calcium that can be added to the sodalite material.[II]

5.2.3   Full range of photochromism colours

Sections 5.2.1 and 5.2.2 have presented new ways of tuning the tenebrescence colour of photochromic sodalites and significantly extended the range of absorption maxima and thus the available colour range. While the redshifting abilities of potassium iodide followed by potassium ion exchange are significant, causing a redshift of up to 80 nm compared to sodium iodosodalite, there is still room to expand the range. Johnson *et al*. showed that potassium aluminogermanate and gallosilicate iodosodalites can be synthesised hydrothermally and subjected to ion exchange without undergoing framework collapse, to produce materials with unit cell parameters ranging from 9.28-9.37 Å.[69,125] These are predicted to have an absorption maximum of > 700 nm.[53,57] Such a material would likely not show much of a visible colour change, but instead the F-centre's absorption would become apparent under infrared illumination when observed with a suitable camera or spectrometer.

Synthesis of photochromic potassium iodosodalites suitable for ion exchange made with gallium or germanium fully replacing aluminium or silicon respectively was unfortunately not successful. The hydrothermal step showed that a small amount of the sodalite phase had formed, however upon reduction (activation of the photochromism), the respective halide-free gallosilicate and aluminogermanate or other phases formed instead, and the resulting product was not photochromic sodalite (**Figure 22**a). It is uncertain why these syntheses were unsuccessful, though the length and temperature of the reduction step may have been a factor. As germanium generally produces greater lattice expansion, the synthesis was repeated using only 20 mol% germanium instead of silicon, with the addition of a sintering step in air to stabilise the material, and this was found to retain the correct structure even after reduction (**Figure 22**b). Above this amount of germanium the synthesis once again failed.
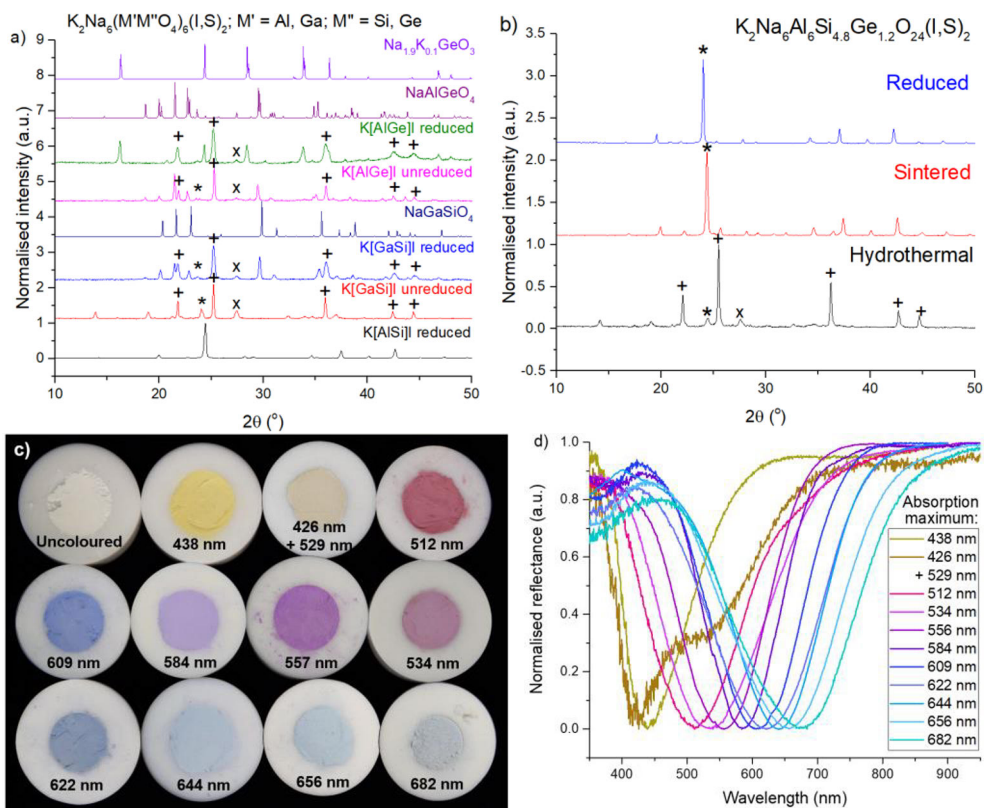
Figure 22. a) PXRD patterns of potassium iodosodalites prepared with Ga or Ge replacing Al or Si respectively. Formulae of the products are nominal. Diffractograms after hydrothermal synthesis (unreduced) and reduction (reduced) are shown. A reference aluminosilicate potassium iodosodalite's diffractogram is shown, along with references for the other predominant phases: $NaGaSiO_4$ (PDF 04-012-1419), $NaAlGeO_4$ (PDF 01-078-1172) and $K_{0.1}Na_{1.9}GeO_3$ (PDF 04-020-5434). Other phases are marked as follows: * = main peak of the sodalite phase, + = KI and × = NaI. b) Diffractograms of a potassium iodosodalite made with 20 mol% Si substituted with Ge. The differences in structure after hydrothermal synthesis, sintering and reduction are clear. The phases are marked as follows: * = main peak of the sodalite phase, + = KI and × = NaI. c) Photographs of the full range of photochromism colours available, including one material in its uncoloured form. The absorbance maxima of each material are indicated.[III] d) Normalised reflectance curves of coloured forms of the materials shown in c).[III]

With 20 mol% germanium substitution and after potassium ion exchange, these materials were found to show marginally lower energy absorption maxima than their germanium-free counterparts. This, in conjunction with the ability of calcium to blueshift the absorption maximum, brings the full range of absorption maxima to 420-682 nm, or almost the entire visible spectrum (**Figure 22**c, d).[III] However, considering that the ion-exchanged potassium iodosodalite of 5.2.1.2 has its

reflectance minimum at 675 nm, the advantage offered by 20 mol% substitution of germanium is small, and not worth the additional expense of this increasingly rare element, nor the increased hassle of such a difficult synthesis. Nevertheless, the ability to control position of the absorption maximum the range of 420-675 nm is impressive for such a simple material and is a true demonstration of its versatility. Note that the closest colour to orange obtained from a single sodalite during this work was still that of a calcium sodalite with $x = 0.11$, where both the pink and yellow absorption bands contribute to the colour (see section 5.2.2.2).[II] A true orange and green are the only colours that photochromic sodalite has not yet been made to show, due to difficulties in making the F-centre absorb in the correct region for these. This is discussed further in section 5.3.2.

5.2.4   Tuning the colouration threshold with selenium

Recent spectroscopic and computational studies of natural hackmanites and synthetic photochromic sodalites have revealed that the activation energy for photochromism, i.e. excitation of an electron from S_2^{2-} to a neighbouring V_{Cl} is 3.5-5.0 eV (250-375 nm).[6,18] Synthetic samples are generally only excited by ≤ 310 nm, while natural minerals can be coloured by lower energy UV, sometimes due to the presence of other activators than S_2^{2-} or impurities of potassium.[11,18,34] In 2018, Norrbo *et al.* studied the effect of alkali metal substitution on the activation energy of photochromism more closely, and found they were able to lower the colouration threshold. K-doped sodalite showed an excitation threshold similar to the erythemal action of human skin, while Rb-doped sodalite would colour under UVA radiation.[6] This is particularly of interest, as UVA is the dominant form of UV radiation that reaches the earth's surface.[128] Nevertheless, as discussed in 5.2.1, introduction of these larger alkali cations can affect the colour of tenebrescence, which is not always desirable, and there are limitations with how much K and Rb can enter the lattice. An alternative was therefore required. TD-DFT analyses predict that the HOMO of a diselenide (Se_2^{2-}) activator is higher than that of disulfide, as is the HOMO of the ditelluride (Te_2^{2-}) ion.[62,72] Photochromic sodalites containing selenium and tellurium instead of sulfur have been prepared before, but the effect of Se and Te on the excitation threshold was never explored.[74,78] In this study, the activation energy of colouration was directly manipulated by replacing sulfur with selenium.[III] Tellurium substitution was attempted, however all samples produced with Te were very dark in colour, and their tenebrescence was not visible to the eye.

Sulfur was replaced with selenium in increasingly large amounts in sodalites prepared with NaCl. All samples showed pink photochromism, with the activation threshold decreasing steadily as the selenium content increased (**Figure 23**a). This is believed to be related to increasing amounts of Se_2^{2-} in the material.[III] It may also

be that in materials containing both sulfur and selenium, some $(SeS)^{2-}$ activators are present, which are predicted to have an activation energy lying between that of S_2^{2-} and Se_2^{2-}. TD-DFT simulations were carried out to complement the experimental observations, and while DFT consistently overestimated the excitation energy, the calculated values followed the same trend as the experimental ones.[III] Hence, the effect of the higher energy HOMO on the transition energy from $E_2^{2-}(\pi^*) \rightarrow V_{Cl}(a_1)$ is clearly observable (**Figure 23**f, E = S, Se; see also **Figure 3**b, **A**).[III] When only selenium was used, colouration began at 410 nm and the strong colouration induced by 375 nm radiation is also a significant improvement on Norrbo *et al.*'s rubidium sodalites. This effect is also visible for other compositions showing yellow and blue tenebrescence (**Figure 23**b). There was also little difference in the position of reflectance minima across the series, showing that selenium does not affect the tenebrescence colour and thus the energy levels of the F-centre, only the activation energy of its formation (**Figure 23**c). The only drawback was the increasingly dark body colour as selenium content increased (**Figure 23**d, e).

Raman spectroscopy was used to investigate the species responsible for the darkening body colour. Sodalites containing 0 mol%, 50 mol% and 100 mol% Se were selected, and the spectra are presented in **Figure 24**a. Assignments of the peaks indicated by comparison to the literature are given in **Table 14**. The main conclusion from this study was identification of the Se_2^- radical ion responsible for the increasingly weak tenebrescence and darkening body colour. This species is responsible for the permanent colour in red ultramarines.[76,78,79] Peaks in the Raman spectrum at 330 cm^{-1} and 650 cm^{-1} from this ion are visible upon introduction of some selenium, though their strengths vary. Peaks from the sodalite structure are also visible in all samples, particularly the intense peak at 460 cm^{-1} from stretching of the $ClNa_4$ tetrahedra.

There is a small signal around 250 cm^{-1}, which may arise from the Se_2^{2-} activator involved in lowering the photochromism threshold, though it is weak and partially hidden by the Na-O vibration at 258 cm^{-1}. Likewise the usual photochromism activator S_2^{2-} may be present, but its 450 cm^{-1} vibrational mode is hidden by the strong peak at 460 cm^{-1}. Nevertheless, when considering these results alongside the reflectance spectra of the uncoloured materials (**Figure 24**b), it can be concluded that the body colour is indeed the result of Se_2^- absorption, with its λ_{max} around 490 nm.[76,78] Interestingly, when looking at the microscope images taken during Raman spectroscopy, the colour comes from orange patches surrounded by white crystals (**Figure 24**c). These areas are likely sodalite crystals rich in Se_2^-, while the white crystals do not contain so much of this colourful anion. Indeed, Raman measurements taken from each region reveal stronger signals from Se_2^- in the orange regions, and more signal from the sodalite structure in the white regions (**Figure 24**d).
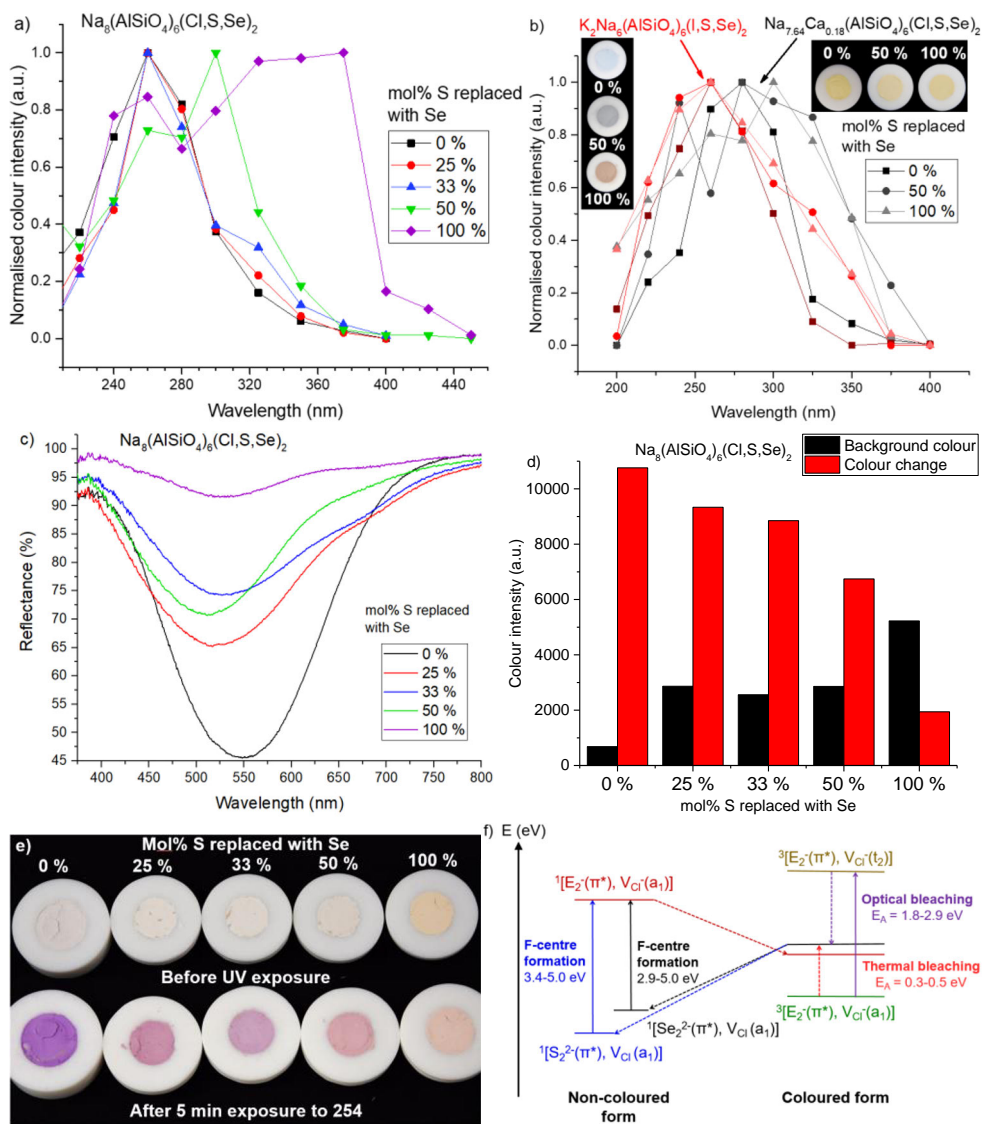
Figure 23. a) Tenebrescence excitation spectra of chlorosodalites made with sulfur and selenium.[III] b) Tenebrescence excitation spectra of sodalites made with sulfur and selenium showing yellow and blue tenebrescence (photographs of coloured forms as inserts).[III] c) Reflectance curves of chlorosodalites containing selenium after 254 nm UV exposure showing their change of colour.[III] d) Relative intensities of the body colours of chlorosodalites made with selenium, compared to the intensity of their colour changes on exposure to 5 min of 254 nm UV.[III] e) Photographs of the chlorosodalites, showing their darkening body colours and coloured forms.[III] f) Effect of selenium on the mechanism of F-centre formation and thermal and optical bleaching. Electron transfers initiated by photoexcitation are marked with solid arrows, while non-radiative thermal and geometrical relaxations are indicated by dotted arrows. As more selenium replaces sulfur, the relative number of $^1[S_2^{2-}(\pi^*), V_{Cl}(a_1)]$ decreases and $^1[Se_2^{2-}(\pi^*), V_{Cl}(a_1)]$ increases. E = S or Se.[III]
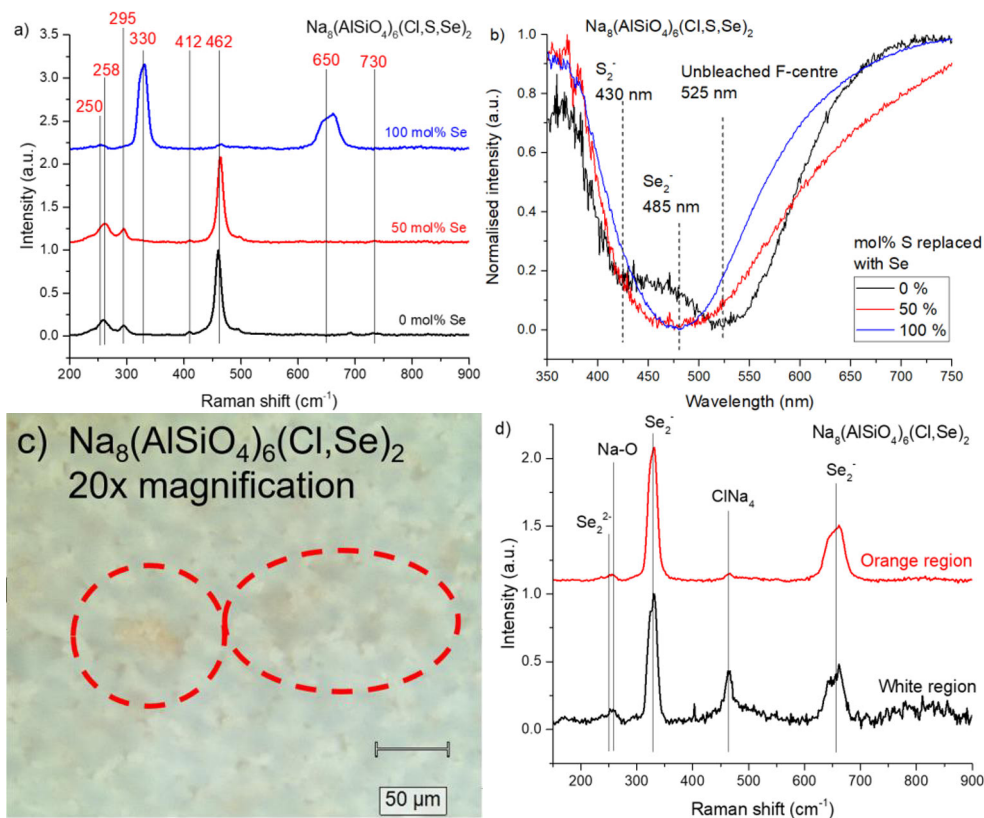
Figure 24. a) Raman spectra of sodium chlorosodalites made with varying amounts of sulfur and selenium. The peaks and their Raman shifts are indicated on the figure.[III] b) Normalised reflectance spectra of the body colours of the materials in a) with the species responsible indicated. The white reference was MgO.[III] c) Microscope images taken during Raman spectroscopy showing variation in body colour and orange, Se_2^--rich regions in the powder (circled in red). d) Raman spectra showing the difference in signal intensities between white and orange regions of the powder.

Table 14. Peaks in the Raman spectra of chlorosodalites made with sulfur and selenium and their assignments based on the literature.[III]

Peak (cm⁻¹)	Assignment	Reference
250	Se_2^{2-}	Reinen & Lindner, 1999[78]
258	Na-O	Zahoransky *et al.,* 2016[7]
295	Symmetric Al/Si-tetrahedra	Zahoransky *et al.,* 2016[7]
330	Se_2^-	Reinen & Lindner, 1999[78]; Clark *et al.,* 1983[76]
412	SO_4^{2-}	Zahoransky *et al.,* 2016[7]
462	$ClNa_4$-tetrahedra	Zahoransky *et al.,* 2016[7]
650	Se_2^-	Clark *et al.,* 1983[76]
730	Bending frequency of T_2 mode of framework	Zahoransky *et al.,* 2016[7]

Optical and thermal bleaching measurements, discussed in **III**, revealed that regardless of S:Se ratio, these materials bleach in the expected region, with optimal bleaching close to the absorption maximum of around 530 nm. This again supports the theory that selenium does not affect the F-centre's energy levels.[III] The gradually decreasing excitation threshold as Se content increased did, as expected, lower the energy at which optical bleaching begins. Thermotenebrescence measurements revealed introduction of selenium lowers the thermal bleaching energy from 0.5 eV to 0.3 eV, possibly due to some destabilisation of the F-centre, similar to that induced by potassium.[62]

This steady control of the excitation threshold that also does not affect the tenebrescence colour allows these materials to be easily controlled for applications where a certain colour and excitation threshold are desired. In particular, simultaneous passive detection and dosimetry of UVA and UVC is possible when a tuned selenosodalite is mixed with a sulfur-containing sodalite of different tenebrescence colour, as explored in 5.3.3 and **III**. The main drawback of using selenium to tune the activation energy of F-centre formation is its tendency to form the Se_2^- ion instead of the desired Se_2^{2-}. This results in weakened photochromism, as the amount of S_2^{2-} activators present decreases with increasing selenium content, and they are not so readily replaced with Se_2^{2-}. This could be mitigated using stronger reducing conditions to ensure full reduction of selenium to Se_2^{2-}, which hopefully would also result in paler body colours. Another pleasing feature of these materials is that they also retain the PL and PeL properties of their sulfur counterparts.[III]

5.2.5 Conclusions

In this section, two new methods for tuning the photochromism colour of photochromic sodalites have been presented. Previously the available range of absorption maxima was between 510-640 nm, corresponding to pink, purple and blue tenebrescence. Through utilising the effects of potassium and calcium on the vacancy size and F-centre's energy levels, this range has been expanded to 420-675 nm, encompassing almost the entire visible spectrum, and without the need for rarer elements like gallium and germanium. Potassium ion exchange can be exploited to further broaden this range, though contrary to predictions by TD-DFT, this was unable to lower the excitation threshold any more than use of a potassium salt during solid-state synthesis.

The mechanism of yellow photochromism in sodalite has been studied and verified through agreeing computational and experimental results. These unusual materials have been shown to contain not one, but two F-centres, which function independently of one another. Attempts to further tune the F-centre's energy levels once degeneracy has been broken were unsuccessful, in part because the unwanted by-product davyne restricts the maximum amount of calcium that can be incorporated in the structure while retaining the yellow photochromic effect. Further study close to the yellow → pink switchover point in calcium-containing bromosodalites may reveal that this is possible.

Finally, the effect of selenium on the activation energy of F-centre formation was shown. Selenium provides a more reliable way to tune the excitation than potassium, with adjustment of the S:Se ratio providing incremental change in the colouration threshold. Moreover, Se does not significantly affect the tenebrescence colour in the same way as potassium, meaning it is the superior choice for lowering the excitation threshold. Destabilisation of the F-centre leading to a lowered thermal bleaching energy is a drawback, though this has been shown in **III** to be no worse than that of potassium. The issue of darkening body colour can also possibly be mitigated by using harsher reducing conditions to try and prevent the formation of the Se_2^- species responsible.

It can therefore be said that photochromic sodalites can be tuned to turn from white to almost any colour under UVA, UVB or UVC radiation through simple adjustments to the formula and stoichiometry. Moreover, the colour can be tuned for the most part independently of the excitation threshold, and vice versa. The next section, 5.3, will cover how these highly tuned materials can be incorporated into a range of applications, in which their robustness and low cost may prove particularly useful.

5.3 Applications

5.3.1 Blue light detection

The first application for photochromic sodalites to be discussed in this thesis is that of blue light detection. As discussed in section 2.6.1, the human eye is sensitive to blue light and overexposure can damage the retina and disrupt the circadian rhythm. As humans spend increasing amounts of time indoors under cool LED lighting and in front of computer and smartphone screens, there is an increasing need for them to monitor and regulate their exposure to blue light.

The bleaching spectra obtained from yellow photochromic sodalites made with calcium (see section 5.2.2) reveal that these types of sodalites are particularly sensitive to blue light (**Figure 25**a).[II] Their suitability for blue light detection was further tested by measuring the fading of the yellow colour under five different light sources (**Figure 25**b). The additional sensitivity of the pink Na_4 F-centres to green light (**Figure 20**a) means that the colour was best bleached by a WLED-LCD computer screen, which emits blue and green light strongly (**Figure 25**c).[II] A schematic of how this kind of sodalite could be used in a small device used for monitoring blue light exposure is shown in **Figure 25**e. In **1**, the yellow sodalite is coloured with UV radiation. The colour intensity can be read using a mobile phone application (**2**),[6] and with a suitable application and calibration curve (**Figure 25**d) the dose of blue light to which the user was exposed (**3**) can be estimated (**4**).[129,130] Such a device could be used in an office or home environment.
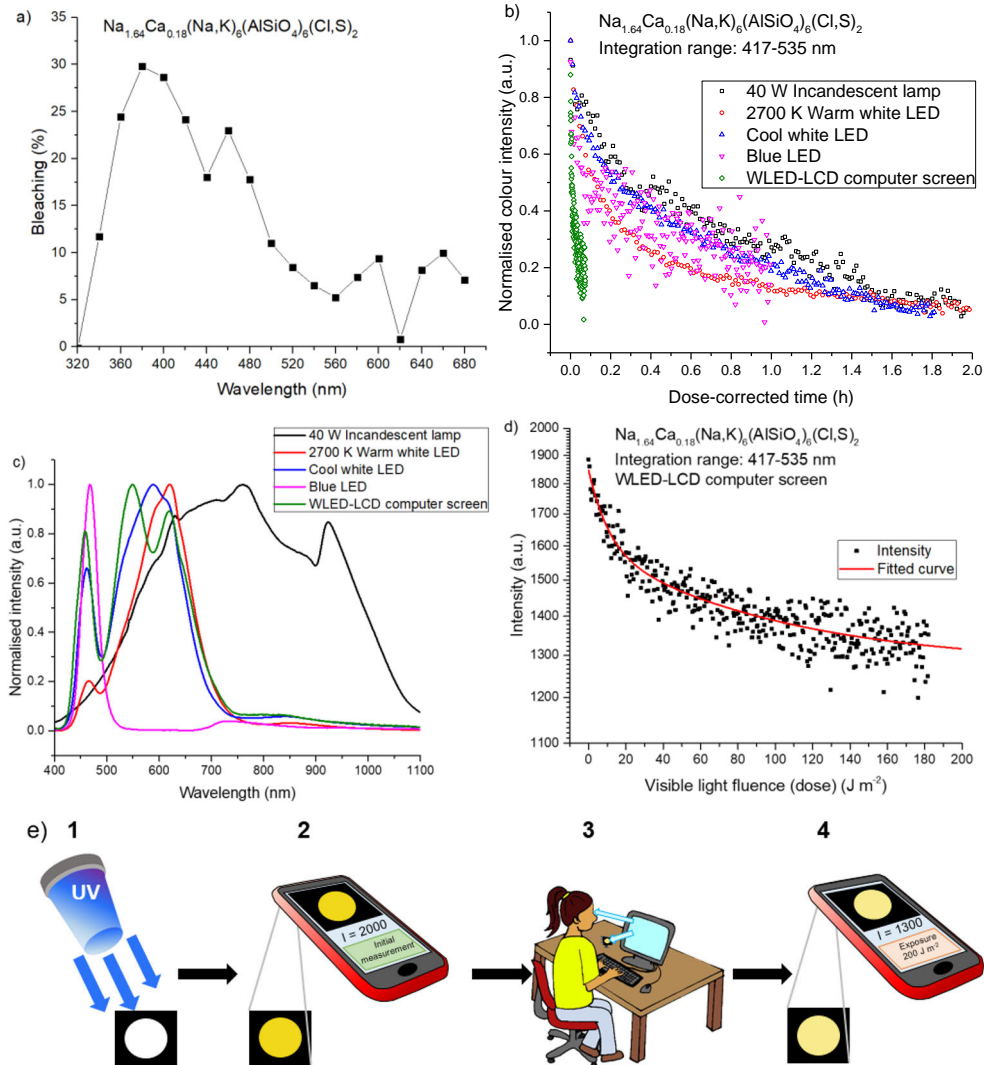
Figure 25. a) Optical bleaching spectrum of yellow photochromic sodalite.[II] b) Dose-corrected fading of yellow photochromism under different light sources.[II] c) Emission spectra of the light sources used in b).[II] d) Calibration curve for blue light dosimetry. e) Schematic showing how yellow photochromic sodalite could be used in everyday blue light exposure monitoring. In **2**, the user can save the initial measurement (I = 2000) and in **4** the measured intensity is I = 1300, corresponding to an exposure of 200 J m^{-2}.

5.3.2 Photochromic sodalite mixes for complete colour tuning

In section 5.2.3, the full range of possible colours photochromic sodalite can be tuned to display are shown. Sections 5.2.2.2 and 5.2.3 discuss the issues in obtaining a white-to-orange colour change, due to difficulty in shifting the energy levels of the

F-centre to absorb in the 450-490 nm region.[II] A white-to-green colour change is also difficult to obtain, because photochromic sodalites usually only contain one F-centre, and absorption in both the red and blue regions are required for a green colour. While some photochromic sodalites do have two types of F-centre in their structures, the difficulties of tuning them independently from one another (see 5.2.2.2) makes obtaining a white-to-green photochromic material challenging.[II] However, in **III** it is shown that this shortfall can easily be mitigated by mixing pink, blue and yellow photochromic sodalites in appropriate ratios, similarly to paints or pigments. These three colours can easily and reliably be obtained from the following compositions: pink – $Na_8(AlSiO_4)_6(Cl,S)_2$, yellow – $Na_{1.64}Ca_{0.18}(Na,K)_6(AlSiO_4)_6(Cl,S)_2$ and blue – $Na_8(AlSiO_4)_6(I,S)_2$ or $K_2Na_6(AlSiO_4)_6(Br,S)_2$ (**Figure 26**a).
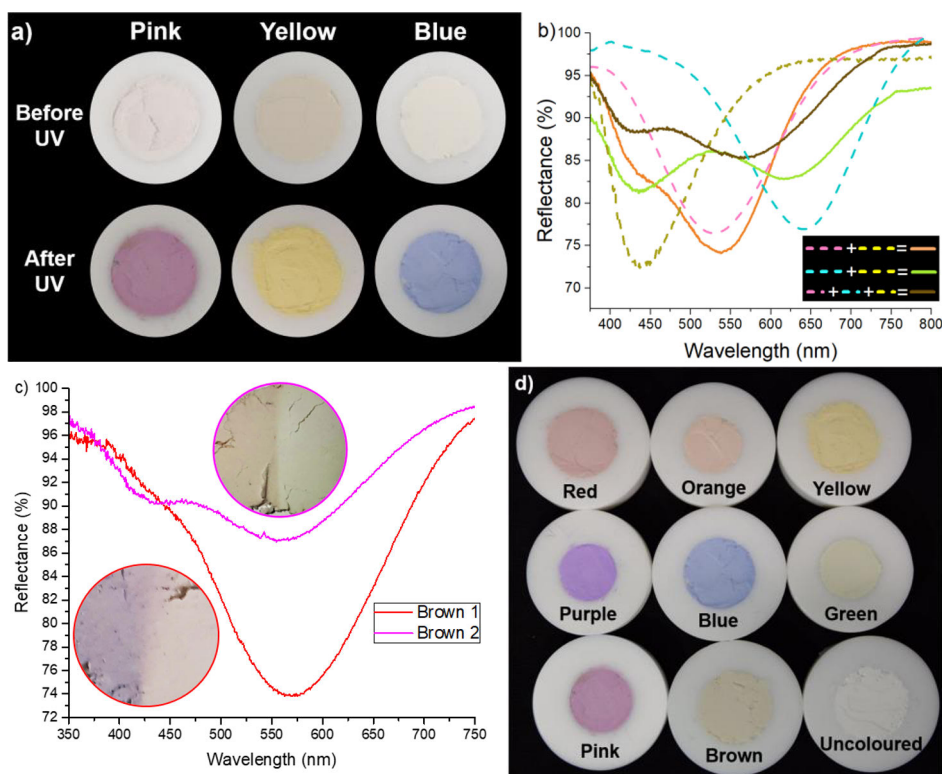
Figure 26.   a) Easily synthesisable pink, yellow and blue photochromic sodalites before and after UV irradiation used to produce green, orange and brown photochromic mixes. b) Reflectance spectra of the coloured forms of the pink, yellow and blue components (dashed lines), as well as those of mixes showing orange, green and brown photochromism (solid lines). The parent sodalites used in each mix are indicated in the legend.[III] c) Brown 1 is the result of mixing roughly equal amounts of pink, blue and yellow sodalites, and appears purple. Brown 2 has been corrected by addition of extra yellow sodalite. d) The full portfolio of photochromic colours available in sodalites.[III]

Mixing these materials presents some challenges, since they are all usually colourless. However, quick irradiation of a small sample with 254 nm UV can be done to confirm the current colour. Approximate ratios can be estimated from the relative absorbance intensities of each of the three starting materials (**Figure 26**b) and an understanding of how the eye perceives colour – for example, even though the absorption intensities of all three components may be the same, comparatively more yellow sodalite may be needed to obtain the desired colour, as yellow appears to be the palest of the three primary colours. In **Figure 26**c, a brown mix was made by initially mixing all three colours in roughly equal amounts. The result was too purple, as evidenced by the uneven absorption intensities in reflectance spectrum. Brown 2 was corrected by adding more yellow sodalite to the mix, and the result is a warm brown with a more uniform absorption in the visible region. In a commercial setting, large batches of pink, yellow and blue sodalite would be tested and characterised after mixing in different ratios to produce a palette of available colours, after which mixing could be automated. This provides a very cheap and easy way of producing robust, low-cost and sustainable photochromic materials able to change from white to truly any desired colour (**Figure 26**d). These could then see use in any of the applications already mentioned in the literature, with the added bonus of colour customisation. The mixes also retain the luminescence properties of their parent sodalites, which provides an added nuance for applications such as security marking and tagging. This is discussed more in section 5.3.3.

5.3.3   Photochromic sodalite mixes as passive detectors and security markers

The pink, yellow and blue sodalites of 5.3.2 used to make green, brown and other colours were all excitable only by UVC or UVB radiation. However, following the success of selenium substitution of section 5.2.4, it came to mind to attempt to mix two sodalites of contrasting colours and with different excitation thresholds, to produce a material which changes from white to one of two or three colours, depending on the wavelength of UV it is exposed to (**Figure 27**a).[III] Such a material could serve as a qualitative passive detector of UV radiation, by means of comparing the colour to a chart similarly to how pH paper is used. The colour would indicate the type of radiation the sodalite mix was exposed to, with the exact shade also dependent on the exposure time (**Figure 27**b).[III] The material would identify the radiation type passively, making use of sodalite's robust nature in situations where electronics may get damaged, such as in extremes of temperature. In **Figure 27**b the mix has been cast into a film, however this application also works using pure powder or when the mix has been embedded into another medium.
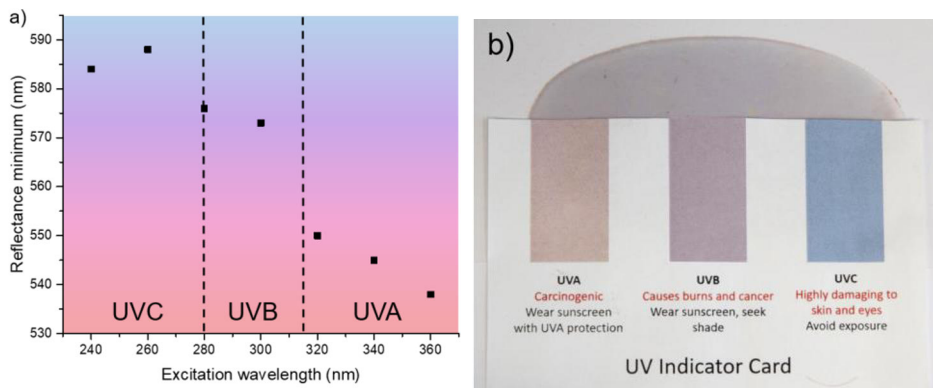
Figure 27. a) Change in reflectance minimum and therefore tenebrescence colour of a sodalite mix after excitation by different wavelengths of UV.[III] b) Demonstration of how such a mix could be used as a passive detector for qualitative detection of radiation type. After exposure to an unknown source of radiation, the colour is compared to a reference card and the radiation type identified.[III]

A variety of compositions were considered, based on the material's tenebrescence colour and measured excitation threshold. Those excited by UVA radiation contained selenium or potassium, which are both known to lower the excitation threshold (**Figure 28**a, **Table 15**).[6,III] Those excited by higher energy radiation were also chosen based on their colour and excitation thresholds, this time aiming for an excitation threshold in the UVB-UVC region (**Figure 28**b). Two sodalites of contrasting colours were then paired up and tested by mixing in roughly equal amounts. In **Figure 28**c, the compatibility of a blue sodalite excited by UVA and a pink sodalite excited by UVC are considered, while in **Figure 28**d, a yellow sodalite excited with UVA is considered as a possible pair to the same pink sodalite in **Figure 28**c. Though both the blue and yellow sodalites in **Figure 28**c-d are excited by UVC, the pink sodalite is much more strongly coloured by this type of radiation, and thus will dominate the mix's reflectance spectrum and the observed colour change.
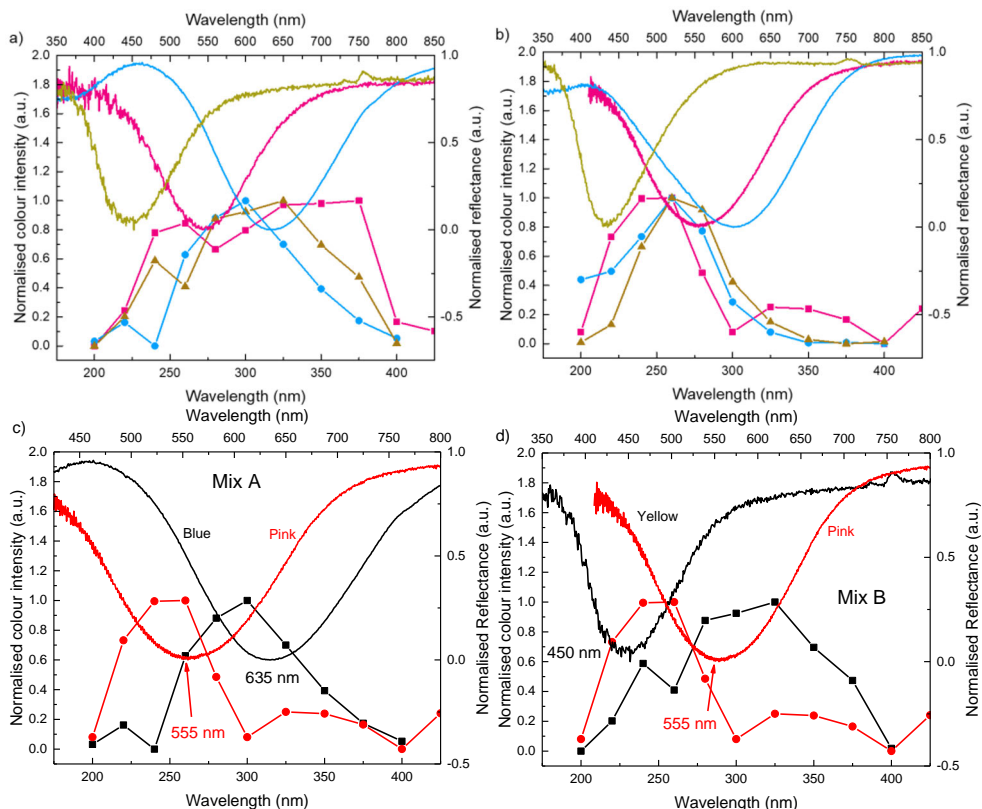
Figure 28. a) Pink, yellow and blue photochromic sodalites excitable by UVA radiation considered for sodalite mix preparation. Photochromism colours are indicated by the line colours on the graph. b) Pink, yellow and blue photochromic sodalites excitable by UVB and UVC radiation considered for sodalite mix preparation. Photochromism colours are indicated by the line colours on the graph. c) Excitation spectra and reflectance spectra of the two parent sodalites chosen to make mix A.[III] d) Excitation spectra and reflectance spectra of the two parent sodalites chosen to make mix B.[III]

Table 15. Further details of the photochromic properties of the sodalites used for preparing mixes in **Figure 28**, including their compositions.

Excitation region	Excitation threshold (nm)	Tenebrescence colour	λ_{max} (nm)	Composition
UVA	425	Pink	545	$Na_8(AlSiO_4)_6(Cl,Se)_2$
	375	Blue	635	$K_2Na_6(AlSiO_4)_6(I,S)_2$
	375	Yellow	450	$Na_{7.64}Ca_{0.18}(AlSiO_4)_6(Cl,Se)_2$
UVC	280	Pink	555	$LiNa_7(AlSiO_4)_6(Br,S)_2$
	300	Blue	601	$LiNa_7(AlSiO_4)_6(I,S)_2$
	300	Yellow	430	$Na_{1.69}Ca_{0.155}(Na,K)_6 (AlSiO_4)_6(Cl,S)_2$

Many combinations of the above materials were tested. In the best cases, the difference in the mixes' tenebrescence colour upon excitation with UVA or UVC radiation is clearly visible to the eye (**Figure 29**a, b).[III] To study this further, reflectance spectra were measured after excitation by several wavelengths of UV produced by a Xe lamp coupled to a monochromator. The changes in reflectance spectra with respect to excitation wavelength are clear (**Figure 29**c, d). Interestingly, when a yellow sodalite was used, the two bands remain separate, with their relative intensities changing depending on excitation wavelength, whereas for the pink and blue mix, the bands appear to merge and instead the observed position of the reflectance minimum shifts.
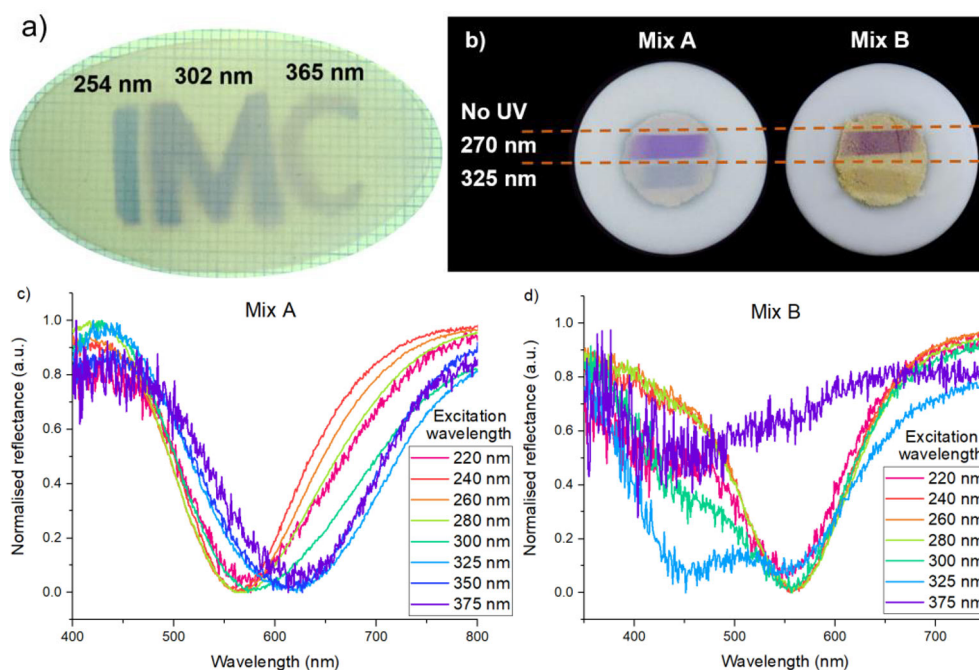
Figure 29.   a) A film cast from a sodalite mix showing three different tenebrescence colours dependent on excitation wavelength. The acronym "IMC" was written on the tape using three different UV lamps and the aid of a stencil.[III] b) Photographs of mixes A and B after excitation with UVA (325 nm) and UVC (270 nm) radiation, showing their two different tenebrescence colours.[III] c) Reflectance spectra of mix A after 5 min excitation by 8 different wavelengths of UV.[III] d) Reflectance spectra of mix B after 5 min excitation by 7 different wavelengths of UV.[III]

In **III**, one such mix was used to demonstrate how these materials could be used to passively detect and quantify the dose of two types of UV radiation simultaneously. The mix used was much like that of **Figure 29**c (Mix A), where the reflectance minimum gradually shifts as the excitation wavelength increased. In **III**, a

mathematical model was developed and tested for its ability to estimate the doses of UVA and UVC radiation the material received. It was found to be able to predict the fluences of each radiation type received with reasonable accuracy, provided the UVC dose was greater than that of UVA.[III] This is thought to be due to the strength of the response under each radiation type. This was also tested on a smaller scale for another mix, and was found to work in the same way, though with the same issues. Nevertheless, the model could be further improved to accurately estimate the fluences of UVA and UVC radiation regardless of their relative intensities, though that was out of the scope of this work.

These mixes would also make attractive security markers. Not only do they show unique photochromism properties, but they also retain the luminescence properties of the two components used to produce the mix. **Figure 30**a shows photographs of the mix presented in **Figure 28**c and **Figure 29**b-c (Mix A) under the illumination of three different UV wavelengths, where we see orange-red luminescence excited by 365 nm and blue-white luminescence under 302 nm and 254 nm, as well as persistent luminescence.[III] **Figure 30**b shows the luminescence spectra compared to those of the blue sodalite component, which are identical. The weakened intensity is the result of dilution of the blue sodalite component by the pink sodalite, which did not show any strong luminescence. With five different optical signals originating from the same material, this would make an ideal component for anti-counterfeiting inks or coatings or for invisible tagging. Were both sodalite components to be luminescent, yet another layer of complexity would be added, making these materials even more challenging to imitate.
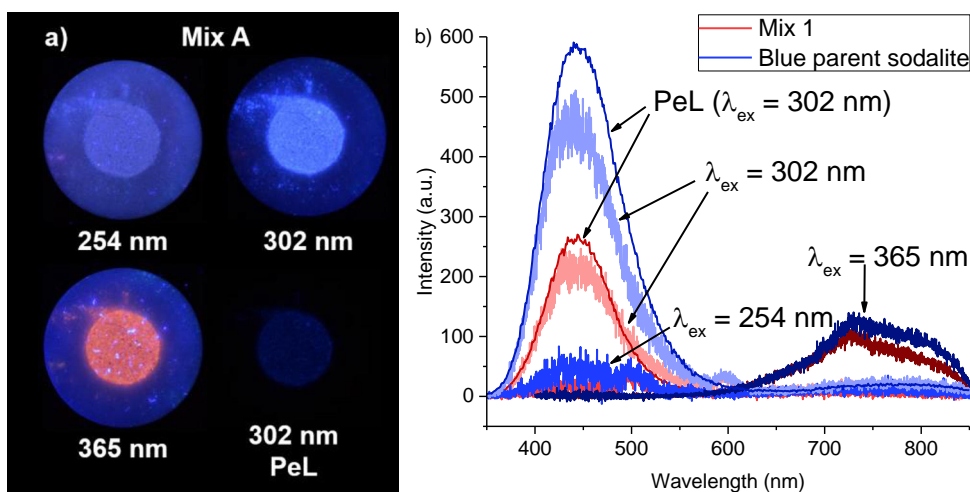
Figure 30.   a) Photographs of photo- (PL) and persistent luminescence (PeL) of Mix A under the given UV wavelengths.[III] b) PL and PeL spectra of Mix A compared to its blue sodalite component, showing identical, if weaker luminescence of the mix.[III]

5.3.4   Tuned photochromic sodalites for X-ray imaging

When X-rays interact with matter, they interact with the electron cloud surrounding each atom, which can cause a variety of effects such as scattering of the X-rays, photoelectric absorption and Compton effects.[101,103] The X-ray induced tenebrescence efficiency curves of Vuori *et al*. for different sodalites seem to follow a similar trend to that of their photoelectric absorption coefficients at different X-ray energies, suggesting photoelectric absorption, particularly close to the K-edge, is crucial for good colouration.[5] The decrease in colouration intensity with increasing X-ray energy is disadvantageous from the perspective of application in X-ray imaging, which is often done using X-rays of ≥ 20 keV in energy, or for non-destructive testing ≥ 100 keV.[101,102,131] Moreover, the doses required for photochromic sodalite to produce a clear image of an organic sample are high (105 mSv), meaning sodalite requires some optimisation for this application.

Considering the broad range of compositions tested in 5.2.1, many of which contain heavier elements than those of chlorosodalite, it was of interest to test their response under X-rays. Due to the penetrating nature of X-rays compared to UV radiation, it was impossible to compare doses of the two, and the resources to measure the photon fluxes of each radiation type were not available. However, by measuring each material's response to UV radiation (**Figure 31**a), a sense of the depth of colouration achievable with respect to exposure time (i.e., dose) can be gauged, and then compared to the response under X-rays to see if sensitisation was achieved (**Figure 31**b). The X-ray source used was the silver anode of the XRF device described in section 4.2.1.4, with a characteristic emission of 22 keV but working at a tension of 50 kV, meaning bremsstrahlung emission up to 50 keV was produced by the tube.[132,133] This emission goes beyond the K-edge of iodine, and when looking at a plot of the photoelectric absorption coefficients of these sodalites (**Figure 31**c), we see that iodosodalite absorbs X-rays over 10 times as strongly as chlorosodalite for photons of energy ≥ 33 keV.[III]
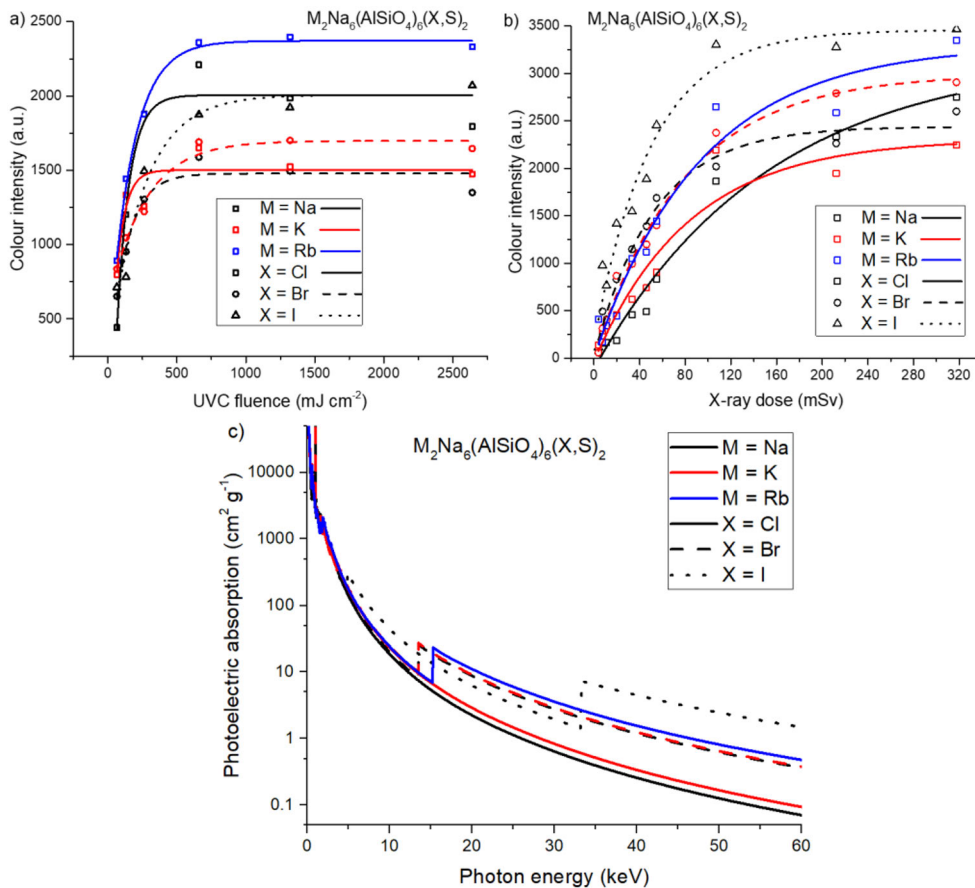
Figure 31.　a) Rise in colouration intensity with respect to UV fluence (dose) for photochromic sodalites of nominal formula $M_2Na_6(AlSiO_4)_6(X,S)_2$.[III] b) Rise in colouration of the same materials upon exposure to X-rays from a 50 kV Ag-anode X-ray tube.[III] c) Photoelectric absorption coefficients for the same materials as determined from the NIST X-ray Form Factor, Attenuation and Scattering tables.[134,III]

When comparing **Figure 31**a and **Figure 31**b, sensitisation to X-rays is indeed observed. Under UV, the rubidium sodalite colours the most strongly, followed by sodium chloro- and iodosodalite.[III] It is assumed that the plateau regions in **Figure 31**a correspond to the point where all possible F-centres have formed in the material. Therefore, the rubidium sodalite contains the most F-centres, and the sodium chloro- and iodosodalites roughly equal amounts of F-centres. Under X-rays, however, the iodosodalite colours most strongly, and also most rapidly, i.e., smaller doses are needed to produce the same colour intensity in iodosodalite as its rubidium- and sodium-containing chlorosodalite counterparts. Rubidium chlorosodalite is the second best performer under X-rays, which is in fitting with the position of its K-edge at 15.2 keV.[134,135] At low doses, the bromosodalites are superior to the

chlorosodalites, though at higher doses their generally weaker colour becomes a limiting factor (**Figure 31**a). The sudden rise of colour intensity at doses of > 120 mSv for the sodium chlorosodalite suggests that at high enough doses, i.e. long enough exposure times, all the F-centres will be populated, similarly to after long exposure to UV. However, due to the weak photoelectric absorption of X-rays by chlorosodalite compared to bromo and iodosodalites, the colour changes more slowly. In fact, the maximum colour intensities obtained by fitting curves to the data points in **Figure 31**a and **Figure 31**b show that regardless of excitation radiation type, the relative maximum colour intensities of the six compositions tested remains constant: RbCl ~ NaI ~ NaCl > KBr > KCl ~ NaBr (**Table 16**). This fits the theory that colour intensity relates to F-centre density, and colour intensity plateaus once all F-centres are populated. Sensitisation is evident in the rate at which the materials colour under each radiation type. These rates are compared in **Table 16**. The reason why those sodalites with larger ions colour more slowly under UV is unclear, and is contrary to the accounts of Williams and Chang, who claimed that their bromo- and iodosodalites colour faster than chlorosodalites.[20,21]

Table 16.   Maximum colour intensities obtained from fitting the data points in **Figure 31**a and **Figure 31**b. The materials' compositions are described as $M_2Na_6(AlSiO_4)_6(X,S)_2$. The times taken to reach 95 % of the colour intensity under UV and X-rays are indicated to show the relative rates of colouration.

Metal, M	Halogen, X	Maximum colour intensity (a.u.)		Time to reach 95 % of maximum colour intensity	
		254 nm UV	X-ray	UV (min)	X-ray (h)
Na	Cl	2000	3200	1.20	4.38
Na	Br	1500	2400	1.43	1.50
Na	I	2000	3500	2.70	1.74
K	Cl	1500	2300	0.80	2.38
K	Br	1700	3000	2.57	2.24
Rb	Cl	2400	3300	1.83	2.67

In light of iodosodalite's increased sensitivity to X-rays, its suitability for X-ray imaging was tested. In **III**, it was demonstrated that iodosodalite film is able to produce images of an organic sample (in this case, a deceased flying ant) of equal clarity using less than half the dose required of chlorosodalite. The blue colour also appears darker to the eye, improving the perceived contrast (**Figure 32**a). Vuori *et al.*'s proposed application in electronics quality control was also tested,[5] and the iodosodalite film was able to produce a clear image of the internal electronics of a

micro SD adapter, despite the X-ray source being softer than those usually used in such quality control (**Figure 32**b).[101,102] It is believed that this material would perform even better under harder X-rays, which would pass more readily through the sample, and also be more strongly absorbed by the iodosodalite. Chlorosodalite was not able to image such a dense sample at the 107 mSv dose used.
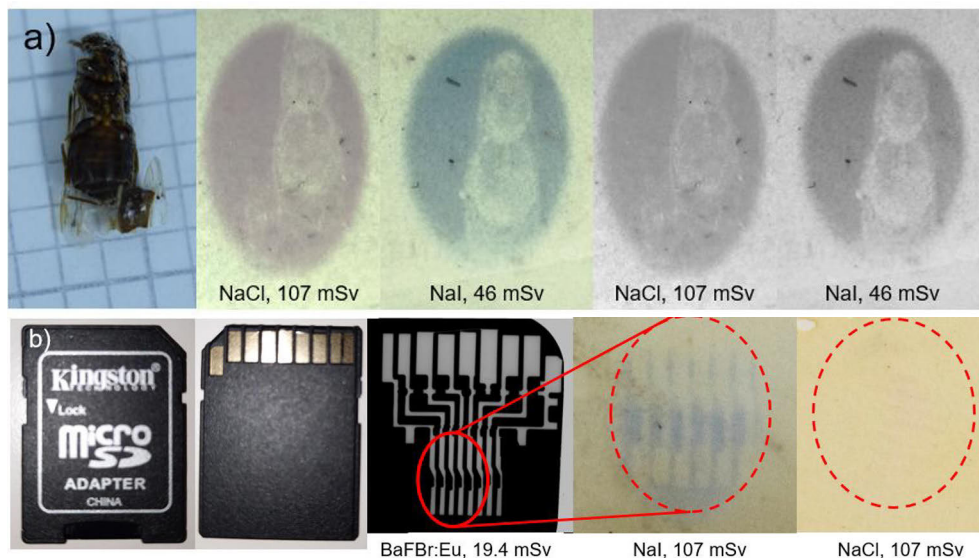
Figure 32. a) X-ray images of a deceased flying ant (left) taken with chlorosodalite (NaCl) and iodosodalite (NaI) using different doses. The images are also shown in greyscale to highlight the stronger contrast produced by the blue iodosodalite.[III] b) X-ray images of the internal electronics of an SD adapter. As the internal structure is not visible to the eye, a reference image was taken using a commercial computed radiography imaging plate. The structure is visible on the iodosodalite film after 107 mSv of radiation, but is not clear on the chlorosodalite film with the same dose.[III]

Thus, it is clear that photochromic sodalites can be sensitised to X-rays simply by substituting chlorine for iodine during synthesis. As discussed in **III**, a marginal improvement to the photoelectric absorption could be made through potassium or rubidium substitution, though incorporating enough rubidium into the structure for a significant effect may be challenging (see section 5.2.1). Nevertheless, cutting the required dose in half is a notable improvement, and these materials are expected to respond even better to higher-energy X-rays.

5.3.5   Conclusions

Section 5.3 presents two new applications for highly tuned photochromic sodalites: a passive blue light detector and dosimeter, which makes use of the particular

sensitivity the yellow photochromic sodalites of 5.2.2 have to blue light, and for use in passive dosimetry of two types of radiation simultaneously. The mathematical model used for simultaneous UVA and UVC dosimetry could be adjusted with the calibration data obtained from other mixes and subsequently commercialised. This section also shows how the tuning methods used throughout this thesis and in the associated publications can be used to improve already proposed applications, such as X-ray imaging.

The idea of mixing two different sodalites with different properties is simple, yet facilitates an expansion in the portfolio of available tenebrescence colours. There are certainly other robust inorganic photochromic materials available which are able to change from white to similar colours, though the low cost, low toxicity and abundancy of all starting materials needed to produce the key pink, yellow and blue sodalites required for complete colour tuning undoubtedly strengthen sodalite's position as an attractive alternative to these. Furthermore, due to the retention of any luminescence properties and the possibility to incorporate materials with differing excitation thresholds, these sodalite mixes would make very durable and unique security markers. Meanwhile, many other proposed applications are made more viable and attractive with the addition of colour customisation and control of the excitation thresholds, including UV indexing, radiation sensing and optical multiplexing. This is even further improved when considering that many of these tuned materials also show photo- and persistent luminescence properties, often of different colours, though further discussion of those is outside the scope of this work.

6 Summary and Outlook

This doctoral thesis and associated publications represent an in-depth study of all the known ways to tune the photochromism of sodalite, including ones never presented in the literature before this research, to gain as much control as possible on the colour and excitation threshold. Such control has improved photochromic sodalite's suitability for previously proposed applications (dosimetry, sensing, security marking, imaging, optical multiplexing)[6,58,85,108] as well as demonstrating its suitability for new ones, including as a blue light detector.

Three zeolite-free synthesis methods were tested alongside synthesis from zeolite A, to test whether greater structural tuning and thus control over the colour and excitation threshold could be obtained by using simpler starting materials. Of these, only the hydrothermal method produced good quality tenebrescent materials, and the advantages it offered were small. Excellent control of the photochromism property is obtainable via a solid-state synthesis from zeolite A, though the hydrothermal method is required for introduction of gallium and germanium into the structure for maximum unit cell expansion.

The work describes how simple substitutions of one salt for another, particularly the use of potassium salts and calcium chloride, facilitated a significant expansion in the range of available absorption maxima from 520-640 nm to 420-680 nm, and discusses how the exact colour can be chosen from within that range. Of these, the most surprising discovery was that of yellow photochromism through partial substitution of sodium with calcium. Potassium-exchanged sodalites were also shown to be able to change from white to a blue-green shade similar to those made with germanium,[53] but without the need for this increasingly rare element. Despite the range of available λ_{max} encompassing almost the entire visible spectrum, a true white-to-orange colour change was not achieved from a single sodalite in this work. However, the discovery of yellow tenebrescence allowed this shortfall to be made up for by mixing pink and yellow photochromic sodalites together. The availability of all three primary colours in fact means any desired colour is achievable in photochromic sodalites, without compromising their low cost and robust nature.

The activation energy of colouration was also controlled through gradual substitution of sulfur with selenium. This was shown to have a less significant effect

on the photochromism colour compared to other methods of tuning the excitation threshold.[6] Hence, the colour and excitation threshold can be tuned independently of one another. This allows almost complete customisation of the material for the user's needs.

Nevertheless, there are still many things left unstudied concerning the tuning of photochromic sodalites. For example, the effect of other cations of 2+ charge, such as Mg^{2+}, Sr^{2+}, Ba^{2+} and Zn^{2+}, could be investigated to see if a similar effect to that of calcium is produced or not. The effect on the F-centre's energy levels as a result of changing crystal field and vacancy size from these ions may reveal a pathway to intrinsic orange tenebrescence. Alternatively, sodium-calcium chlorobromosodalites could be studied closer to the changeover from yellow to pink photochromism to see if the ratio of pink to yellow F-centres could be adjusted to give a stronger orange colour than that of the material in **Figure 22**c.

During the yellow photochromism study, the total amount of NaCl and $CaCl_2$ used was kept constant relative to the metals, meaning as calcium content increased, so did the amount of chlorine. A study by TGA similar to that done during the zeolite-free synthesis (**Figure 7**b) could reveal a better synthesis temperature for these materials in which more chlorine escapes the structure, thus creating more vacancies and a stronger yellow colour. However, care must be taken to avoid the production of nepheline or any other unwanted by-products.

Further study on selenium-containing sodalites is required to limit the darkening of the body colour as selenium content increases. This could be extended to tellurium as well. It is mentioned in section 5.2.4 that tellurium sodalites were all dark in colour – this may also be due to the formation of unwanted radical anions, or of low starting material purity. In any case, this could be studied in the future in the hopes of further lowering the excitation threshold.

The attempts to synthesise aluminogermanate and gallosilicate sodalites during this work were particularly disappointing. The considerable unit cell expansion obtained before framework collapse of Johnson *et al*. means these materials are still of interest,[69,125] particularly when prepared with potassium iodide and subjected to further ion exchange. Moreover, Ga and Ge have higher-energy K-edges than aluminium and silicon, meaning they may be more sensitive to X-rays. However, whether the improved sensitivity offered is worth the increase in cost from these elements is to be considered upon studying them.

Finally, most materials discussed in this work also showed some luminescence, be it PL, PeL or both. The study of such luminescence was out of the scope of this thesis, but in conjunction with the photochromism of these materials, it could make an interesting topic of research in the future.

Acknowledgements

Finally, I must thank the most important people in my life. I have no words to express how grateful I am to my parents, Alan and Harriet, for their unwavering support for the last 26 years. You have always let me follow my dreams, even when they have led me far away from home, and have supported me through every challenge I have faced, no matter how big or small. Thank you both so, so much. And last but not least, my partner Aleksi. I can't imagine how I would have managed this without you. You have been so patient with me through the difficult times, and never fail to make me laugh when I need it. Thank you for everything, and I look forward to taking the next steps in life with you.

Turku, May 2023

Hannah Byron

List of References

(1) *Hackmanite Is a Miracle Material*. https://www.utu.fi/en/news/news/hackmanite-is-a-miracle-material (accessed 2022-12-22).

(2) Norrbo, I.; Gluchowski, P.; Paturi, P.; Sinkkonen, J.; Lastusaari, M. Persistent Luminescence of Tenebrescent $Na_8Al_6Si_6O_{24}(Cl,S)_2$: Multifunctional Optical Markers. *Inorg. Chem.* **2015**, *54* (16), 7717–7724. https://doi.org/10.1021/acs.inorgchem.5b00568.

(3) *Hackmanite*. https://www.mindat.org/min-1789.html (accessed 2023-02-20).

(4) International Mineralogical Association. *List of Minerals*. http://cnmnc.main.jp/IMA_Master_List_%282022-11%29.pdf (accessed 2022-11-22).

(5) Vuori, S.; Colinet, P.; Norrbo, I.; Steininger, R.; Saarinen, T.; Palonen, H.; Paturi, P.; Rodrigues, L. C. V.; Göttlicher, J.; Le Bahers, T.; Lastusaari, M. Detection of X-Ray Doses with Color-Changing Hackmanites: Mechanism and Application. *Advanced Optical Materials* **2021**, *9* (20), 2100762. https://doi.org/10.1002/adom.202100762.

(6) Norrbo, I.; Curutchet, A.; Kuusisto, A.; Mäkelä, J.; Laukkanen, P.; Paturi, P.; Laihinen, T.; Sinkkonen, J.; Wetterskog, E.; Mamedov, F.; Le Bahers, T.; Lastusaari, M. Solar UV Index and UV Dose Determination with Photochromic Hackmanites: From the Assessment of the Fundamental Properties to the Device. *Mater. Horiz.* **2018**, *5* (3), 569–576. https://doi.org/10.1039/C8MH00308D.

(7) Zahoransky, T.; Friis, H.; Marks, M. A. W. Luminescence and Tenebrescence of Natural Sodalites: A Chemical and Structural Study. *Phys. Chem. Miner.* **2016**, *43* (7), 459–480. https://doi.org/10.1007/s00269-016-0810-0.

(8) Finch, A. A.; Friis, H.; Maghrabi, M. Defects in Sodalite-Group Minerals Determined from X-Ray-Induced Luminescence. *Phys. Chem. Miner.* **2016**, *43* (7), 481–491. https://doi.org/10.1007/s00269-016-0816-7.

(9) Wight, W. The Gems of Mont Saint-Hilaire, Quebec, Canada. *J. Gemm.* **1996**, *25* (1), 24–44.

(10) Chukanov, N. V.; Sapozhnikov, A. N.; Shendrik, R. Y.; Vigasina, M. F.; Steudel, R. Spectroscopic and Crystal-Chemical Features of Sodalite-Group Minerals from Gem Lazurite Deposits. *Minerals* **2020**, *10* (11), 1042. https://doi.org/10.3390/min10111042.

(11) Agamah, C.; Vuori, S.; Colinet, P.; Norrbo, I.; de Carvalho, J. M.; Okada Nakamura, L. K.; Lindblom, J.; van Goethem, L.; Emmermann, A.; Saarinen, T.; Laihinen, T.; Laakkonen, E.; Lindén, J.; Konu, J.; Vrielinck, H.; Van der Heggen, D.; Smet, P. F.; Bahers, T. L.; Lastusaari, M. Hackmanite—The Natural Glow-in-the-Dark Material. *Chem. Mater.* **2020**, *32* (20), 8895–8905. https://doi.org/10.1021/acs.chemmater.0c02554.

(12) Kirk, R. D. Role of Sulfur in the Luminescence and Coloration of Some Aluminosilicates. *J. Electrochem. Soc.* **1954**, *101* (9), 461–465. https://doi.org/10.1149/1.2781301.

(13) Banerjee, A. Correlation between Colour and Fluorescence of Lapis Lazuli. *Zeitschrift für Naturforschung A* **1993**, *48* (12), 1267–1268. https://doi.org/10.1515/zna-1993-1222.

(14)   S. F. McClure; G. R. Rossman; J. E. Shigley. Tenebrescent Scapolite from Afghanistan. *Gems & Gemology* **2005**, *41* (3), 269–271.

(15)   Claffy, E. W. Composition, Tenebrescence and Luminescence of Spodumene Minerals. *American Mineralogist* **1953**, *38* (11–12), 919–931.

(16)   Lee, O. I. A New Property of Matter: Reversible Photosensitivity in Hackmanite from Bancroft, Ontario. *Am. Mineral.* **1936**, *21*, 764–776.

(17)   Aage Jensen; Ole V. Petersen. Tugtupite: A Gemstone from Greenland. *Gems & Gemology* **1982**, *18* (2), 90–94.

(18)   Colinet, P.; Byron, H.; Vuori, S.; Lehtiö, J.-P.; Laukkanen, P.; Van Goethem, L.; Lastusaari, M.; Le Bahers, T. The Structural Origin of the Efficient Photochromism in Natural Minerals. *Proceedings of the National Academy of Sciences* **2022**, *119* (23), e2202487119. https://doi.org/10.1073/pnas.2202487119.

(19)   Ch. Baerlocher; L.B. McCusker. *Database of Zeolite Structures*. Database of Zeolite Structures. http://www.iza-structure.org/databases/ (accessed 2023-02-15).

(20)   Chang, I. F. Synthesis of Photochromic and Cathodochromic Sodalite. *J. Electrochem. Soc.* **1974**, *121* (6), 815. https://doi.org/10.1149/1.2401925.

(21)   Williams, E. F.; Hodgson, W. G.; Brinen, J. S. Synthetic Photochromic Sodalite. *J. Am. Ceram. Soc.* **1969**, *52* (3), 139–144. https://doi.org/10.1111/j.1151-2916.1969.tb11200.x.

(22)   Marckwald, W. Ueber Phototropie. *Zeitschrift für Physikalische Chemie* **1899**, *30U* (1), 140–145. https://doi.org/10.1515/zpch-1899-3007.

(23)   Fischer, E. Y. Y. Hirshberg—In Memoriam. *J. Chem. Educ.* **1963**, *40* (3), 112. https://doi.org/10.1021/ed040p112.

(24)   Hirshberg, Y.; Fischer, E. 128. Low-Temperature Photochromism and Its Relation to Thermochromism. *J. Chem. Soc.* **1953**, 629–636. https://doi.org/10.1039/JR9530000629.

(25)   Purkait, M. K.; Sinha, M. K.; Mondal, P.; Singh, R. Chapter 4 - Photoresponsive Membranes. In *Interface Science and Technology*; Purkait, M. K., Sinha, M. K., Mondal, P., Singh, R., Eds.; Stimuli Responsive Polymeric Membranes; Elsevier, 2018; Vol. 25, pp 115–144. https://doi.org/10.1016/B978-0-12-813961-5.00004-8.

(26)   Sekkat, Z.; Knoll, W. *Photoreactive Organic Thin Films*; Elsevier, 2002.

(27)   Yager, K. G.; Barrett, C. J. Chapter 17:Azobenzene Polymers as Photomechanical and Multifunctional Smart Materials. In *Intelligent Materials*; 2007; pp 424–446. https://doi.org/10.1039/9781847558008-00424.

(28)   Leistner, A.-L.; Pianowski, Z. L. Smart Photochromic Materials Triggered with Visible Light. *European Journal of Organic Chemistry* **2022**, *2022* (19), e202101271. https://doi.org/10.1002/ejoc.202101271.

(29)   Zhang, J.; Zou, Q.; Tian, H. Photochromic Materials: More Than Meets The Eye. *Adv. Mater.* **2013**, *25* (3), 378–399. https://doi.org/10.1002/adma.201201521.

(30)   Smith, G. P. Photochromic Glasses: Properties and Applications. *J Mater Sci* **1967**, *2* (2), 139–152. https://doi.org/10.1007/BF00549573.

(31)   Badour, Y.; Jubera, V.; Andron, I.; Frayret, C.; Gaudon, M. Photochromism in Inorganic Crystallised Compounds. *Optical Materials: X* **2021**, *12*, 100110. https://doi.org/10.1016/j.omx.2021.100110.

(32)   Schrauben, J. N.; Hayoun, R.; Valdez, C. N.; Braten, M.; Fridley, L.; Mayer, J. M. Titanium and Zinc Oxide Nanoparticles Are Proton-Coupled Electron Transfer Agents. *Science* **2012**, *336* (6086), 1298–1301. https://doi.org/10.1126/science.1220234.

(33)   Kanu, S. S.; Binions, R. Thin Films for Solar Control Applications. *Proc. R. Soc. A* **2010**, *466* (2113), 19–44. https://doi.org/10.1098/rspa.2009.0259.

(34)   Norrbo, I.; Gluchowski, P.; Hyppänen, I.; Laihinen, T.; Laukkanen, P.; Mäkelä, J.; Mamedov, F.; Santos, H. S.; Sinkkonen, J.; Tuomisto, M.; Viinikanoja, A.; Lastusaari, M. Mechanisms of Tenebrescence and Persistent Luminescence in Synthetic Hackmanite $Na_8Al_6Si_6O_{24}(Cl,S)_2$. *ACS Appl. Mater. Interfaces* **2016**, *8* (18), 11592–11602. https://doi.org/10.1021/acsami.6b01959.

(35)   Jin, Y.; Lv, Y.; Wang, C.; Ju, G.; Wu, H.; Hu, Y. Design and Control of the Coloration Degree for Photochromic $Sr_3GdNa(PO_4)_3F:Eu^{2+}$ via Traps Modulation by Ln^{3+} (Ln=Y, La-Sm, Tb-Lu) Co-Doping. *Sensors and Actuators B: Chemical* **2017**, *245*, 256–262. https://doi.org/10.1016/j.snb.2017.01.129.

(36)   Lv, Y.; Jin, Y.; Wang, C.; Chen, L.; Ju, G.; Hu, Y. $Sr_3YLi(PO_4)_3F:Eu^{2+},Ln^{3+}$: Colorless-Magenta Photochromism and Coloration Degree Regulation through Ln^{3+} Co-Doping. *RSC Adv.* **2017**, *7* (69), 43700–43707. https://doi.org/10.1039/C7RA08090E.

(37)   Naoi, K.; Ohko, Y.; Tatsuma, T. TiO_2 Films Loaded with Silver Nanoparticles: Control of Multicolor Photochromic Behavior. *J. Am. Chem. Soc.* **2004**, *126* (11), 3664–3668. https://doi.org/10.1021/ja039474z.

(38)   Ohko, Y.; Tatsuma, T.; Fujii, T.; Naoi, K.; Niwa, C.; Kubota, Y.; Fujishima, A. Multicolour Photochromism of TiO_2 Films Loaded with Silver Nanoparticles. *Nature Mater* **2003**, *2* (1), 29–31. https://doi.org/10.1038/nmat796.

(39)   Dong, X.; Wu, Z.; Guo, Y.; Tong, Y.; Liu, X.; Zhang, L.; Lu, Y. Rational Modification in the Photochromic and Self-Bleaching Performance of Hierarchical Microsphere Cu@h-$WO_3/WO_3 \cdot nH_2O$ Composites. *Solar Energy Materials and Solar Cells* **2021**, *219*, 110784. https://doi.org/10.1016/j.solmat.2020.110784.

(40)   Bechinger, C.; Wirth, E.; Leiderer, P. Photochromic Coloration of WO_3 with Visible Light. *Appl. Phys. Lett.* **1996**, *68* (20), 2834–2836. https://doi.org/10.1063/1.116340.

(41)   Miyazaki, H.; Inada, M.; Suzuki, H.; Ota, T. Molybdenum Doping Effects on Photochromic Properties of WO_3 Based Composite Films. *Journal of the Ceramic Society of Japan* **2013**, *121* (1409), 106–108. https://doi.org/10.2109/jcersj2.121.106.

(42)   Avellaneda, C. O.; Bulhões, L. O. S. Photochromic Properties of WO_3 and WO_3:X (X=Ti, Nb, Ta and Zr) Thin Films. *Solid State Ionics* **2003**, *165* (1), 117–121. https://doi.org/10.1016/j.ssi.2003.08.023.

(43)   Shen, Y.; Pan, L.; Ren, Z.; Yang, Y.; Xiao, Y.; Li, Z. Nanostructured WO_3 Films Synthesized on Mica Substrate with Novel Photochromic Properties. *Journal of Alloys and Compounds* **2016**, *657*, 450–456. https://doi.org/10.1016/j.jallcom.2015.10.103.

(44)   Nishio, S.; Kakihana, M. Evidence for Visible Light Photochromism of V_2O_5. *Chem. Mater.* **2002**, *14* (9), 3730–3733. https://doi.org/10.1021/cm0204270.

(45)   Ju, G.; Hu, Y.; Chen, L.; Wang, X. Photochromism of Europium and Gadolinium Co-Doped Barium Haloapatite. *ECS Solid State Lett.* **2012**, *1* (1), R1. https://doi.org/10.1149/2.001201ssl.

(46)   Zhang, Y.; Luo, L.; Li, K.; Li, W.; Hou, Y. Light-Controlled Reversible Photoluminescence Modulation in Photochromic $Sr_2SnO_4:Eu^{3+}$. *J. Phys. D: Appl. Phys.* **2018**, *51* (36), 365102. https://doi.org/10.1088/1361-6463/aad531.

(47)   Lv, Y.; Li, Z.; Jin, Y.; Wu, H.; Wang, C.; Ju, G.; Chen, L.; Hu, Z.; Hu, Y. A Novel Photochromic Material Based on Halophosphate: Remote Light-Controlled Reversible Luminescence Modulation and Fluorescence Lifetime Regulation. *Ceramics International* **2019**, *45* (5), 5971–5980. https://doi.org/10.1016/j.ceramint.2018.12.067.

(48)   Lv, Y.; Jin, Y.; Wang, C.; Ju, G.; Xue, F.; Hu, Y. Reversible White-Purple Photochromism in Europium Doped $Sr_3GdLi(PO_4)_3F$ Powders. *Journal of Luminescence* **2017**, *186*, 238–242. https://doi.org/10.1016/j.jlumin.2017.02.052.

(49)   Jin, Y.; Hu, Y.; Fu, Y.; Chen, L.; Ju, G.; Mu, Z. Reversible Colorless-Cyan Photochromism in Eu^{2+}-Doped $Sr_3YNa(PO_4)_3F$ Powders. *J. Mater. Chem. C* **2015**, *3* (36), 9435–9443. https://doi.org/10.1039/C5TC01797A.

(50)   Yang, Z.; Du, J.; Martin, L. I. D. J.; Poelman, D. Reversible Yellow-Gray Photochromism in Potassium-Sodium Niobate-Based Transparent Ceramics. *Journal of the European Ceramic Society* **2021**, *41* (3), 1925–1933. https://doi.org/10.1016/j.jeurceramsoc.2020.10.046.

(51)   Rouhani, M.; Foo, Y. L.; Hobley, J.; Pan, J.; Subramanian, G. S.; Yu, X.; Rusydi, A.; Gorelik, S. Photochromism of Amorphous Molybdenum Oxide Films with Different Initial Mo^{5+} Relative   Concentrations.   *Applied   Surface   Science*   **2013**,   *273*,   150–158. https://doi.org/10.1016/j.apsusc.2013.01.218.

(52)   Pardo, R.; Zayat, M.; Levy, D. Photochromic Organic–Inorganic Hybrid Materials. *Chem. Soc. Rev.* **2011**, *40* (2), 672–687. https://doi.org/10.1039/C0CS00065E.

(53)   Williams, E. R.; Simmonds, A.; Armstrong, J. A.; Weller, M. T. Compositional and Structural Control of Tenebrescence. *J. Mater. Chem.* **2010**, *20* (48), 10883–10887. https://doi.org/10.1039/c0jm02066d.

(54)   *The   Periodic   Table   of   Endangered   Elements*.   American   Chemical   Society. https://www.acs.org/greenchemistry/research-innovation/endangered-elements.html (accessed 2022-12-16).

(55)   Hodgson, W. G.; Brinen, J. S.; Williams, E. F. Electron Spin Resonance Investigation of Photochromic Sodalites. *The Journal of Chemical Physics* **1967**, *47* (10), 3719–3723. https://doi.org/10.1063/1.1701527.

(56)   Goettlicher, J.; Kotelnikov, A.; Suk, N.; Kovalski, A.; Vitova, T.; Steininger, R. Sulfur K X-Ray Absorption near Edge Structure Spectroscopy on the Photochrome Sodalite Variety Hackmanite. **2013**, *228* (3), 157–171. https://doi.org/10.1524/zkri.2013.1587.

(57)   Colinet, P.; Gheeraert, A.; Curutchet, A.; Le Bahers, T. On the Spectroscopic Modeling of Localized Defects in Sodalites by TD-DFT. *J. Phys. Chem. C* **2020**, *124* (16), 8949–8957. https://doi.org/10.1021/acs.jpcc.0c00615.

(58)   Vuori, S.; Colinet, P.; Lehtiö, J.-P.; Lemiere, A.; Norrbo, I.; Granström, M.; Konu, J.; Ågren, G.; Laukkanen, P.; Petit, L.; Airaksinen, A. J.; Goethem, L. van; Bahers, T. L.; Lastusaari, M. Reusable Radiochromic Hackmanite with Gamma Exposure Memory. *Mater. Horiz.* **2022**, *9*, 2773–2784. https://doi.org/10.1039/D2MH00593J.

(59)   R. Radler; C. Chenot. *SYNTHESIS OF INORGANIC PHOTOTROPIC MATERIALS FOR HIGH DENSITY COMPUTER MEMORY APPLICATIONS.*; Defense Technical Information Center, 1964. https://apps.dtic.mil/sti/citations/AD0608426 (accessed 2022-11-23).

(60)   Phillips, W. Properties of Cathodochromic Sodalite. *J. Electrochem. Soc.* **1970**, *117* (12), 1557–1561. https://doi.org/10.1149/1.2407383.

(61)   Dawson, R. K.; Pooley, D. F Band Absorption in Alkali Halides as a Function of Temperature. *physica status solidi (b)* **1969**, *35* (1), 95–105. https://doi.org/10.1002/pssb.19690350107.

(62)   Colinet, P. Tenebrescent Minerals by in Silico Modelling. These de doctorat, Lyon, 2022. https://www.theses.fr/2022LYSEN002 (accessed 2022-10-20).

(63)   Doorn, C. Z. van; Schipper, D. J.; Bolwijn, P. T. Optical Investigation of Cathodochromic Sodalite. *J. Electrochem. Soc.* **1972**, *119* (1), 85–92. https://doi.org/10.1149/1.2404141.

(64)   Schipper, D. J.; Doorn, C. Z. V.; Bolwijn, P. T. Preparation of Cathodochromic Sodalites. *Journal of the American Ceramic Society* **1972**, *55* (5), 256–259. https://doi.org/10.1111/j.1151-2916.1972.tb11275.x.

(65)   Todd, L. T. Investigation of Luminescence in Ge-Doped Sodalite Powders. *J. Electrochem. Soc.* **1978**, *125* (7), 1133–1138. https://doi.org/10.1149/1.2131635.

(66)   Todd, L. T. U.V. Absorption Band in Ge-Doped Sodalite Powders. *J. Electrochem. Soc.* **1980**, *127* (2), 435–438. https://doi.org/10.1149/1.2129683.

(67)   Fleet, M. E. Structures of Sodium Alumino-Germanate Sodalites [$Na_8(Al_6Ge_6O_{24})A_2$, A = Cl, Br, I]. *Acta Crystallogr C Cryst Struct Commun* **1989**, *45* (6), 843–847. https://doi.org/10.1107/S0108270188013964.

(68)   Johnson, G. M.; Weller, M. T. A Powder Neutron Diffraction Study of Lithium-Substituted Gallosilicate and Aluminogermanate Halide Sodalites. *Inorg. Chem.* **1999**, *38* (10), 2442–2450. https://doi.org/10.1021/ic9812510.

(69)   Johnson, G. M.; Mead, P. J.; Weller, M. T. Synthesis of a Range of Anion-Containing Gallium and Germanium Sodalites. *Microporous and Mesoporous Materials* **2000**, *38* (2–3), 445–460. https://doi.org/10.1016/S1387-1811(00)00169-4.

(70)   Johnson, G. M.; Mead, P. J.; Weller, M. T. Structural Trends in the Sodalite Family. *Phys. Chem. Chem. Phys.* **1999**, *1* (15), 3709–3714. https://doi.org/10.1039/a903373d.

(71)   Norrbo, I.; Carvalho, J. M.; Laukkanen, P.; Mäkelä, J.; Mamedov, F.; Peurla, M.; Helminen, H.; Pihlasalo, S.; Härmä, H.; Sinkkonen, J.; Lastusaari, M. Lanthanide and Heavy Metal Free Long White Persistent Luminescence from Ti Doped Li-Hackmanite: A Versatile, Low-Cost Material. *Adv. Funct. Mater.* **2017**, *27* (17), 1606547. https://doi.org/10.1002/adfm.201606547.

(72)   Colinet, P.; Bahers, T. L. Engineering Aluminosilicate's Photochromism by Quantum Chemistry. *J. Mater. Chem. C* **2023**, *11* (2), 730–741. https://doi.org/10.1039/D2TC04312B.

(73)   Radler, R. *INORGANIC PHOTOTROPIC MATERIALS FOR HIGH DENSITY COMPUTER MEMORIES:*; Defense Technical Information Center: Fort Belvoir, VA, 1963. https://doi.org/10.21236/AD0407796.

(74)   Ballentyne, D. W. G.; Bye, K. L. The Nature of Photochromism in Chlorosodalites from Optical Data. *J. Phys. D: Appl. Phys.* **1970**, *3* (10), 1438–1443. https://doi.org/10.1088/0022-3727/3/10/308.

(75)   Hammond, K. D.; Dogan, F.; Tompsett, G. A.; Agarwal, V.; Conner, W. C. Jr.; Grey, C. P.; Auerbach, S. M. Spectroscopic Signatures of Nitrogen-Substituted Zeolites. *J. Am. Chem. Soc.* **2008**, *130* (45), 14912–14913. https://doi.org/10.1021/ja8044844.

(76)   Clark, R. J. H.; Dines, T. J.; Kurmoo, M. On the Nature of the Sulfur Chromophores in Ultramarine Blue, Green, Violet, and Pink and of the Selenium Chromophore in Ultramarine Selenium: Characterization of Radical Anions by Electronic and Resonance Raman Spectroscopy and the Determination of Their Excited-State Geometries. *Inorg. Chem.* **1983**, *22* (19), 2766–2772. https://doi.org/10.1021/ic00161a024.

(77)   Lindner, G. G.; Reinen, D. Synthese, Farbe und Struktur eines roten Selen-Ultramarins. *Z. Anorg. Allg. Chem.* **1994**, *620* (7), 1321–1328. https://doi.org/10.1002/zaac.19946200729.

(78)   Reinen, D.; Lindner, G.-G. The Nature of the Chalcogen Colour Centres in Ultramarine-Type Solids. *Chem. Soc. Rev.* **1999**, *28* (2), 75–84. https://doi.org/10.1039/a704920j.

(79)   Schlaich, H.; Lindner, G.-G.; Feldmann, J.; Göbel, E. O.; Reinen, D. Optical Properties of Se_2^- and Se_2 Color Centers in the Red Selenium Ultramarine with the Sodalite Structure. *Inorg. Chem.* **2000**, *39* (13), 2740–2746. https://doi.org/10.1021/ic990223u.

(80)   Kirk, R. D. The Luminescence and Tenebrescence of Natural and Synthetic Sodalite. *American Mineralogist* **1955**, *40* (1–2), 22–31.

(81)   Van Doorn, C. Z.; Schipper, D. J. Luminescence of O_2^-, Mn^{2+} and Fe^{3+} in Sodalite. *Physics Letters A* **1971**, *34* (3), 139–140. https://doi.org/10.1016/0375-9601(71)90792-4.

(82)   Deb, S. K.; Gallivan, J. B. Photoluminescence of O_2^- and S_2^- Ions in Synthetic Sodalities. *Journal of Luminescence* **1972**, *5* (5), 348–360. https://doi.org/10.1016/0022-2313(72)90025-7.

(83)   Gaft, M.; Panczer, G.; Nagli, L.; Yeates, H. Laser-Induced Time-Resolved Luminescence of Tugtupite, Sodalite and Hackmanite. *Phys Chem Minerals* **2009**, *36* (3), 127–141. https://doi.org/10.1007/s00269-008-0263-1.

(84)   Warner, T. E. *Synthesis, Properties and Mineralogy of Important Inorganic Materials*; Wiley: Somerset, GB, 2011.

(85)   Norrbo, I.; Hyppänen, I.; Lastusaari, M. Up-Conversion Luminescence – A New Property in Tenebrescent and Persistent Luminescent Hackmanites. *J. Lumin.* **2017**, *191*, 28–34. https://doi.org/10.1016/j.jlumin.2017.02.046.

(86)   Thapan, K.; Arendt, J.; Skene, D. J. An Action Spectrum for Melatonin Suppression: Evidence for a Novel Non-Rod, Non-Cone Photoreceptor System in Humans. *The Journal of Physiology* **2001**, *535* (1), 261–267. https://doi.org/10.1111/j.1469-7793.2001.t01-1-00261.x.

(87)   Tosini, G.; Ferguson, I.; Tsubota, K. Effects of Blue Light on the Circadian System and Eye Physiology. *Mol Vis* **2016**, *22*, 61–72.

(88)   Li, D.; Fang, P.; Liu, H.; Chen, L.; Fu, Y.; Liu, J.; Xie, B.; Liu, Y.; Ye, H.; Gu, P. The Clinical Effect of Blue Light Therapy on Patients with Delayed Sleep-Wake Phase Disorder. *Nat Sci Sleep* **2022**, *14*, 75–82. https://doi.org/10.2147/NSS.S344616.

(89)   Glickman, G.; Byrne, B.; Pineda, C.; Hauck, W. W.; Brainard, G. C. Light Therapy for Seasonal Affective Disorder with Blue Narrow-Band Light-Emitting Diodes (LEDs). *Biol Psychiatry* **2006**, *59* (6), 502–507. https://doi.org/10.1016/j.biopsych.2005.07.006.

(90)   Wang, H.-B.; Whittaker, D. S.; Truong, D.; Mulji, A. K.; Ghiani, C. A.; Loh, D. H.; Colwell, C. S. Blue Light Therapy Improves Circadian Dysfunction as Well as Motor Symptoms in Two Mouse Models of Huntington's Disease. *Neurobiology of Sleep and Circadian Rhythms* **2017**, *2*, 39–52. https://doi.org/10.1016/j.nbscr.2016.12.002.

(91)   Zhao, Z.-C.; Zhou, Y.; Tan, G.; Li, J. Research Progress about the Effect and Prevention of Blue Light on Eyes. *Int J Ophthalmol* **2018**, *11* (12), 1999–2003. https://doi.org/10.18240/ijo.2018.12.20.

(92)   Organisciak, D. T.; Darrow, R. M.; Barsalou, L.; Kutty, R. K.; Wiggert, B. Circadian-Dependent Retinal Light Damage in Rats. *Invest Ophthalmol Vis Sci* **2000**, *41* (12), 3694–3701.

(93)   Vaughan, D. K.; Nemke, J. L.; Fliesler, S. J.; Darrow, R. M.; Organisciak, D. T. Evidence for a Circadian Rhythm of Susceptibility to Retinal Light Damage. *Photochem Photobiol* **2002**, *75* (5), 547–553. https://doi.org/10.1562/0031-8655(2002)075<0547:efacro>2.0.co;2.

(94)   White, M. P.; Fisher, L. J. Degree of Light Damage to the Retina Varies with Time of Day of Bright Light Exposure. *Physiol Behav* **1987**, *39* (5), 607–613. https://doi.org/10.1016/0031-9384(87)90160-0.

(95)   Cameron, J. Radiation Dosimetry. *Environmental Health Perspectives* **1991**, *91*, 45–48. https://doi.org/10.1289/ehp.919145.

(96)   Soubra, M.; Cygler, J.; Mackay, G. Evaluation of a Dual Bias Dual Metal Oxide-Silicon Semiconductor Field Effect Transistor Detector as Radiation Dosimeter. *Med Phys* **1994**, *21* (4), 567–572. https://doi.org/10.1118/1.597314.

(97)   Senthil Srinivasan, V. S.; Pandya, A. Dosimetry Aspects of Hafnium Oxide Metal-Oxide-Semiconductor (MOS) Capacitor. *Thin Solid Films* **2011**, *520* (1), 574–577. https://doi.org/10.1016/j.tsf.2011.07.010.

(98)   Kevles, B. *Naked to the Bone: Medical Imaging in the Twentieth Century*; New Brunswick, N.J. : Rutgers University Press, 1997.

(99)   Pardue, L. A. *Photographic Film as a Pocket Radiation Dosimeter*; Atomic Energy Commission, 1947.

(100)   J. Izewska; G. Rajan. Chapter 3: Radiation Dosimeters. In *Radiation Oncology Physics: A Handbook for Teachers and Students*; E. B. Podgorsak, Ed.; International Atomic Energy Agency-IAEA, 2005.

(101)   GE Inspection Technologies. *Industrial Radiography: Image Forming Techniques*; Pennsylvania, USA, 2008.

(102)   Rolf Behling. *Modern Diagnostic X-Ray Sources: Technology, Manufacturing, Reliability*; Ringgold Inc: Beaverton, United States, 2015; Vol. 2.

(103)   Curry, T. S.; Dowdey, J. E.; Murry, R. C. *Christensen's Physics of Diagnostic Radiology*; Lippincott Williams & Wilkins, 1990.

(104)   Jin, Y.; Hu, Y.; Yuan, L.; Chen, L.; Wu, H.; Ju, G.; Duan, H.; Mu, Z. Multifunctional Near-Infrared Emitting Cr^{3+}-Doped $Mg_4Ga_8Ge_2O_{20}$ Particles with Long Persistent and Photostimulated Persistent Luminescence, and Photochromic Properties. *J. Mater. Chem. C* **2016**, *4* (27), 6614–6625. https://doi.org/10.1039/C6TC01640E.

(105)   Medved, D. B. Hackmanite and Its Tenebrescent Properties. *Am. Mineral.* **1954**, *39*, 615–629.

(106)   Armstrong, J. A.; Weller, M. T. New Sodalite Frameworks; Synthetic Tugtupite and a Beryllosilicate Framework with a 3 : 1 Si : Be Ratio. *Dalton Trans.* **2006**, No. 24, 2998–3005. https://doi.org/10.1039/b600579a.

(107)   Abhinay, S.; Mazumder, R.; Seal, A.; Sen, A. Tape Casting and Electrical Characterization of $0.5Ba(Zr_{0.2}Ti_{0.8})O_3$–$0.5(Ba_{0.7}Ca_{0.3})TiO_3$ (BZT–0.5BCT) Piezoelectric Substrate. *Journal of the European Ceramic Society* **2016**, *36* (13), 3125–3137 . https://doi.org/10.1016/j.jeurceramsoc.2016.04.017.

(108)   Vuori, S.; Byron, H.; Norrbo, I.; Tuomisto, M.; Lastusaari, M. Photochromic Photography with Hackmanite Obtained by Large-Scale Synthesis. *Journal of Industrial and Engineering Chemistry* **2023**, *120*, 361–373. https://doi.org/10.1016/j.jiec.2022.12.043.

(109)   Langford, J. I.; Wilson, A. J. C. Scherrer after Sixty Years: A Survey and Some New Results in the Determination of Crystallite Size. *J. Appl. Cryst.* **1978**, *11*, 102–113.

(110)   Alexander, L.; Klug, H. P. Determination of Crystallite Size with the X-Ray Spectrometer. *J. Appl. Phys.* **1950**, *21* (2), 137–142. https://doi.org/10.1063/1.1699612.

(111)   Garlick, F. J.; Gibson, F. The Electron Trap Mechanism of Luminescence in Sulphide and Silicate Phosphors. *Proc. Phys. Soc.* **1948**, *60*, 574–590.

(112)   Phosphorescent pigments and products – Part 1: Measurement and marking at the producer. DIN 67510-1:2009-11, Berlin, Germany. Phosphorescent pigments and products – Part 1: Measurement and marking at the producer. DIN 67510-1:2009-11, 2009.

(113)   Van den Eeckhout, K.; Bos, A. J. J.; Poelman, D.; Smet, P. F. Revealing Trap Depth Distributions in Persistent Phosphors. *Phys. Rev. B* **2013**, *87* (4), 045126. https://doi.org/10.1103/PhysRevB.87.045126.

(114)   R. Dovesi; V. R. Saunders; C. Roetti; R. Orlando; C. M. Zicovich-Wilson; F. Pascale; B. Civalleri; K. Doll; N. M. Harrison; I. J. Bush; P. D'Arco; M. Llunell; M. Causà; Y. Noël; L. Maschio; A. Erba; M. Rerat; S. Casassa. CRYSTAL17, 2017.

(115)   Adamo, C.; Barone, V. Toward Reliable Density Functional Methods without Adjustable Parameters: The PBE0 Model. *J. Chem. Phys.* **1999**, *110* (13), 6158–6170. https://doi.org/10.1063/1.478522.

(116)   Nada, R.; Nicholas, J. B.; McCarthy, M. I.; Hess, A. C. Basis Sets for Ab Initio Periodic Hartree—Fock Studies of Zeolite/Adsorbate Interactions: He, Ne, and Ar in Silica Sodalite. *International Journal of Quantum Chemistry* **1996**, *60* (4), 809–820. https://doi.org/10.1002/(SICI)1097-461X(1996)60:4<809::AID-QUA3>3.0.CO;2-0.

(117)   Demichelis, R.; Noel, Y.; Civalleri, B.; Roetti, C.; Ferrero, M.; Dovesi, R. The Vibrational Spectrum of α-AlOOH Diaspore: An Ab Initio Study with the CRYSTAL Code. *J. Phys. Chem. B* **2007**, *111* (31), 9337–9346. https://doi.org/10.1021/jp072501d.

(118)   Corno, M.; Busco, C.; Civalleri, B.; Ugliengo, P. Periodic Ab Initio Study of Structural and Vibrational Features of Hexagonal Hydroxyapatite $Ca_{10}(PO_4)_6(OH)_2$. *Phys. Chem. Chem. Phys.* **2006**, *8* (21), 2464–2472. https://doi.org/10.1039/B602419J.

(119)   Hariharan, P. C.; Pople, J. A. The Influence of Polarization Functions on Molecular Orbital Hydrogenation Energies. *Theoret. Chim. Acta* **1973**, *28* (3), 213–222. https://doi.org/10.1007/BF00533485.

(120)   G. Sophia; P. Baranek; C. Sarrazin; M. Rerat; R. Dovesi. *www.crystal.unito.it/basissets.php*. www.crystal.unito.it/basissets.php.

(121)   Vilela Oliveira, D.; Laun, J.; Peintinger, M. F.; Bredow, T. BSSE-Correction Scheme for Consistent Gaussian Basis Sets of Double- and Triple-Zeta Valence with Polarization Quality for Solid-State Calculations. *Journal of Computational Chemistry* **2019**, *40* (27), 2364–2376. https://doi.org/10.1002/jcc.26013.

(122)   M. J. Frisch; G. W. Trucks; H. B. Schlegel; G. E. Scuseria; M. A. Robb; J. R. Cheeseman; G. Scalmani; V. Barone; G. A. Petersson; H. Nakatsuji; X. Li; M. Caricato; A. V. Marenich; J. Bloino; B. G. Janesko; R. Gomperts; B. Mennucci; H. P. Hratchian; J. V. Ortiz; A. F. Izmaylov; J. L. Sonnenberg; D. Williams-Young; F. Ding; F. Lipparini; F. Egidi; J. Goings; B. Peng; A. Petrone; T. Henderson; D. Ranasinghe; V. G. Zakrzewski; J. Gao; N. Rega; G. Zheng; W. Liang; M. Hada; M. Ehara; K. Toyota; R. Fukuda; J. Hasegawa; M. Ishida; T. Nakajima; Y. Honda; O. Kitao; H. Nakai; T. Vreven; K. Throssell; J. A. Montgomery Jr.; J. E. Peralta; F. Ogliaro; M. J. Bearpark; J. J. Heyd; E. N. Brothers; K. N. Kudin; V. N. Staroverov; T. A. Keith; R. Kobayashi; J. Normand; K. Raghavachari; A. P. Rendell; J. C. Burant; S. S. Iyengar; J. Tomasi; M. Cossi; J. M. Millam; M. Klene; C. Adamo; R. Cammi; J. W. Ochterski; R. L. Martin; K. Morokuma; O. Farkas; J. B. Foresman; D. J. Fox. Gaussian 16 Revision C.01, 2016.

(123)   Dong, B.; Xu, Y.; Lin, S.; Dai, X. Characterizing and Exploring the Formation Mechanism of Salt Deposition by Reusing Advanced-Softened, Silica-Rich, Oilfield-Produced Water (ASOW) in Superheated Steam Pipeline. *Scientific Reports* **2015**, *5* (1), 17274. https://doi.org/10.1038/srep17274.

(124)   Geoffrey Mark Johnson. Synthesis and Characterisation of Aluminosilicate and Framework Modified Sodalites. PhD Thesis, University of Southampton, Faculty of Science, Department of Chemistry, 1996.

(125)   Johnson, G. M.; Mead, P. J.; Dann, S. E.; Weller, M. T. Multinuclear MAS NMR Studies of Sodalitic Framework Materials. *J. Phys. Chem. B* **2000**, *104* (7), 1454–1463. https://doi.org/10.1021/jp9929521.

(126)   Shannon, R. D. Revised Effective Ionic Radii and Systematic Studies of Interatomic Distances in Halides and Chalcogenides. *Acta Crystallographica Section A* **1976**, *32* (5), 751–767. https://doi.org/10.1107/S0567739476001551.

(127)   Warner, T. E.; Hutzen Andersen, J. The Effects of Sulfur Intercalation on the Optical Properties of Artificial 'Hackmanite', $Na_8[Al_6Si_6O_{24}]Cl_{1.8}S_{0.1}$; 'Sulfosodalite', $Na_8[Al_6Si_6O_{24}]S$; and Natural Tugtupite, $Na_8[Be_2Al_2Si_8O_{24}](Cl,S)_{2-\delta}$. *Phys. Chem. Miner.* **2012**, *39* (2), 163– 168. https://doi.org/10.1007/s00269-011-0471-y.

(128)   Hoffmann, G. Principles and Working Mechanisms of Water-Filtered Infrared-A (WIRA) in Relation to Wound Healing. *GMS Krankenhaushygiene interdisziplinär* **2007**, *2*, Doc54.

(129)   Fang, W.; Sairanen, E.; Vuori, S.; Rissanen, M.; Norrbo, I.; Lastusaari, M.; Sixta, H. UV-Sensing Cellulose Fibers Manufactured by Direct Incorporation of Photochromic Minerals. *ACS Sustainable Chem. Eng.* **2021**, *9* (48), 16338–16346. https://doi.org/10.1021/acssuschemeng.1c05938.

(130)   T. Laine; I. Norrbo; J. Holvitie; M. Lastusaari. An Android Application for Determining UV Index and UV Dose from Hackmanite, 2020.

(131)   *Nuclear Physics Experience*. http://nupex.eu/index.php?g=textcontent/nuclearapplications/xraymed&lang=en (accessed 2023-02-01).

(132)   *Mini-X2 X-Ray Tube System for XRF – Amptek – X-Ray Detectors and Electronics*. https://www.amptek.com/products/mini-x2-x-ray-tube (accessed 2023-02-01).

(133)   Szalóki, I.; Pintér, T.; Szalóki, I.; Radócz, G.; Gerényi, A. A Novel Confocal XRF-Raman Spectrometer and FPM Model for Analysis of Solid Objects and Liquid Substances. *J. Anal. At. Spectrom.* **2019**, *34* (8), 1652–1664. https://doi.org/10.1039/C9JA00044E.

(134)   C. T. Chantler; K. Olsen; R. A. Dragoset; J. Chang; A. R. Kishore; S. A. Kotochigova; D. S. Zucker. *NIST X-Ray Form Factor, Attenuation and Scattering Tables (Version 2.1)*. https://physics.nist.gov/PhysRefData/FFast/html/form.html (accessed 2023-01-24).

(135)   R. D. Deslattes; E. G. Kessler Jr.; P. Indelicato; L. de Billy; E. Lindroth; J. Anton; J. S. Coursey; D. J. Schwab; C. Chang; R. Sukumar; K. Olsen; R. A. Dragoset. *X-Ray Transition Energies Database (Version 1.2)*. NIST. https://www.nist.gov/pml/x-ray-transition-energies-database (accessed 2023-02-08).